Doctoral theses at NTNU, 2018:314

Are Håvard Høien

Applicability of reinforced ribs of sprayed concrete in sections of poor quality and swelling rock mass

Norwegian University of
Science and Technology

NTNU

Doctoral thesis

Are Håvard Høien

ISBN 978-82-326-3418-7 (printed ver.)
ISBN 978-82-326-3419-4 (electronic ver.)
ISSN 1503-8181

NTNU
Norwegian University of Science and Technology
Thesis for the Degree of
Philosophiae Doctor
Faculty of Engineering
Department of Geoscience and Petroleum

Doctoral theses at NTNU, 2018:314

NTNU
Norwegian University of
Science and Technology

Are Håvard Høien

Applicability of reinforced ribs of sprayed concrete in sections of poor quality and swelling rock mass

Thesis for the Degree of Philosophiae Doctor

Trondheim, October 2018

Norwegian University of Science and Technology
Faculty of Engineering
Department of Geoscience and Petroleum

NTNU
Norwegian University of
Science and Technology

NTNU
Norwegian University of Science and Technology

Thesis for the Degree of Philosophiae Doctor

Faculty of Engineering
Department of Geoscience and Petroleum

ISBN 978-82-326-3418-7 (printed ver.)
ISBN 978-82-326-3419-4 (electronic ver.)
ISSN 1503-8181

Doctoral theses at NTNU, 2018:314

Printed by NTNU Grafisk senter

Abstract

When excavating tunnels, reinforcement and support is required depending on the quality of the rock mass. In good quality rock mass, simple reinforcement such as sprayed concrete and rock bolts is usually adequate as support. In areas with very weak rock mass and unfavourable stresses, more comprehensive support methods need to be applied to avoid large deformations in the rock mass. In Norwegian hard rock tunnelling, the geology is characterised mostly by hard rock intersected by weakness zones that often contain swelling minerals. The common rock support in such weakness zones is rebar reinforced ribs of sprayed concrete (RRS) combined with rock bolts and reinforced sprayed concrete between the ribs. This practice is mostly based on experience and the scientific basis to support the practise and its best application is limited.

The main objective of this thesis was to explore deformations in sections of weak rock in hard rock tunnels, with the purpose of developing a better understanding of the use of RRS in tunnelling. A special focus have been placed on how swelling minerals may affect the system. This has been achieved by performing full-scale in-situ monitoring, laboratory testing, numerical modelling and collection and systemization of existing data.

Field monitoring of RRS in Norwegian road tunnels has shown only small deformations in the rock mass and no substantial strain in the rebar of the RRS. When evaluating the field measurements based on numerical modelling, it has been found that the RRS have not been subjected to any load, and hence have had no load-bearing function.

By comparing data from a parameter study based on numerical modelling with data extracted from The Norwegian Public Roads Administration (NPRA) tunnel data base, it was discovered that that RRS has been applied in tunnels where the conditions probably would not require load-bearing support. In the literature, a convergence of 1% is suggested as the limit for the rock to require load-bearing support. This implies that there is an interval where the need for rock support exceeds bolts and sprayed concrete, but where load-bearing support is too extensive.

To explore how swelling minerals may affect the support construction, reconstituted cores of swelling gouge have been tested triaxially. The registered deformation was found to be dominated by creep in the material and no swelling was observed during the saturation of the initially dry specimens. This implies that swelling was insignificant compared to other deformation processes, but as the deformation rate increased during saturation, it may have accelerated the creep process.

Oedometer testing on the swelling gouge with different initial water contents was conducted on the fraction < 20 μm. The behaviour of the material suggests that one could find the water content for where the intracrystalline swelling ends and the osmotic swelling begins. This is important since the rock stress in many cases exceeds the osmotic swelling stress, while it will not exceed the intracrystalline swelling stress. Related to in-situ gouge, one may thus be able to predict whether the material will swell if exposed to water or if the rock stress may force water out, making it shrink. The oedometer testing also showed that the swelling pressure was dependent on the density of the material.

The results described above imply that the current design of the RRS is in most cases over-dimensioned and that a leaner design, which is not load-bearing, is probably sufficient for

most cases. Earlier, reinforced but unarched RRS was used, which require less material (steel, concrete) compared to the load-bearing arched RRS used today. By performing surveillance of the deformations based on total stations, the use of unarched RRS could be safely implemented, first at a project level and later, when having more data, on a systematic level. As part of implementing such a leaner RRS, it is important that effort is also devoted to characterizing the weakness zones and identifying the most important parameters of their deformability.

Preface

This thesis presents research performed during a PhD study conducted at the Research Group for Engineering Geology, Department of Geoscience and Petroleum, Norwegian University of Science and Technology.

The work has been funded by the Norwegian Public Roads Administration (NPRA), which also has been my employer for the last 12 years. The focus of the study was developed over several years while working on different tunnelling projects and, at the same time, having a main base at the NPRA's research and development department. With this work, I hope we are one small step closer to understanding the use of RRS, and the effect that swelling gouge may have on the support structure.

Acknowledgements

First, I would like to express my gratitude to my supervisors: Professor Bjørn Nilsen, thank you for critical and constructive feedback. It has been a great reassurance having an supervisor with your extensive experience to guide me through this work, knowing that you know what it takes. A special thanks for tidying up my messy article drafts. I hope I now have learned. Professor Roger Olsson, thank you for showing great interest for, and the detailed examination, of the scientific results. I have also greatly appreciated the times we have met to discuss article drafts and the following technical and academic discussions.

I would also like to express my gratitude to my former manager in the NPRA, Kjersti Kvalheim Dunham, which facilitated and encouraged me to start on this PhD-work. I would also like to thank my current manager Claus K. Larsen for giving me time to finish the study and group leader Alf Kveen and the rest of my colleagues at the NPRA for support during the work.

Thank you, mom, for always believing in me, the help you have given me and my wife during this work, and for letting me start my engineering career as a kid. Thanks also to my brother Pål, for always being a great guy. I wish my father and grandparents also could have experienced this, particularly as my father went to the same school and my grandfather have worked as a miner. Also a great thank you to my family in-law that have helped us out during the last years.

Finally, thank you dear Inger, you are the best, in general. Always interested, ready to help when needed, and giving encouraging words. It is also a great inspiration to see how you perform your research work and you are more or less a walking course in research methodology and publication, which is very helpful. Tanks also to my sons Peder and Olav who arrived with a blast during this work. You guys rock!

Content

Abbreviations

a	Constant dependent on the rock mass characteristics
c	Cohesion
D	Blast damage
E_i	Intact E-modulus
E_{rm}	E-modulus of the rock mass
GSI	Geological Strength Index
J_a	Joint alteration number in the Q-system
J_n	Joint set number in the Q-system
J_r	Joint roughness number in the Q-system
J_w	Joint water reduction factor in the Q-system
k	Horizontal to vertical stress ratio
m_b	Reduced value of the material constant mi
MPBX	Multipoint Borehole Extensometers
NGI	The Norwegian Geotechnical Institute
NPRA	Norwegian Public Roads Authority
NTNU	Norwegian University of Science and Technology
RMR	Rock Mass Rating
RQD	Rock Quality Designation
RRS	Rebar Reinforced ribs of Sprayed concrete
s	Constant which depends upon the rock mass characteristics
SRF	Stress reduction factor in the Q-system
UCS	Uniaxial Compressive Strength
z	Overburden/depth
γ	Specific gravity
θ	Fracture angle
σ'_1	Maximum effective principal stress
σ'_3	Minimum effective principal stress
σ_1	Major principal stress
σ_3	Minor principal stress
σ_{ci}	Strength of intact rock
σ_h	Horizontal stress
σ_n	Normal stress on a failure plane
σ_r	Radial stress
σ_v	Vertical stress
τ	Shear stress
τ_θ	Shear stress on a fracture plane
φ	Friction angle

1 Introduction

1.1 Background

When excavating underground openings, the reinforcement and support of the rock mass are normally required to ensure a stable and lasting construction. The necessary reinforcement and support vary greatly, from almost none in good rock mass with favourable stresses to massive support in poor and swelling rock masses with unfavourable stresses.

In good quality rock mass, a simple reinforcement is usually enough to make it self-bearing. This reinforcement is usually performed by applying shotcrete, which "glues" fragments/blocks together and creates wedges that keep the contour in place, and by installing rock bolts that reinforce the rock mass. In very weak rock mass, the rock stress deforms the rock and to make a stable tunnel, this deformation needs to be controlled and ultimately stopped. This is accomplished by installing support that interacts with the rock and balances the forces between them. Between these two extremities of good quality rock mass that requires only simple reinforcement and very weak rock mass that needs extensive support, there is a transition zone that will comprise one of the main subjects in this thesis.

Rock support for weak rock mass follows different traditions in different countries. For instance, in the Alp countries, very rigid systems are commonly used (Aksoy et al. 2012b; Schwingenschloegl and Lehmann 2009), while in Norwegian tunnelling tradition, it is common to use much leaner support systems (NFF 2008). Among the rigid systems commonly used in many countries are steel sets and lattice girders, and in extreme cases elements that deform at a certain load are included. These are used together with rock bolts, reinforcing mesh and sprayed concrete between the steel beams (Barla et al. 2011).

The Norwegian tradition is to use rebar reinforced ribs of sprayed concrete (RRS), with rock bolts and fibre-reinforced sprayed concrete between the ribs (NFF 2008). The ribs usually consist of six rebars mounted in brackets attached to rock bolts along the tunnel periphery; see Fig. 1. After mounting the rebars, shotcrete is applied to form the final rib. In Norway today, the rib system is the preferred choice of rock support in weak and swelling rock mass. The current practice in the use of these ribs is largely based on experience/empiricism.

Fig. 1 Mounting of rebars for two RRS for permanent support (2). Further toward the face, two (1) blast rounds are temporarily supported with spiling bolts held in place by steel straps and radial rock bolts. The finished RRS is shown to the right (3).

There are many reasons to use these ribs. First of all, construction-wise they are easy and quick to build as an integrated part of the blasting and rock support cycle. Combined with spiling bolts, the ribs can be used to excavate through almost any kind of poor quality rock mass. They represent an early, integrated part of the permanent rock support, while other support systems require more effort later in the construction process. Because of their quick construction and limited material requirements (steel and concrete), they also represent a cost-efficient alternative.

In recent years, there has been a discussion in Norway on the boundary regarding rock conditions that are reasonable for RRS, relative to cast concrete lining for rock support (Holmøy and Aagaard 2002). The discussion has been characterized by limited scientific documentation and considerable subjectivity depending upon individual experience. In recent years, the Norwegian Public Roads Administration (NPRA) has revised its guideline from requiring that all zones containing swelling clay must be supported by cast concrete lining to stating that RRS can be used in most rock conditions (Statens vegvesen 2016b). NPRA also stated that cast concrete lining, in the few cases where it is required, can normally be constructed behind the face, which means that support during excavation in any case will normally be provided by spiling bolts and RRS. This standard is also practised by other builders, like the Norwegian national rail administration, Bane NOR SF, (Bane NOR 2018).

There has also been a discussion on how to design the shotcrete ribs. The two different main opinions in this discussion hinge on whether the rib needs to form an arch (arched RRS) or if the rib may follow the rock contour (unarched RRS); see Fig. 2. The discussion is fuelled to a great extent by limited knowledge of the mechanical behaviour of the RRS, its interaction with the rock mass, and of how and why the rock deforms under different kinds of weak rock conditions.

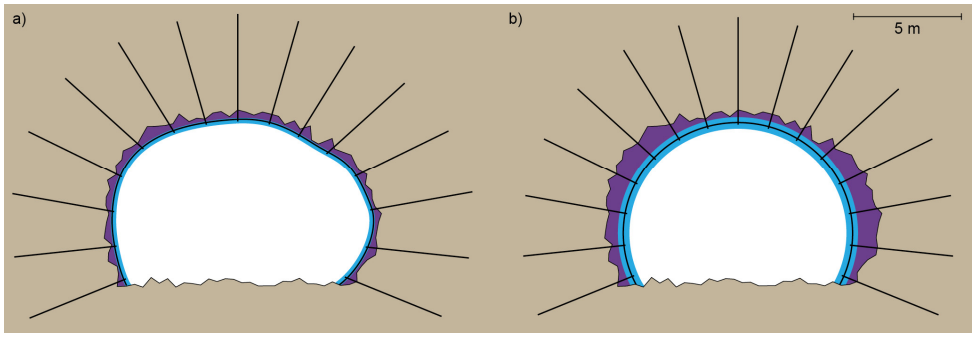

Fig. 2 Principle sketches of a) unarched RRS and b) arched RRS. The black lines represent rebar and rock bolts, purple is the sprayed concrete smoothing layer and the light blue final layer is the sprayed concrete covering the rebar. The rugged contour represents the blasted profile.

The Norwegian Geotechnical Institute (NGI) and Norwegian University of Science and Technology (NTNU) have previously conducted some research related to RRS. NGI has performed numerical modelling to define dimensioning guidelines (Grimstad et al. 2002), and also calculated loads based on in-situ measurements in the Finnfast and Bærum Tunnel (Grimstad et al. 2008). The RRS dimensioning guiQ-delines have been integrated into the rock support chart of the rock mass quality classification and support design system – the Q-system (NGI 2015). The dataset from the Finnfast Tunnel has also been studied at NTNU by Mao et al. (2011), wherein a 3D numerical model was used to analyse the loading effects on the reinforced ribs of sprayed concrete.

The Norwegian geology is characterised primarily by hard rock, which is intersected by weakness zones originating from tectonic activity. The weakness zones very often contain swelling minerals, and the proper method of coping with these swelling minerals constitutes a major concern. Little literature is available on how to interpret the results from laboratory tests of the swelling gouge in term of tunnel support design.

There is also limited knowledge of other mechanical properties characterising the sections of poor quality rock mass material, such as UCS, E-modulus and properties related to water, which are important for time-dependent deformation development. When assessing these parameters, the external factors are also important, such as rock stress and the geometry of the tunnel. More research is therefore needed on how to characterise the weakness zones to better facilitate adequate rock support.

As indicated above, the current state of knowledge on the subject does not present a satisfactory background for solving the problems described above. To advance one step further, the main intention of this PhD project is to evaluate the RRS design for weak and swelling rock, with a particular focus on deformation in weakness zones.

1.2 Thesis scope and objective

The thesis focuses on underground constructions for infrastructure use i.e. road and railway tunnels. The research results will, however, also be relevant for other types of underground excavations. The main emphasis will be geological situations where hard rock is intersected by weakness zones that often contain swelling minerals.

The objective is to explore deformations under different kinds of weak rock conditions, with the purpose of developing a better understanding of the function of RRS in tunnelling.

In order to achieve this objective, the following sub-tasks have been defined:

- An evaluation of measurement data for poor quality rock mass and monitoring data for RRS instrumentation
- A comparison of Norwegian conditions with international theory to evaluate the current Norwegian rock support strategies, with a particular focus on deformations
- An investigation of the properties of the swelling weakness zone gouge through experimental laboratory testing
- An investigation of the swelling fraction of gouge material with a particular focus on the water content

1.3 Organisation of thesis and note on contribution

The thesis consists of four papers and a synthesis. The synthesis presents the background, explains the overall problem and describes the interrelationship between the articles and research carried out. The following four papers constitute the main part of the thesis:

Paper I
Analysis of the stabilizing effect of ribs of reinforced sprayed concrete (RRS) in the Løren Road Tunnel
Høien, Are Håvard; Nilsen, Bjørn
Published online in Bulletin of Engineering Geology and the Environment https://doi.org/10.1007/s10064-018-1238-1
The planning of the measurement setup was performed by Are Håvard Høien in cooperation with Lloyd Tunbridge (NGI), Arild Neby (NPRA), Alf Kveen (NPRA) and others. The

installation of RRS measurement equipment and collection of data was supervised by Lloyd Tunbridge. Data was collected by site engineers, including Are Håvard Høien. Stress measurements were planned by Are Håvard Høien and Arild Neby and executed by Trond Larsen (SINTEF). The paper was written by Are Håvard Høien and reviewed during the process by Bjørn Nilsen.

Paper II
Main aspects of deformation and rock support in Norwegian road tunnels
Høien, AH, Nilsen, B, Olsson, R
Submitted, 31/01/2018, to Tunnelling and Underground Space Technology. Under review.
Data collection and analysis were performed by Are Håvard Høien. The paper was written by Are Håvard Høien and reviewed by Bjørn Nilsen and Roger Olsson.

Paper III
Experimental triaxial testing of swelling gouge materials
Høien, AH, Nilsen, B, Vistnes, G, Olsson, R
Submitted, 23/03/2018, to Rock Mechanics and Rock Engineering. Under review.
Planning of triaxial test methodology and specimen preparation was done by Are Håvard Høien. Triaxial testing was done in cooperation by Gunnar Vistnes (NTNU) and Are Håvard Høien. The additional tests were performed by Are Håvard Høien, Per Olav Solli (NPRA), Johnny Bergersen (NPRA) and Daniel Voll (SINTEF). The paper was written by Are Håvard Høien and reviewed by Bjørn Nilsen, Gunnar Vistnes and Roger Olsson.

Paper IV
Oedometer testing of swelling clay from gouge material at different water contents
Høien, AH, Nilsen, B, Olsson, R
Abstract to be submitted, 07/2018, to ISRM 14th International Congress of Rock Mechanics 2019, Iguassu Falls, Brazil.
Planning of test methodology was done by Are Håvard Høien with technical input from Tom-Andrè Kynbråten (NPRA) and Jan-Inge Senneset (NPRA). Laboratory testing was supervised by Are Håvard Høien and executed by Tom-Andrè Kynbråten and Jan-Inge Senneset. The paper was written by Are Håvard Høien and reviewed by Bjørn Nilsen and Roger Olsson.

2 Theoretical basis and background

In the following section, important basic aspects of the properties and behaviour of rock mass will be described. This background knowledge is considered important for understanding the intention of the individual papers, which are briefly commented on in Section 5.1.

2.1 Rock mass quality

There are several tools or systems that may be used to describe rock mass quality. These tools are often also used for designing support, evaluations of alternative excavation methods or estimations of inputs for rock engineering applications (Palmstrom and Stille 2007). The systems that are most relevant to this thesis are the GSI and Q-system. The Q-system is described later in Section 4.3 and will not be further commented on in this section.

The Geological Strength Index was introduced in the mid-1990s by Hoek (1994). The system provides a number which, when combined with the intact rock properties, can be used to estimate rock mass strength under different geological conditions (Hoek 2006), based on the Hoek-Brown failure criterion (see Section 2.4). In addition, it can be used to estimate the E-modulus of the rock mass (E_{rm}) (see Section 2.2). Because of its applicability in these matters, it is commonly used in rock engineering applications, such as numerical modelling, as in this thesis.

The GSI can be estimated in-situ by using diagrams describing the structure and joint surface conditions. To obtain the GSI value or rather a range of values describing the rock mass, the rock structure and the surface of the discontinuities are combined based on a diagram. The GSI values ranges from 0 (poorest) to 100 (best).

One of the most recent contributions regarding GSI is a quantification of the two sides of the GSI chart that makes it possible to calculate GSI values from parameter values registered with the Rock Mass Rating (RMR) and Q-system (Hoek et al. 2013). In this thesis, recalculations of Rock Quality Designation (RQD) and Q-parameters, J_r and J_a, into GSI values have been used. This was done to create tunnelling conditions based on a large dataset of mapped Norwegian road tunnels comparable to results obtained from numerical modelling. This kind of conversion is known to involve some degree of uncertainty, but the large amount of data is believed, to some degree, to compensate for this uncertainty. This topic is discussed in more detail in Paper II.

2.2 Properties of rock mass and weak rock

The Young's modulus, or E-modulus, is a basic parameter when considering deformations. Theoretically, strain (relative deformation) is a function of applied stress and E-modulus. Knowing the E-modulus of the rock mass is therefore important when considering support with respect to deformations.

In contrast to the E-modulus of intact rock, which is quite easy to obtain in the laboratory, the E-modulus of the rock mass is more difficult to obtain, and is normally estimated based on a rock mass quality classification system. More than 15 different formulas have been proposed for this estimation by different authors. These formulas are based on the inputs of different rock mass quality parameters, such as the Q-value from the Q-system, the Rock Mass Rating (RMR) and the Geological Strength Index (GSI) (Aksoy et al. 2012a; Palmström and Singh 2001; Hoek and Diederichs 2006). Most of these estimates are based on a limited amount of data (Hoek and Diederichs 2006).

Hoek and Diederichs (2006) proposed two equations that can be used to estimate the E-modulus of the rock mass with the GSI as an input. These equations are based on a dataset of nearly 500 tests. In addition to an equation proposed earlier (Hoek et al. 2002), these equations are probably the most commonly used today because they are well documented and easy to use, based on computer software. The equations provide a rock mass E-modulus, E_{rm}, and have slightly different input parameters to suit different premises:

- *Generalized Hoek & Diederichs (2006)*, which considers the E-modulus of intact rock (E_i), blast damage (D) and GSI;
- *Simplified Hoek & Diederichs (2006)*, which considers D and GSI; and
- *Hoek, Carranza-Torres, Corkum (2002)*, which considers the strength of intact rock (σ_{ci}), D and GSI.

The strain can be calculated based on Hooke's law, as indicated in the beginning of this section; strain = E-modulus/stress. To illustrate the relationship between the three parameters, strain has been plotted versus different probable values of stress and E-modulus in Fig. 3. Vertical stresses representing overburdens from 25 to 1000 m have been used, with 0.7 MPa representing the gravitational stress at 25 m and 2.6 MPa representing the gravitational stress at 100 m, and the following stresses representing each subsequent even 100 m. The E-modulus ranges from 40 000 MPa to 313 MPa, where the high value represents e.g. a massive gneiss and the lowest value represents e.g. a crushed, clayey gouge material. The plot is intended merely to illustrate the sensitivity of the deformation with respect to the E-modulus at different, relevant stress states and must not be confused with actual strain in a tunnel.

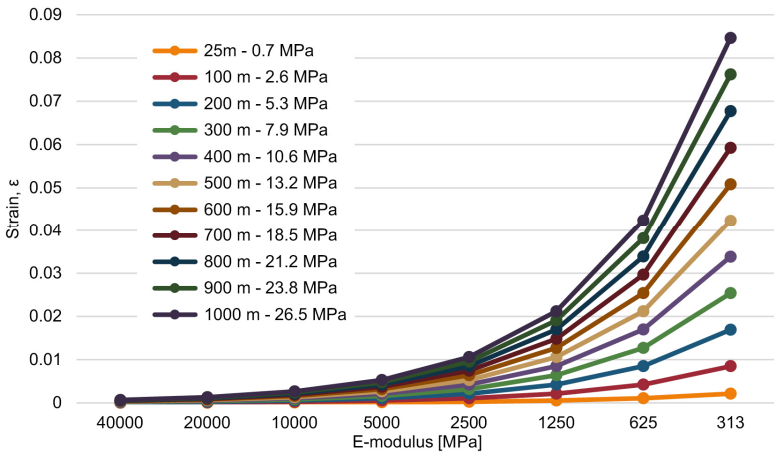

Fig. 3 Strain vs. E-modulus calculated based on Hooke's law for different (vertical) stresses.

The main message based on Fig. 3 is that the E-modulus and stress have a far greater impact on strain on the right side of the plot, where the rock mass is weak with low E-values, than on the middle and high E-values. In addition, Fig. 3 illustrates that the strain for low stresses, representing shallow tunnels, is very small, even for low E-values.

According to ISRM (1978), a rock is characterised as weak when the UCS is below 25 MPa. Hoek (1999) had a more complex definition based on including in-situ stress as well and suggested that a rock is weak when the uniaxial strength is less than about one-third of the in-situ stress acting upon the rock mass. The latter approach implies that the "weakness" of

the rock is not only defined by the rock mass strength, but also by the stress conditions of the rock mass in which the tunnel was excavated.

2.3 Rock stress

The in-situ stress condition in the rock mass is, together with the material properties and tunnel geometry, the main input used in evaluating tunnel deformation. The stress in flat topography is usually defined by a gravity-driven vertical stress, representing the weight of the overburden and a horizontal stress which is a ratio of the vertical, as shown in Eq. 1 and 2:

$$\sigma_v = \gamma z \quad (1)$$

$$\sigma_h = k\sigma_v \quad (2)$$

Where σ_v is vertical stress [kPa]
σ_h is horizontal stress [kPa]
γ is specific gravity [kN/m^3]
z is overburden/depth [m]
k is horizontal to vertical stress ratio

Considerable uncertainty is connected to the ratio k, but it is generally agreed upon in the literature that the horizontal stress is usually larger than the vertical stress, especially near the surface (Brown and Hoek 1978; Herget 1988; Myrvang 1993; Sheorey 1994; Hoek 2006). Local conditions may, however, greatly influence the stress situation in terms of both magnitude and direction e.g. topography, tectonic stress and rock mass quality.

As input for stresses in the numerical modelling in Paper II, an equation suggested by Sheorey (1994) is considered to be the best option for estimating the ratio k, and has been used. The k-ratio is dependent on the E-modulus of the rock and for the chosen E-modulus in the paper, the horizontal stress is equal to the vertical stress at a depth of approximately 250 m. For depths lower than 250 m in the study, the vertical and horizontal stresses are set to be equal. This decision was based on two arguments: 1) Myrvang (1993) found that at least down to 500 m the vertical stress is the minor stress, indicating that there is a point somewhere at depth that the horizontal and vertical stress converge, and 2) that according to Hoek (1999), it is a reasonable assumption to consider the horizontal and vertical stresses equal for very weak rock mass, such as in a weakness zone. Since the numerical modelling focused on the performance of weak rock, it was considered reasonable based on this to set the horizontal stress equal to the vertical stress.

2.4 Failure criterions — Hoek-Brown and Mohr-Coulomb

The two most commonly used failure criterions in rock engineering are Hoek-Brown and Mohr-Coulomb. The first is used in the numerical modelling performed in the papers, while the second is used to understand the triaxial tests described later.

For the purpose of obtaining reliable estimates of the strength characteristics of rock masses, Hoek and Brown (1980) proposed a new failure criterion. The criterion uses properties of the intact rock, which are reduced based on the characteristics of the joints in the rock mass (Hoek et al. 2002). There have been several minor and major revisions and adjustments to this criterion through the years, with the latest edition being the criterion from 2002, called *Generalized Hoek-Brown Criterion* (see Eq. 3).

$$\sigma_1' = \sigma_3' + \sigma_{ci}\left(m_b\frac{\sigma_3'}{\sigma_{ci}} + s\right)^a \qquad 3$$

Where σ_1' and σ_3' are the maximum and minimum effective principal stresses at failure
m_b is a reduced value of the material constant m_i, were the reduction is based on GSI and blast damage (D)
s and a are constants which depend upon the rock mass characteristics. s is calculated by using GSI and D and a is calculated using only the GSI
σ_{ci} is the uniaxial compressive strength of the intact rock pieces

The failure envelope for Hoek-Brown is curved, as indicated by the red dotted line in Fig. 4. The m_i value depends on the frictional characteristics of the rock and can be obtained by triaxial rock core testing.

The red solid line in Fig. 4 is the failure envelope for the Mohr-Coulomb criterion. As shown, this envelope is linear, and shear stress is defined by the equation:

$$\tau = c + \tan\varphi \qquad 4$$

Where τ is the shear stress
c is the cohesion
φ is the friction angle

In Fig. 4, the major principal stress (σ_1) is equal to the axial stress (σ_a) and the minor principal stress (σ_3) is equal to the radial stress (σ_r). If a half circle crosses the strength envelope, the material fails. For example, if σ_3 is lowered, the size of the half circle will grow, making it cross the line, and the material will fail. What happens is that the stabilizing normal stress (σ_n) on the fracture plane decreases and the fracture plane shear stress (τ_θ) increases at the same time, causing the sample to fail.

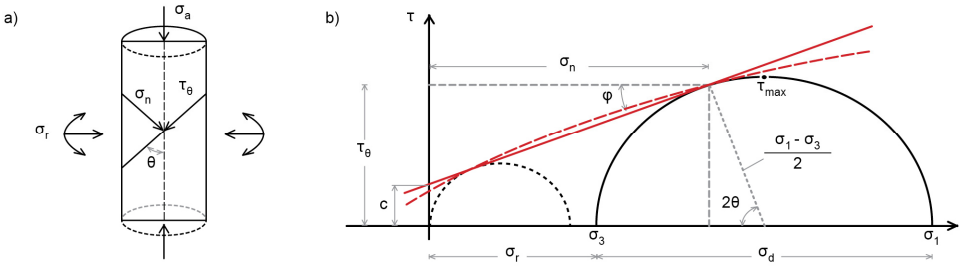

Fig. 4 Principle of failure for a triaxial test. a) Stresses on a core sample under radial and axial stress. b) The red solid line is the Mohr-Coulomb failure envelope and the red dotted line is Hoek-Brown failure envelope.

3 Deformation of rock mass due to tunnelling

When excavating a tunnel, there are two main types of deformations one may encounter:, immediate and time-dependent (Barla 1999). The immediate deformations are dependent on the elastic and plastic material properties of the rock mass (see Fig. 5). In clayey and silty rock mass, with water present, immediate and time-dependent deformations will be associated with an undrained and drained phase, respectively. The immediate deformations take place without/before the flow of water and the drained, or time-dependent, deformations occur with water flowing. Drained and undrained behaviours are extreme conditions that hardly appear in the field, but since they represent limiting conditions, they offer valuable guidelines (Terzaghi and Peck 1967).

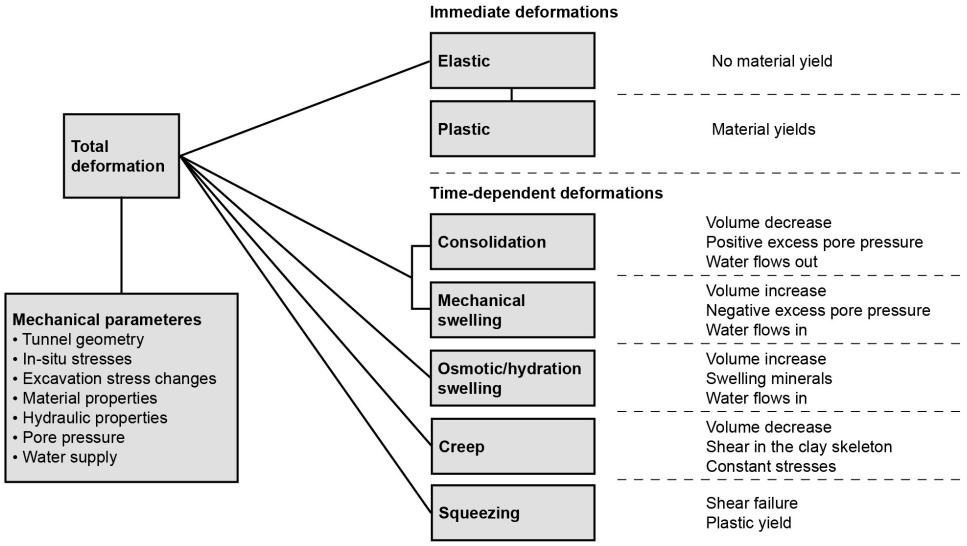

Fig. 5 Types of deformations related to tunnelling

3.1 Immediate deformations

The immediate deformations are caused by the in-situ stress and the stress changes in the remaining rock mass due to the excavation. The displacement caused by rock stress is dependent on the elastic and plastic properties of the rock mass, where the elastic is the property of the intact rock mass and the plastic is the property of the rock mass if it yields. The rock mass yields if the stresses exceed its strength. The plastic properties of a rock mass are lower or, for very weak rock, they may be the same as the elastic properties (Crowder and Bawden 2004).

When a tunnel is excavated, the face advances through the rock mass and deformations occur. According to Hoek et al. (1997), the deformation starts about one-half of the tunnel diameter ahead of the face and at the face about one-third of the deformations have taken place. At about one to one and a half tunnel diameters behind the face, the deformations have reached their final value. This is further discussed in Paper II.

3.2 Time-dependent deformations

The time-dependent deformations are more complex than the afore mentioned, with many possible processes causing them. The main different processes are (mineral) swelling, squeezing, creep, consolidation and mechanical swelling, which all cause convergence of

the tunnel walls. The particular process that takes place is dependent on the rock mass and stresses, and more than one may occur at the same time.

When it comes to swelling and squeezing, Einstein (1996) pointed out that these phenomena are often strongly interrelated and that one may lead to the other. He also provided some short definitions for the two, where swelling is defined as the *"Time-dependent volume increase of the ground, leading to inward movement of the tunnel perimeter"* and squeezing is defined as the *"Time-dependent shearing of the ground, leading to inward movement of the tunnel perimeter."*

When the tunnel advances, changes in stress occur, which may result in negative or positive excess pore pressure. If the excess pore pressure is positive, the water will flow out and the material will consolidate. Further, if it is negative, the water will flow toward the area and it will mechanically swell. This processes are also referred to as the primary consolidation phase (Bellwald 1990).

Creep is defined as deformation due to shear failure over time and under constant stress. It may or may not happen at the same time as the (mechanical) swelling/consolidation and is also referred to as the second consolidation phase. Creep is related to the time-dependent properties of the grain skeleton and is usually associated with drained behaviour. Creep can be divided into three phases: primary, secondary and tertiary (see Fig. 6). The creep mechanism is divided into two types: the volumetric creep caused by volumetric stress and the deviatoric creep caused by deviatoric stress. The volumetric stress is, using the core in Fig. 4 a) as an example, the uniform stress in the radial and axial direction, and the deviatoric stress is the stress additional to the volumetric in one of these directions.

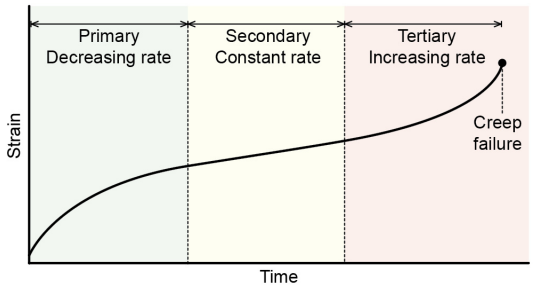

Fig. 6 Creep phases. Based on Einstein (1989)

The primary creep phase is a result of volumetric creep and possibly deviatoric creep if the deviatoric stresses are large enough. The rate of strain during primary creep decreases until it stops, or the strain/time is constant. When the strain-rate is constant, the secondary creep phase, which is caused by deviatoric stress, begins. Deviatoric creep is a time-dependent shear deformation caused by a serial change in the soil structure through the rearrangement of the grain contacts. The tertiary creep phase is also caused by deviatoric creep and starts when the strainrate starts to accelerate. The tertiary creep phase ends in failure and it is therefore important to avoid. Einstein (1996) defined creep as shear failure and stated that this shear failure also is squeezing, indicating that the background process of squeezing is creep.

During time-dependent deformations, there will be a redistribution of stresses around the tunnel profile. The new stress regime may start new deformation processes at locations that were stable earlier. The processes causing the deformations are, as described above, hard to

determine and more than one process may occur at the same time. To identify the deformation processes, a good approach might be to consider the mechanical parameters for the area (e.g. those given in Fig. 5), with a focus on the background of the processes.

3.3 Swelling process for smectite minerals

The weakness zones in Norwegian geology are mainly formed by faulting and/or, in some cases, deep weathering. The origin of swelling minerals in weakness zones is believed mainly to be caused by on alternation of feldspar into different types of smectites.

There are two types of swelling processes, according to Madsen and Müller-Vonmoos (1989), for this kind of material; intracrystalline/hydration (see Fig. 7) and osmotic (see Fig. 8), which happen in sequence. A clay quasicrystal (see Fig. 8 a) consists of two to thousands of clay layers stacked together and the intracrystalline swelling is swelling occurring between these layers, while the osmotic is between quasicrystals (Laird 2006). The intra-crystalline swelling is caused by the hydration of the exchangeable cations of the dry clay layer surface and can expand the grain up to about 100%. The water arranges itself in layers between the clay layers. For montmorillonite, swelling pressures ranging between several hundred MPa for one layer of water to about 27 MPa for the third and fourth layer of water have been found (Madsen and Müller-Vonmoos 1989; Kraehenbuehl et al. 1987). The osmotic process relates to the ion concentration differences near the quasicrystal surface and in the pore water. The osmotic swelling in the second phase can create a pressure ranging up to about 2 MPa.

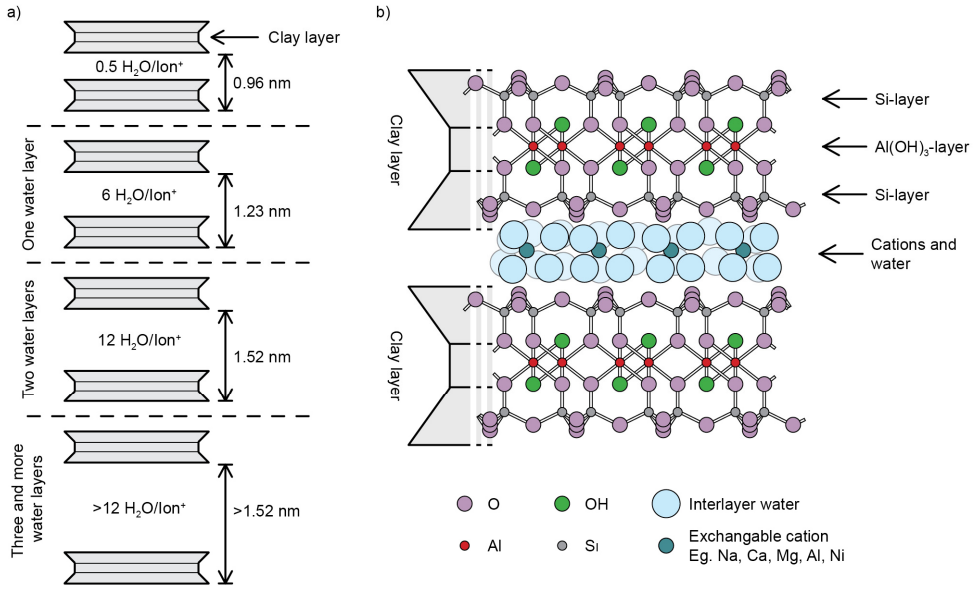

Fig. 7 a) Intracrystalline swelling/hydration of sodium montmorillonite with distances as a function of water adsorption. b) The basic structure of montmorillonite. Each clay layer consists of two Si-layers (tetrahedral) and one Al(OH_3)-layer (octahedral). Based on Kraehenbuehl et al. (1987), Selmer-Olsen (1980), Nilsen (2016) and Weil and Brady (2017)

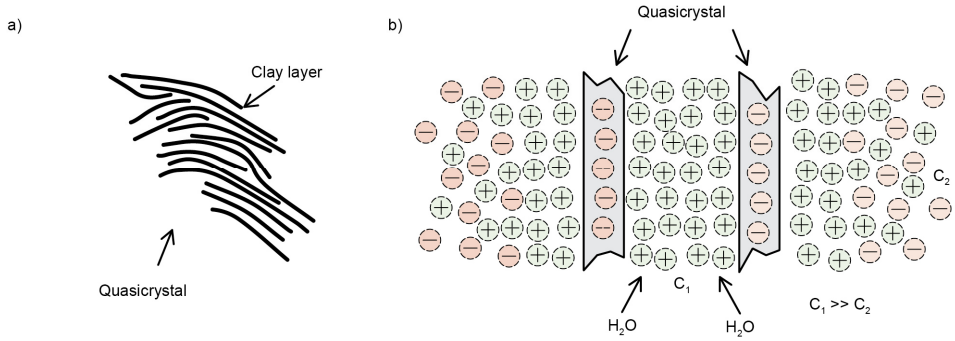

Fig. 8 a) Example of a quasicrystal consisting of fifteen clay layers. b) Osmotic swelling. Quasicrystals are negatively charged at the surfaces and between them there is a high ion concentration, C1. This concentration is much higher than in the pore water, C2, and an equilibrium is reached through the penetration of the water between the quasicrystals. Based on Madsen and Müller-Vonmoos (1989) and Laird (2006)

3.4 Rock support related to deformations

Evaluation of expected deformations can be used to distinguish between which rock masses that need to be supported by load-bearing constructions and which only requires reinforcement.

Fig. 9 illustrates the relationship between rock mass strength, in-situ stress and strain as published in Hoek (1999); Hoek and Marinos (2000); Hoek (2001). The relationship is a result of statistical simulation based on using the Monte Carlo method according to the theory of Duncan Fama (1993) and Carranza-Torres and Fairhurst (1999), with input representing weak rock and overburdens down to 800 m.

The strain, or tunnel convergence, in the figure has been divided into different squeezing classes, each with general support suggestions for the respective classes A-E. Of particular interest is the transition from class A to B, where class A has recommended rock reinforcement provided by bolts and sprayed concrete and class B has recommended load-bearing constrictions such as lattice girders or steel sets. The amount of strain in this transition, 1%, is based on Sakurai's work (Sakurai 1981; Sakurai 1983) on critical strain, which can be explained as the strain of a rock or rock mass at yield load. Both the work of Sakurai and Hoek and Marinos are discussed in more detail in Paper II.

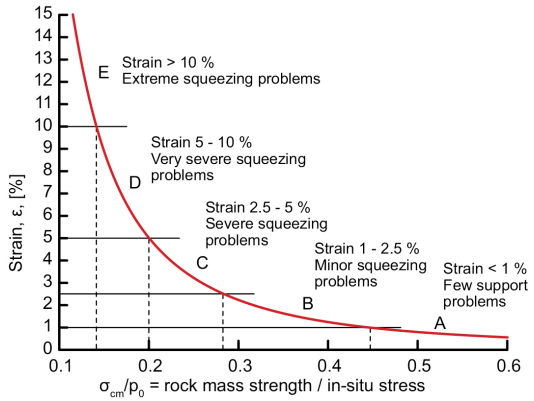

Fig. 9 The relationship between strain and the ratio between rock mass strength and in-situ stress. The curve is for unsupported rock. Based on Hoek and Marinos (2000)

4 Main characteristics of Norwegian ground conditions and rock support

4.1 Geological overview

The bedrock in Norway is mainly Precambrian and Cambro-Silurian (Caledonian); see Fig. 10. The bedrock of Precambrian age is mainly gneiss and intrusive granite and gabbro, while the Caledonian rocks are mainly metamorphosed, originally sedimentary rocks. In the Oslo region in the southeast of Norway, some Permian volcanic and igneous rocks are found. In the Mesozoic era, there was a weathering of the bedrock and later, in the Pleistocene, glaciers eroded and shaped the landscape. Because of this glacial erosion, the bedrock today mainly consists of unweathered hard rock, which is intersected by weakness zones of different extents and characters caused by tectonic activity and, in some cases, Mesozoic weathering.

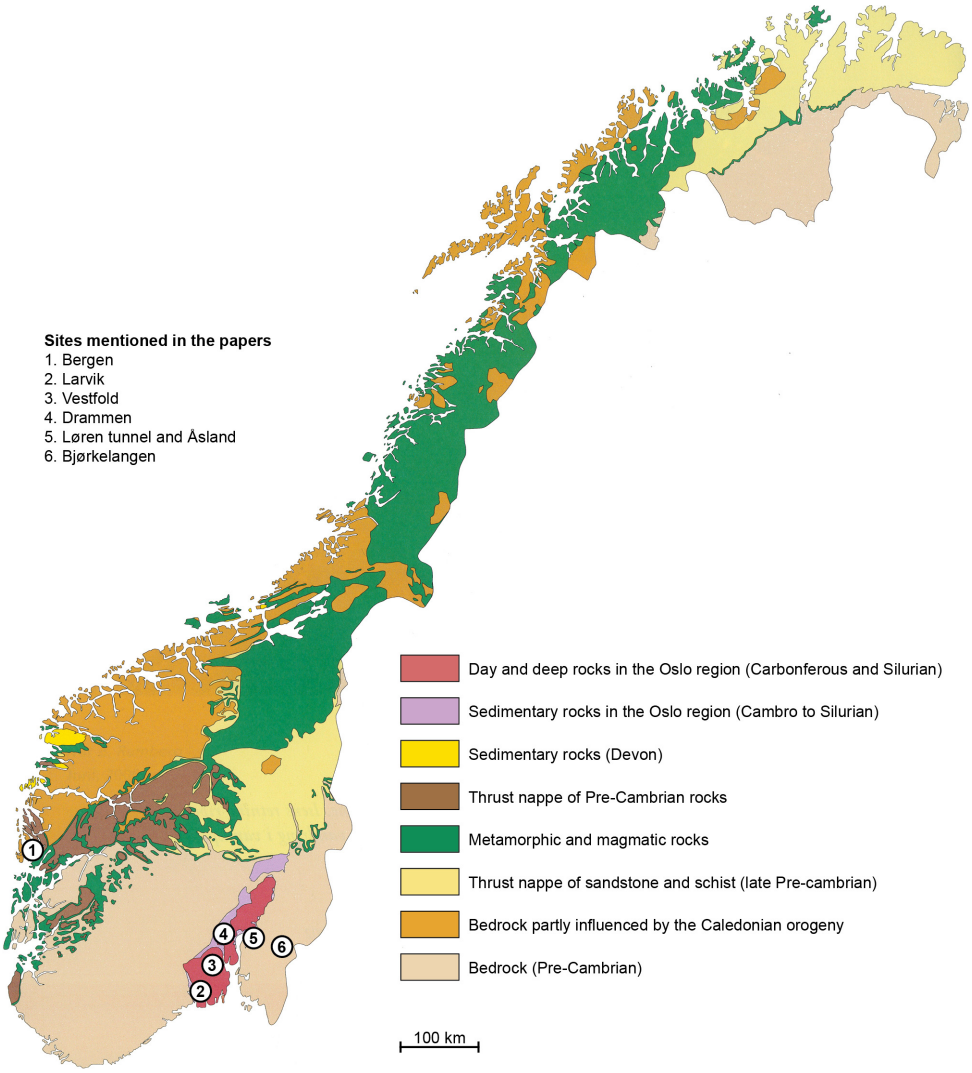

Fig. 10 Overview of Norwegian regional geology and sites discussed in the papers. Based on NGU (2018).

The stresses in Norway according to Myrvang (1993, 2001) are characterized by much higher horizontal stress than the vertical component would indicate. As mentioned earlier, this is at least the case down to a 500 m overburden. Myrvang also found that the directions show an overall tendency for the principal stress to be either parallel or normal to the Caledonian mountain range.

Values of UCS and E-modulus of Norwegian rocks are mainly large or very large. In Paper II, the significance of UCS and E-modulus based on the Norwegian research foundation SINTEF's database of rock properties (SINTEF 2016) are further discussed.

4.2 Characteristics of weakness zones

The character of weakness zones may vary within wide ranges. It is not the intention here to provide a complete description of a weakness zone, but rather to give a few examples to illustrate some of the possible variations that may be encountered during tunnelling in hard rock conditions. For a more comprehensive description, reference is made to e.g. Hoek et al. (1997) or Nilsen and Palmstrøm (2000).

Fig. 11 shows a network of weakness zones as seen from the air. This illustration is from a mountainous area in southeastern Norway, where no Quaternary deposits or vegetation hide the bedrock structures as they usually do in the lower parts of the country.

Fig. 11 Network of weakness zones in a mountainous area in southwest Norway. One can see the weakness zones as lines in the landscape due to glacial erosion. The depth of depressions is mainly a result of the rock quality, zone width and glacial motion direction. The road crossing the image is 10 km from edge to edge (Google Maps 2018).

In some cases, i.e. as shown in Fig. 1 and Fig. 16, a weakness zone is characterized by intense fracturing/crushing, with limited extent of gouge material or joint filling. In other cases, the weakness zone contains more clay gouge, often rich in swelling minerals, which

the laboratory work in this thesis is particularly focused on. The examples in Fig. 12-15 are from projects/sites where the material for laboratory testing has been collected. Fig. 12 and Fig. 13, represent examples from the E39 highway tunnel Svagatjørn–Rådal in Bergen. Fig. 12 shows weak rock mass in the entire face, but highest content of clay at the right side. A hydraulic hammer could with little effort excavate this rock mass. In Fig. 13, a more limited zone with a high content of clay is shown, which was so loose that one could easily dig it out by using the back end of a geological hammer. See also Paper IV, Fig. 4.

Fig. 12 Chainage 13251 in tube T52 at the E39 Svagatjørn–Rådal project

Fig. 13 Chainage 13616 in tube T52 at the E39 Svagatjørn–Rådal project. Material from this zone is used in Paper IV.

Fig. 14 Road cut just outside the Martineås tunnel at the E18 Bommestad–Sky project close to Larvik

Fig. 15 Road cut just outside Drammen. This weakness zone crosses the Kleivene tunnel on highway E18.

In Fig. 14, the origin of material referred to as "Larvik" in Fig. 10 and Paper III is shown. The structure running diagonally in the middle of the photo is a very clay-rich zone with material that can be easily scraped loose by using the back end of a geological hammer. Some places, there are harder rock fragments separated by filled joints. The rock fragments can also with little effort be loosened using the back end of the geological hammer and broken into several pieces with a firm blow. See also Paper III, Fig. 5 a).

The zone shown in Fig. 15 is referred to as "Drammen" in Paper III. The left side of the zone is very clay rich and the pointed end of a geological hammer may easily be pushed into the material. On the right side, small pieces may be broken loose by using the geological hammer and further broken by hand into small pieces. See also Paper III, Fig. 7 and 8.

The examples shown in this section represent quite narrow weakness zones. Zones forming large valleys and fjords may be of much larger sizes with widths of tens of meter or more, causing fjord-crossing subsea tunnels to be especially vulnerable to stability problems.

4.3 Rock support in Norwegian road tunnelling

The strategy used most for dimensioning support in Norwegian infrastructure tunnels is based on the Q-system (NGI 2015). The system involves mapping of six rock mass parameters and based on this calculate the Q-value (see Eq. 5). By also taking into account the tunnel dimensions and the required safety level, the Q-value can be used to find recommended rock support by using the chart shown in Fig. 16. The chart refers to three different RRS classes shown in Table 1. The background for the RRS-dimensioning according to these classes is given in Grimstad et al. (2002).

For many projects, the Q-system's support chart is used directly, but for Norwegian road tunnels, a support table developed by the NPRA is used, wherein different support classes are linked to the Q-value (see Table 2). The recommended support is an integrated part of the drill and blast excavation cycle and the dimensioning is largely based on the Q-system support chart (Statens vegvesen 2016a, b).

$$Q = \frac{RQD}{J_n} \times \frac{J_r}{J_a} \times \frac{J_w}{SRF} \qquad 5$$

Where RQD is the Rock Quality Designation
J_n is the joint set number
J_r is the joint roughness number
J_a is the joint alteration number
J_w is the joint water reduction factor
SRF is the stress reduction factor

Table 1 RRS-classes in the Q system. Ex. D45/6+2 Ø16-20, Si = single rebar layer, D = double rebar layer, 45 = thickness in cm, 6+2 = 6 rebar in first layer, 2 in second, Ø16-20 = rebar diameter in mm (NGI 2015)

RRS class	5 m span	10 m span	20 m span
I		Si30/6 Ø16 - Ø20	D40/6+2 Ø16-20
II	Si35/6 Ø16-20	D45/6+2 Ø16-20	D55/6+4 Ø20
III	D40/6+4 Ø16-20	D55/6+4 Ø20	Special consideration

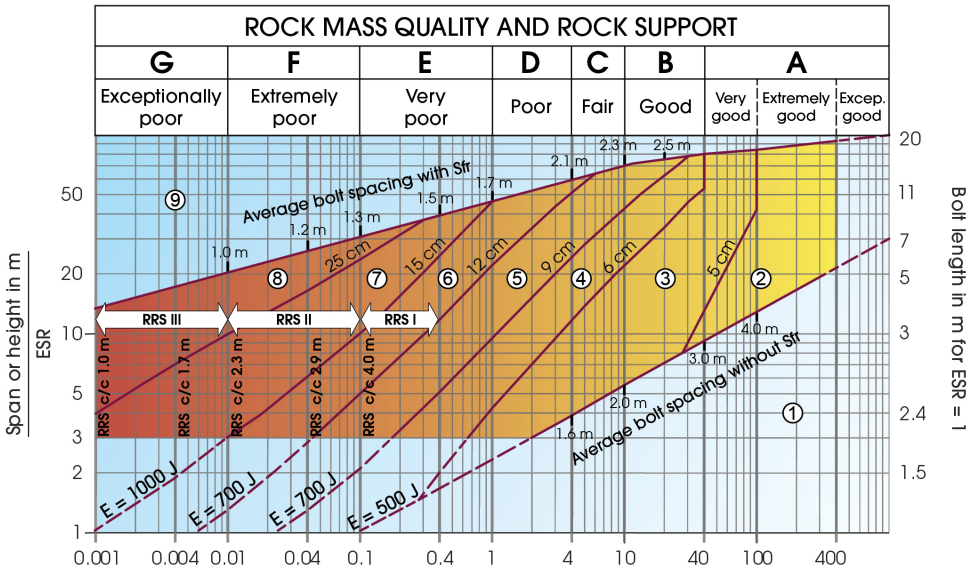

Fig. 16 The Q-systems rock support chart (NGI 2015). For RRS dimensioning, see Table 1.

Table 2 Support table for Norwegian road tunnels developed by the NPRA (Statens vegvesen 2016b; Pedersen et al. 2010)

Rock mass class	**Rock conditions** **Q-value**	**Support class** **Permanent support**
A/B	Weakly jointed rock mass Average joint spacing > 1m. Q = 100–10	*Support class I* - Scattered bolting - Sprayed concrete B35 E700, thickness 80 mm
C	Moderate jointed rock mass Average joint spacing 0.3–1 m. Q = 10 – 4	*Support class II* - Systematic bolting, c/c 2 m - Sprayed concrete B35 E700, thickness 80 mm
D	Strongly jointed rock mass or bedded schistose rock Average joint spacing < 0.3 m. Q = 4–1	*Support class III* - Sprayed concrete B35 E1000, thickness 100 mm - Systematic bolting, c/c 1.75 m
E	Very poor rock mass Q = 1–0.2 ---------- Q = 0.2–0.1	*Support class IVa* - Systematic bolting, c/c 1.5 m - Sprayed concrete B35 E1000, thickness 150 mm ---------- *Support class IVb* - Systematic bolting, c/c 1.5 m - Sprayed concrete B35 E1000, thickness 150 mm - RRS: · Rib dimension E30/6 Ø20 mm, c/c 2–3 m, · Bolting along arch c/c 1.5 m, length 3–4 m - Invert cast concrete must be evaluated
F	Extremely poor rock mass Q = 0.01–0.1	*Support class V* - Systematic bolting, c/c 1.0–1.5 m - Sprayed concrete B35 E1000, thickness 150–250 mm - RRS: · Rib dimension D30/6+4 Ø20 mm, c/c 1.5–2 m, · Bolting along arch c/c 1.0 m, length 3–6 m · Can be replaced with lattice girders - Invert cast concrete, pitch min. 10% of tunnel width
G	Exceptionally poor rock mass Q < 0.01	*Support class VI* - Excavation and support design to be evaluated for each case

4.4 Construction process of RRS

As described in Section 1.1, there are basically two main RRS designs, the one that forms an arch, and the one with rebar following the blasted surface. The two different versions use different rebar dimensions; the arched has pre-bent Ø20 mm rebar, while the unarched uses 16 mm rebar. The reason for this is that the Ø20 mm rebar is too stiff for to bend out of shape which make it is easier to form the arch properly. For the unarched RRS, Ø16 mm is used since they can be bent by hand to follow the uneven blasted rock surface.

Except for the arching and rebar dimensions, and that the need to use a surveyor is lower with an unarched RRS, the construction process is more or less identical. The common process, as illustrated also in Fig. 17, is as follows:

- A surveyor defines where the radial bolts are to be placed and how far out from the existing profile the sprayed concrete smoothing layer is to be applied. In addition, the positions of the spiling bolts are marked.
- Bolt holes are drilled.
- The radial bolts for the RRS are mounted. The threads are covered to protect them from sprayed concrete and, at the same time, marks to show the thickness of the smoothing layer are provided.
- Spiling bolts for the next blasting round are installed and fastened with rock bolts and steel straps.
- The smoothing layer is sprayed and, at the same time, the fastenings of the spiling bolts are sprayed to fix them in place.
- The protection on the threads are removed, brackets and the rebar are mounted on the bolts. The usual distance between rebars is 100 mm.
- The RRS is sprayed with fibre-free concrete to ensure as good as possible coverage with no voids.

For more details regarding the construction and use of RRS, reference is made to Holmøy and Aagaard (2002) and Statens vegvesen (2016a).

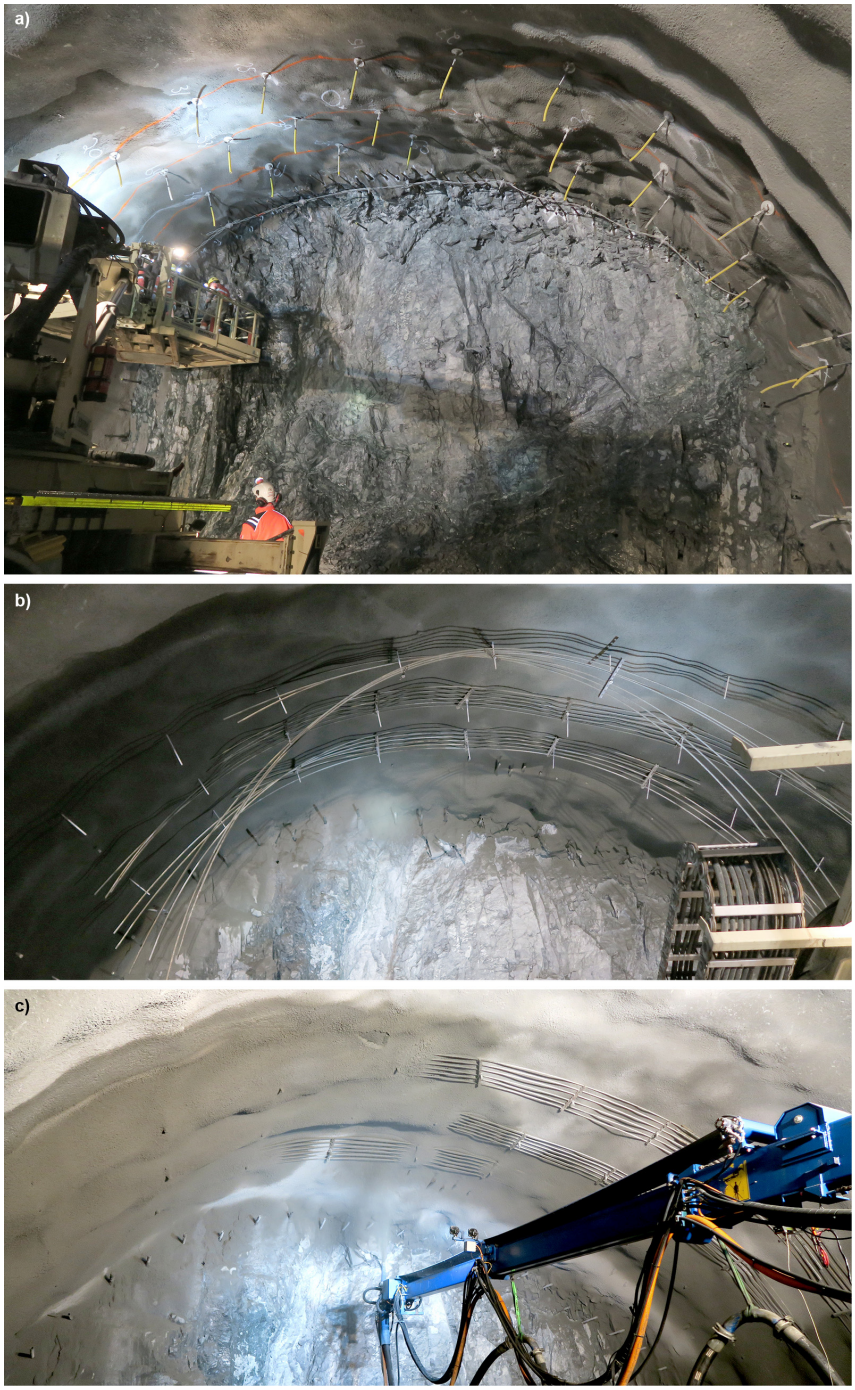

Fig. 17 Construction process of RRS. a) Ready for smoothening layer. The bolt ends have been elongated using a connecting coupling and threaded bar. Threads are covered with a hose (yellow) to protect them from the sprayed concrete. Spiling bolts combined with steel straps and rock bolts can be seen at the periphery of the face. b) The smoothening layer and the spiling arrangement are sprayed and the rebar is being mounted. c) Spraying of ribs. At the face, one can see that the perimeter blast holes are already drilled and protected by a piece of tube. The holes are drilled before RRS construction because the ribs will block the drill rig boom position.

5 Research methodology

This PhD research project includes full-scale field measurements, laboratory testing, numerical modelling and collection as well as systemization of data. The field work consisting of an extensive measurement program of loads and deformations on three RRS, is discussed in Paper I. In both Papers I and II, numerical modelling has been used; in the former for modelling of the measured RRS, and in the latter for investigating possible tunnel deformation characteristics. In Paper II, data on Norwegian road tunnels and rock properties have also been collected and systemized.

Papers III and IV mainly describe laboratory investigations. In Paper III, a new method for triaxial testing of swelling gouge material was performed to investigate stress and strain during water addition. In Paper IV, a modified procedure for oedometer testing of the swelling fraction gouge material was performed to investigate the effects of initial water content in the material.

5.1 Brief comments on individual papers

5.1.1 Paper I: Analysis of the stabilizing effect of ribs of reinforced sprayed concrete (RRS) in the Løren Road Tunnel

RRS is widely used as support in Norwegian tunnelling based on application of the Q-system support chart and, for road tunnels, based on the NPRA support diagram. The actual mode of operation and the possible loads they may be subjected to are however not well known. A measurement program was therefore designed to investigate deformations in the rock mass and strain in the RRS. In addition, rock mass quality was registered and stresses in the rock mass were measured.

Only small deformations were recorded in the rock mass and no substantial strain in the rebar in the RRS. Numerical modelling for evaluating the stress measurements indicated that the 3D values seemed to be too high and door stopper measurements in the roof were therefore used in further analysis. The final numerical modelling concluded that the RRS in this case was not subjected to any load and that together with the spiling bolts, they only had a rock-reinforcing effect and no load-bearing function.

5.1.2 Paper II: Main aspects of deformation and rock support in Norwegian road tunnels

Traditionally, the RRS were constructed by bending the rebar to follow the blasted tunnel profile after a thin smoothing layer of sprayed concrete was applied. Later, load-bearing RRS that form an arch were described and has become the common design used today. Following the use of this new design, there was an abrupt switch in rock support, from light rock reinforcement by bolt and sprayed concrete to heavier load-bearing structures, such as arched RRS.

This paper analyses the possibility of facilitating a smoother transition between the two rock support principles, rock reinforcement and support by load-bearing structures. International literature on the subject indicates that at a convergence of the tunnel at about 1%, there is a transition from the rock mass only needing to be reinforced, to needing to be supported by load-bearing structures.

The Q-system advises that spiling bolts should be considered for Q-values lower than 0.4 and the NPRA recommends spiling bolts for Q-values lower than 0.2. Both also uses the same respective limits for were one should start to use RRS for support. The limits for spiling bolts are based on experience and fit the data presented in the paper on the Frøya tunnel case.

The results of a numerical parameter study were compared to data extracted from the NPRA tunnel data base. This showed that most of the tunnelling was performed under conditions that only required rock reinforcement and that by far, most of the built RRS was used under conditions that probably do not require load-bearing support.

The above mentioned finding suggests that there is an interval between the limit for the use of RRS and the 1% convergence limit. In this interval, there is a need for more comprehensive support than bolts and sprayed concrete, but load-bearing support is not needed. In this interval, it is believed that the stability problems are mainly gravitational and related to weak rock masses and filled joints, and minor weakness zones and moderate swelling problems under favourable stress conditions. A possible support solution in such conditions may be the use of spiling bolts, including steel straps and radial bolts, and/or unarched RRS.

The aforementioned interval is limited by two factors that are not of the same scale, which makes the interval difficult to define. A possible solution is suggested wherein the GSI is mapped when the Q-value are below 0.4. The GSI value can be used with the rock properties, in-situ stresses and surrounding geology to assess if a load-bearing structure is needed.

5.1.3 Paper III: Experimental testing of swelling gouge materials

This paper describes triaxial testing of the reconstituted cores of swelling gouge material. The experiment setup was mainly designed to investigate the possible swelling pressure of such material, but secondly also to estimate the mechanical material properties. Additional tests were further performed, such as uniaxial testing of cores, the swelling pressure of the clay fraction using an oedometer and the density of "undisturbed" material.

Material was collected from four different weakness zones and fragments larger than 4 mm were removed. Dried material was compacted in a specially built compacter with a pressure of 26 or 34 MPa to create the cores. The density of the cores was in approximately the same range as the samples of "undisturbed" material. However, this is only one of many parameters possibly describing the in-situ material, and it is difficult to state exactly the resemblance between the cores and the in-situ material. Since both the reconstitution of cores and the testing was based on mostly new methods, a great deal of problems were encountered, though eight tests were performed successfully.

The triaxial test consisted of four phases:

1. *Pre-stress 1*
   The radial stress was increased to 2 MPa and the axial stress to 4 MPa. Either by simultaneously increasing the both or first increase both until 2 MPa and then the axial to 4 MPa.
2. *Water addition*
   Before water addition, the machine was set to keep the strain constant. If swelling occurred, the machine would then increase the axial and/or radial stresses to keep the strain constant. The pore pressure system, with some modifications, was used to wet the sample from outside and in, all along its length.

3. *Pre-stress 2*
   The stresses were set back to 2 MPa and 4 MPa.
4. *Failure*
   Both radial and axial stress were reduced by lowering the cell pressure to yield the material i.e. by moving the half circle in Fig. 4 to the left to hit the failure envelope.

The stress strain curves from the Pre-stress 1 and 2 phases were used to find the E-modules before and after saturation. For each test specimen it seems that the E-modules were lower for Pre-stress 2, than for Pre-stress 1. The difference between test specimens is in the same order as between phases, ranging between approximately 100 and 200 MPa. For both phases, the E-modulus were between 133 and 430 MPa.

To find the failure envelope from the failure phase, the software RocData (Rocscience Inc. 2015) was used. Some of the samples gave values that seemed too high and three outlier samples were removed for the sake of the reported data. The stress range was a bit narrow from a tunnelling perspective and small differences could have quite a significant impact on the output values. For Hoek-Brown, the σ_{ci} values were 0.8–1.1 MPa and the m_i values were 5.7–7.5. For Mohr-Coulomb, the cohesion was 0.29–0.34 MPa and the friction angle was 28.2–30.6°.

The water addition stage was dominated by creep in the material and no swelling was observed. It is assumed that this does not mean that swelling did not happen, but rather that the swelling was insignificant compared to other deformation processes and may also have increased the speed of these processes. In the oedometer tests of the fraction under 20 µm, medium and high swelling pressures were recorded, confirming that the materials actually contained swelling minerals.

5.1.4 Paper IV: Oedometer testing of swelling clay from gouge material with different water contents

The initial water content of the in-situ material is of great importance when evaluating problems related to swelling, since it may be a measure of how much of the possible swelling has already happened. To find a relative swelling pressure for swelling gouge material, the fraction < 20 µm can be tested in an oedometer. Usually, dry material is placed in the oedometer and pre-stressed by 2 MPa before the pressure is released and water is added to make the material swell with no possibility to expand.

In the tests reported in this paper, the material had a known initial water content before it was placed in the oedometer. Two different samples series were tested with seven individual samples for series one and eight for series two. Two samples were dry for each series and the rest had an increasing initial water content.

The initial short-term (0.5 to 1 day) behaviour during pre-stressing gave lower sample heights with increasing water content. This occurred until it seemed that all pores in the sample were filled with water, and the sample height increased. It may not be related, but this transition seemed to happen at approximately the same water content as the plastic limit. The long-term behaviour showed a slow decrease of the sample height due to drying and, by that reversal of the swelling, of the samples.

The pre-stressing process made the samples, with some exceptions, a decreased sample height with an increased initial water content. Plotting the swelling pressure with respect to the sample height indicated that the pressure is increasing with decreasing sample height.

Following this finding is the hypothesis that the swelling pressure is dependent on the density of the material.

After the swelling phase, sample series 2 performed a post swelling consolidation phase. The behaviour of the material in this stage suggests that one can find the water content for where the intracrystalline swelling is completed and the osmotic swelling starts. This is important since the rock stress in many cases exceeds the osmotic stress while it will not exceed the intracrystalline. Knowing this limit may enable one to anticipate, if the water content of the in-situ gouge is known, whether water may be absorbed, making the material swell, or forced out, making the material shrink.

5.2 Interrelations of individual papers

The papers in this thesis cover the main subjects cited in the title "Applicability of reinforced ribs of sprayed concrete in sections of poor quality and swelling rock mass" and the objectives given in the introduction.

The first paper evaluates the stabilizing effects of RRS in the Løren Tunnel. The paper concludes that under the given conditions, the RRS have no load-bearing function, but rather have a reinforcing effect on the rock mass. Since there was no load-bearing capacity, it was not possible to use the data for further capacity analysis, which was one of the options. Another path was pursued, and the subject for the next paper. This was the issue that for some rock mass qualities, based on experience, one needs to use stronger rock support than bolts and sprayed concrete and that, based on the results from Paper I, this support does not necessarily need to be load-bearing.

In Paper II, the above-mentioned path was followed by reviewing the literature to try to find the basis for which a rock mass needs to be supported, not only reinforced. The transition is related to squeezing theory and to associate this to hard rock tunnelling conditions, Norwegian road tunnels were used as a case study. Through numerical modelling, it was shown that even in poor rock masses, the stresses need to be unfavourable before there is a need for load-bearing constructions. The results indicate that squeezing may happen in hard rock tunnelling, but since the weak/poor rock usually appears as restricted zones/sections, the more solid side rock limits the effect.

Swelling, in the literature, is closely connected to squeezing and the two are considered interrelated processes. In Paper III, this theory was pursued, and a test was performed to see if it was possible to detect a swelling pressure from gouge material under in-situ and ideal (initially dry material) conditions. This was done to see if a build-up of swelling pressure could occur and if it could be significant when designing support.

In Paper IV, the issue that gouge material in-situ has an initial water content was pursued. This is important regardless of whether the swelling minerals exert pressure on a support construction or not, as it may facilitate other processes, such as creep and finally squeezing. Knowing if swelling is a factor or not, based on the water content, may make it easier to estimate the support as one more factor is accounted for.

6 Main conclusions

The character and material parameters of weakness zones comprise a significant span. From a deformation perspective, weakness zones with heavily jointed rock mass with no clay, via combined eroded rock fragments and clay, to massive clay zones, have a very large range. In addition, one has thinner clay-filled joints that may relieve large blocks and create gravity-driven problems or, under large rock stresses, give deformations/displacements.

Looking at the GSI chart, a disintegrated or heavily jointed rock mass with very good surface conditions would have a value between 40 and 50. In Paper II, a rock mass with these GSI values was given an E-modulus of about 3200–6150 MPa. In Paper III, the E-modulus of clayey material was found to be 133–430 MPa. Looking at Fig. 3, the potential for deformation, based on Hooke's law, between these types of weak rock masses is very large. In addition, the more the rock is altered, the more clay and swelling minerals it may contain and because of that, it may be more susceptible to time-dependent deformations.

The triaxial swelling tests showed no sign of a build-up of swelling pressure. The tests were performed on reconstituted cores in only one stress configuration, hence the results offer only a restricted comparison to in-situ conditions. However, since the rock masses containing swelling minerals are very weak, other processes related to strength and deformation may easily dominate the effect of swelling. The in-situ material will also have an initial water content that has already released some, or all, of the swelling potential. In addition, the stresses even around a tunnel at quite low overburdens may be at a magnitude where they are higher than the (osmotic) swelling pressure, limiting its possible influence.

In the triaxial tests, it seemed that the main deformation process was creep and that the swelling may have accelerated the process. Creep is a process that may lead to squeezing, and according to the literature, swelling and squeezing are interrelated phenomena. It is therefore believed that in looking at deformations associated with swelling gouge material, a large focus must be on the shear strength and the possibilities for creep, in addition to the swelling properties.

The study of the Løren tunnel data showed that no significant load was applied to the arched RRS and the parameter studies in Paper II showed that this will be the case for a large range of conditions. In this range, it is suggested that the design is changed from load-bearing arched RRS to reinforcing unarched RRS. To document both the stability for the individual project and to later evaluate the practice, thorough geological mapping is recommended, including Q-values and GSI, and that deformation monitoring with total stations is conducted. Further, it is suggested that more research be performed to investigate the effect of zone width, geological geometry, rock quality and in-situ stresses on deformation. A study on how to characterise weakness zones with respect to deformability that also examines the impact of heavy jointing, degraded rock fragments and clayey gouge should be conducted.

The papers included in this thesis have examined the use of RRS in poor quality rock mass and the processes associated to deformation of swelling gauge material. The findings may implicate that there is an interval between massive rock and poor quality rock mass, where the level of support as recommended in Norwegian guidelines may be excessive. It has also been found that according to present practice, the swelling properties of weakness zone materials are assigned too much consideration compared to other deformation properties.

References

Aksoy CO, Geniş M, Uyar Aldaş G, Özacar V, Özer SC, Yılmaz Ö (2012a) A comparative study of the determination of rock mass deformation modulus by using different empirical approaches. Eng Geol 131–132:19-28. doi:https://doi.org/10.1016/j.enggeo.2012.01.009

Aksoy CO, Ogul K, Topal I, Ozer SC, Ozacar V, Posluk E (2012b) Numerical modeling of non-deformable support in swelling and squeezing rock. International Journal of Rock Mechanics and Mining Sciences 52:61-70. doi:https://doi.org/10.1016/j.ijrmms.2012.02.008

Bane NOR (2018) Technical regulations. https://trv.jbv.no/wiki/Forside. Accessed 30.01.2018

Barla G, Bonini M, Semeraro M (2011) Analysis of the behaviour of a yield-control support system in squeezing rock. Tunnelling and Underground Space Technology 26 (1):146-154. doi:https://doi.org/10.1016/j.tust.2010.08.001

Barla M (1999) Tunnels in swelling ground: simulation of 3D stress paths by triaxial laboratory testing. Dissertation, Politecnico di Torino, Torino

Bellwald P (1990) A contribution to the design of tunnels in argillaceous rock. Dissertation, Massachusetts Institute of Technology, Cambridge

Brown ET, Hoek E (1978) Trends in relationships between measured in-situ stresses and depth. Int J Rock Mech Min 15 (4):211-215. doi:https://doi.org/10.1016/0148-9062(78)91227-5

Carranza-Torres C, Fairhurst C (1999) The elasto-plastic response of underground excavations in rock masses that satisfy the Hoek–Brown failure criterion. International Journal of Rock Mechanics and Mining Sciences 36 (6):777-809. doi:https://doi.org/10.1016/S0148-9062(99)00047-9

Crowder J, Bawden WF (2004) Review of Post-Peak Parameters and Behaviour of Rock Masses: Current Trends and Research. RocNews, vol 4. Rocscience Toronto

Duncan Fama M (1993) Numerical modelling of yield zones in weak rocks. In: Hudson JA (ed) Comprehensive rock engineering, vol 2. Pergamon, Oxford, pp 49-75

Einstein HH (1989) Design and Analysis of Underground Structures in Swelling and Squeezing Rocks. In: Sinha RS (ed) Developments in Geotechnical Engineering, vol 59. Elsevier, pp 203-262. doi:https://doi.org/10.1016/B978-0-444-87462-7.50013-X

Einstein HH (1996) Tunnelling in difficult ground - Swelling behaviour and identification of swelling rocks. Rock Mech Rock Eng 29 (3):113-124. doi:https://doi.org/10.1007/bf01032649

Google Maps (2018) 3D image of landscape with weakness zones in southeastern Norway. maps.google.com, https://www.google.no/maps/@58.9080525,6.5266178,6696a,35y,180h,38.01t/data=!3m1!1e3

Grimstad E, Kankes K, Bhasin R, Magnussen AW, Kaynia AM (2002) Rock mass quality used in designing reinforced ribs of sprayed concrete and energy absorption. Bergmekanikkdagen, Oslo, November 21-22

Grimstad E, Tunbridge L, Bhasin R, Aarset A (2008) Measurements of deformation and forces in reinforced ribs of sprayed concret. Why do we use cast concrete lining when ribs of sprayed concrete have a large margin? Bergmekanikkdagen, Oslo, November 20-21

Herget G (1988) Stresses in rock. Balkema, Rotterdam

Hoek E (1994) Strength of rock and rock masses. ISRM News Journal 2 (2):12

Hoek E (1999) Support for very weak rock associated with faults and shear zones. International Symposium on Rock Support and Reinforcement Practice in Mining, Kalgoorlie, Australia, March 14-19

Hoek E (2001) Big tunnels in bad rock. J Geotech Geoenviron 127 (9):726-740. doi:https://doi.org/10.1061/(ASCE)1090-0241(2001)127:9(726)

Hoek E (2006) Practical Rock Engineering. www.rocscience.com

Hoek E, Brown ET (1980) Empirical Strength Criterion for Rock Masses. Journal of the Geotechnical Engineering Division 106 (9):1013-1035

Hoek E, Carranza-Torres C, Corkum B (2002) Hoek-Brown Failure Criterion – 2002 Edition NARMS-TAC Conference, Toronto, July 7-10

Hoek E, Carter T, Diederichs M (2013) Quantification of the Geological Strength Index Chart. 47th US Rock Mechanics / Geomechanics Symposium, San Francisco, June 23-26
Hoek E, Diederichs MS (2006) Empirical estimation of rock mass modulus. International Journal of Rock Mechanics and Mining Sciences 43 (2):203-215. doi:http://doi.org/10.1016/j.ijrmms.2005.06.005
Hoek E, Kaiser PK, Bawden WF (1997) Support of underground excavations in hard rock. 3rd edn. A.A. Balkema, Rotterdam
Hoek E, Marinos P (2000) Predicting tunnel squeezing problems in weak heterogeneous rock masses. Tunnels & Tunnelling International vol November and December 2000. Polygon Media Ltd, London
Holmøy KH, Aagaard B (2002) Spiling bolts and reinforced ribs of sprayed concrete replace concrete lining. Tunnelling and Underground Space Technology 17 (4):403-413. doi:https://doi.org/10.1016/S0886-7798(02)00065-2
ISRM (1978) Suggested methods for the quantitative description of discontinuities in rock masses. Int J Rock Mech Min 15 (6):319-368. doi:https://doi.org/10.1016/0148-9062(78)91472-9
Kraehenbuehl F, Stoeckli HF, Brunner F, Kahr G, Müller-Vonmoos M (1987) Study of the water-bentonite system by vapour adsorption, immersion calorimetry and X-ray techniques; I, Micropore volumes and internal surface areas, following Dubinin's theory. Clay Miner 22 (1):1-9. doi:https://doi.org/10.1180/claymin.1987.022.1.01
Laird DA (2006) Influence of layer charge on swelling of smectites. Appl Clay Sci 34 (1):74-87. doi:https://doi.org/10.1016/j.clay.2006.01.009
Madsen FT, Müller-Vonmoos M (1989) The swelling behaviour of clays. Appl Clay Sci 4 (2):143-156. doi:https://doi.org/10.1016/0169-1317(89)90005-7
Mao D, Nilsen B, Lu M (2011) Analysis of loading effects on reinforced shotcrete ribs caused by weakness zone containing swelling clay. Tunnelling and Underground Space Technology 26 (3):472-480. doi:https://doi.org/10.1016/j.tust.2011.01.004
Myrvang AM (1993) Rock Stress and Rock Stress Problems in Norway. In: HUDSON JA (ed) Rock Testing and Site Characterization. Pergamon, Oxford, pp 461-471. doi:https://doi.org/10.1016/B978-0-08-042066-0.50025-2
Myrvang AM (2001) Bergmekanikk. Norwegian University of Science and Technology, Department of Geology and Mineral Resources Engineering, Trondheim
NFF (2008) Tung bergsikring i undergrunnsanlegg. Håndbok, vol 5. Norsk forening for fjellsprengningsteknikk, Oslo
NGI (2015) Using the Q-system - Rock mass classification and support design. Handbook. Norwegian Geotechnical Institute, Oslo
NGU (2018) Geological overview of Norway. https://www.ngu.no/emne/berggrunn
Nilsen B (2016) Reliability of swelling pressure testing for tunnel support evaluation. ITA-AITES World Tunnel Congress 2016, San Francisco, April 22-28
Nilsen B, Palmstrøm A (2000) Engineering geology and rock engineering, vol no. 2. Handbook (Norwegian Group for Rock Mechanics). Norwegian Group for Rock Mechanics, Oslo
Palmstrom A, Stille H (2007) Ground behaviour and rock engineering tools for underground excavations. Tunnelling and Underground Space Technology 22 (4):363-376. doi:https://doi.org/10.1016/j.tust.2006.03.006
Palmström A, Singh R (2001) The deformation modulus of rock masses — comparisons between in situ tests and indirect estimates. Tunnelling and Underground Space Technology 16 (2):115-131. doi:https://doi.org/10.1016/S0886-7798(01)00038-4
Pedersen KB, Kompen R, Kveen AT (2010) Arbeider foran stuff og stabilitetssikring i vegtunneler. Teknologirapport. Norwegian Public Roads Administration, Oslo
Rocscience Inc. (2015) RocData. vol 5.003, 5.006 edn. Rocscience Inc., Toronto
Sakurai S (1981) Direct Strain Evaluation Technique In Construction Of Underground Opening. The 22nd U.S. Symposium on Rock Mechanics (USRMS), Cambridge, Massachusetts, June 29 - July 2
Sakurai S (1983) Displacement Measurements Associated With The Design Of Underground Openings. International Symposium on Field Measurements in Geomechanics, Zurich, September 5-8

Schwingenschloegl R, Lehmann C (2009) Swelling rock behaviour in a tunnel: NATM-support vs. Q-support – A comparison. Tunnelling and Underground Space Technology 24 (3):356-362. doi:https://doi.org/10.1016/j.tust.2008.08.007
Selmer-Olsen R (1980) Ingeniørgeologi: Generell geologi, vol 1. 3rd edn. Tapir, Trondheim
Sheorey PR (1994) A theory for In Situ stresses in isotropic and transverseley isotropic rock. Int J Rock Mech Min 31 (1):23-34. doi:https://doi.org/10.1016/0148-9062(94)92312-4
SINTEF (2016) Rock mechanic properties of rocks tested in Sintef Rock mechanics laboratory.
Statens vegvesen (2016a) Tunnelveiledning. V520. Oslo
Statens vegvesen (2016b) Vegtunneler. N500. Oslo
Terzaghi K, Peck RB (1967) Soil mechanics in engineering practice. 2nd edn. Wiley, New York
Weil RR, Brady NC (2017) The Nature and Properties of Soils. 15th edn. Pearson, Boston

Paper I

Bulletin of Engineering Geology and the Environment
https://doi.org/10.1007/s10064-018-1238-1

ORIGINAL PAPER

Analysis of the stabilising effect of ribs of reinforced sprayed concrete (RRS) in the Løren road tunnel

Are Håvard Høien[1,2] · Bjørn Nilsen[1]

Received: 20 June 2017 / Accepted: 29 January 2018

Abstract
The Løren tunnel is a road tunnel at Ring road 3 in Oslo, Norway. The tunnel has a length of 915 m in rock, has two tubes with three lanes and breakdown fields, and was first opened in 2013. For rock support in the case of weak rock masses, ribs of reinforced sprayed concrete (RRS) were used. The scope of this article is to present and analyse the results of a measurement programme carried out on three of these ribs. This is done by focusing on deformations in the rock and the support function of the ribs due to these deformations. The instrumented RRS had strain meters installed in the reinforcement and the concrete. From the surface above the RRS, multipoint borehole extensometers were placed to survey the soil and rock mass deformations caused by tunnel advancement. In addition, 2D and 3D rock stress measurements and rock property testing were conducted. The measurements and numerical modelling show that the deformations are too small to cause a considerable load on the installed support construction and that the 2D stress measurements seem to best fit the in-situ stress conditions. The rock mass quality in the area of this study is on the verge of where one usually starts using reinforced ribs. It is concluded that the RRS are not required because of deformations in the rock but, rather, because of the need to lock blocks, increase the friction in joints and prevent movement in larger filled joints. For this purpose, the RRS should probably be designed differently to get the most out of the materials used.

Keywords Rock support · Ribs of reinforced sprayed concrete (RRS) · Displacement monitoring · Support design

Introduction

To create stable and durable underground openings, reinforcement and support of the rock mass is required. The needed reinforcement and support vary greatly, from almost none in good-quality rock mass with favourable stress conditions to massive support in poor and swelling masses with unfavourable stress conditions.

The rock support in weak rock masses follows different traditions around the world. For instance, in the Alpine countries, rigid systems with deformable elements are common (Aksoy et al. 2012; Schwingenschloegl and Lehmann 2009), while the Norwegian tradition is to use lean support, which improves the self-bearing capacity of the rock mass (Norsk Forening for Fjellsprengningsteknikk, NFF 2008).

The more rigid systems include steel beams with parts that deform at a certain load, together with rock bolts, reinforcing mesh and sprayed concrete between the beams (Barla et al. 2011). In Norway today, a system of rebar-reinforced ribs of sprayed concrete (RRS) is the preferred choice for rock support in weak and swelling rock mass. These RRS are used in combination with spiling bolts, radial rock bolts and sprayed concrete as an integrated part of the excavation process (NFF 2008). The current practice regarding the use of ribs is largely based on experience and empiricism.

The Norwegian Geotechnical Institute (NGI) and Norwegian University of Science and Technology (NTNU) have performed research related to the performance of RRS. The NGI has applied numerical modelling to develop dimensioning rules (Grimstad et al. 2002) and calculated loads based on the in-situ monitoring in the Finnfast road and Bærum railway tunnels (Grimstad et al. 2008). These dimensioning rules have been incorporated in the rock support chart of the

✉ Are Håvard Høien
are.hoien@vegvesen.no

[1] Norwegian University of Science and Technology, Sem Sælands veg 1, 7491 Trondheim, Norway

[2] Norwegian Public Roads Administration, Postboks 8142 Dep, 0033 Oslo, Norway

Published online: 10 February 2018

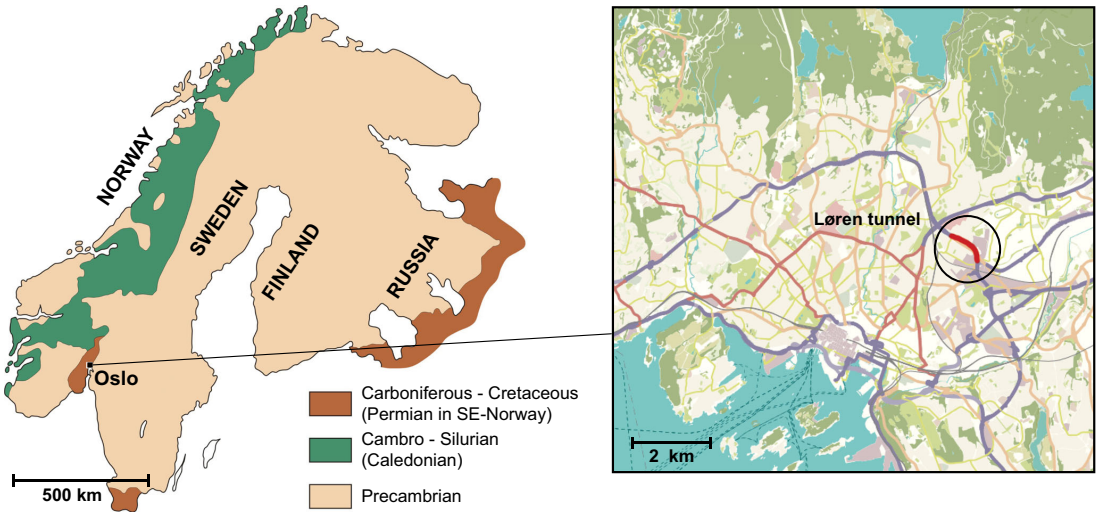

Fig. 1 Location of Oslo and the Løren tunnel in the Scandinavian regional geology

rock mass quality classification and support design system—the NGI Q-system (NGI 2013). The monitoring data from the Finnfast tunnel have also been studied at the NTNU by Mao et al. (2011), who used a 3D numerical model to analyse the loading effects of swelling rock on RRS.

However, to fully understand the mode of operation of the RRS concept, more monitoring, analysis and documentation are required. As a contribution to this, testing of rock mass properties and monitoring of the RRS at the Løren tunnel project have been done and will be described in this article.

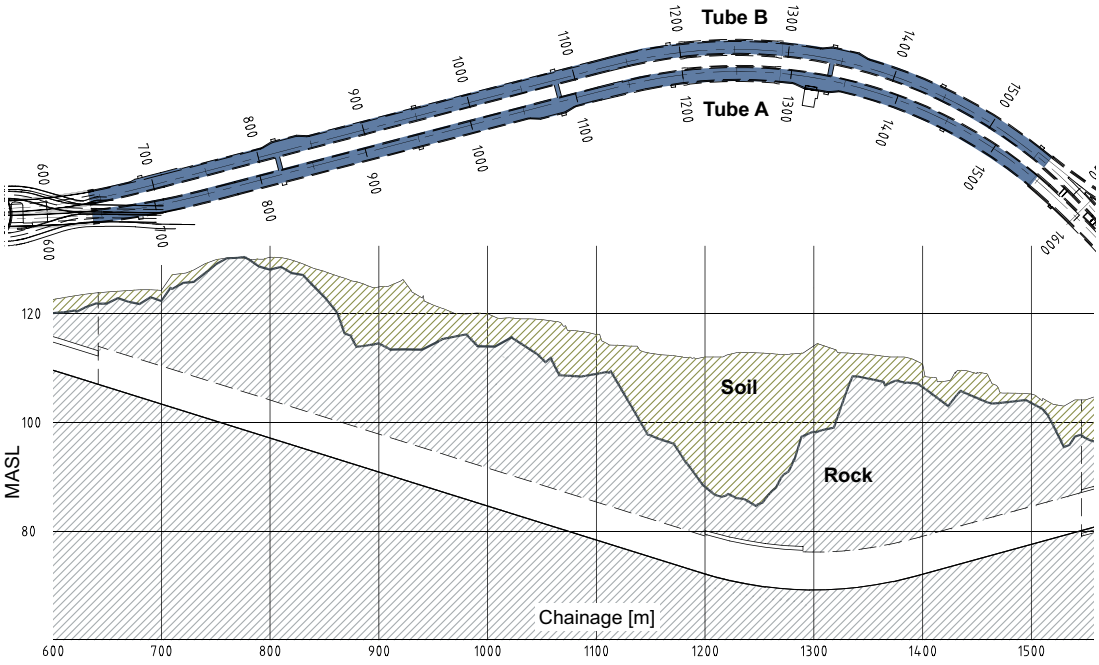

Fig. 2 Plan view and longitudinal profile of the Løren road tunnel

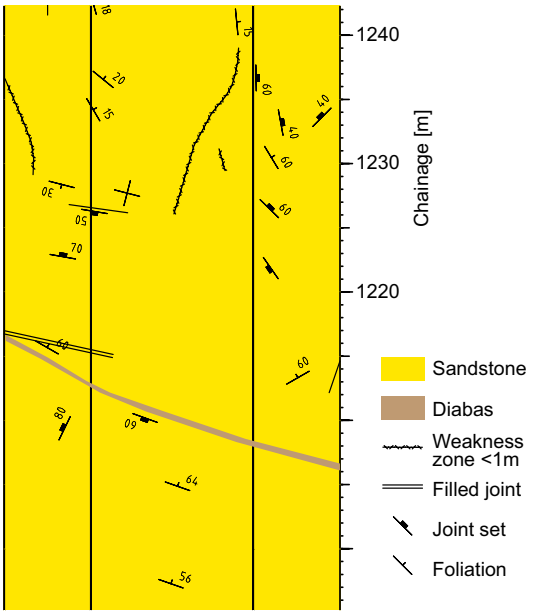

Fig. 3 Geology of tube B, mapped during excavation. The map is drawn as a fold-out tunnel profile. For more details, see Høien and Nilsen (2014)

The results have been used as input in a two-step numerical analysis.

Description of the Løren tunnel

The Løren tunnel is a 915-m road tunnel located in Oslo, Norway (see Fig. 1). The tunnel was excavated from one end by drilling and blasting technique and continuous grouting. It has two tubes with three lanes and emergency stop fields, which results in tunnel widths of 13–16 m and face areas of 105–135 m^2. Tube B was excavated approximately 30 m ahead of tube A on descending profile numbers (see Fig. 2). Above the tunnel, there is a mix of residential and commercial buildings founded on soft, sensitive clay and sandy, gravelly soil with a thickness of up to 30 m. The tunnel opened for traffic in 2013.

During the excavation of the tunnel, its geology was mapped (Fig. 3) and a Q-value was estimated after each blast by an engineering geologist. The geological information was compiled in the tunnel documentation software Novapoint Tunnel (Vianova Systems 2011) using a fold-out tunnel profile (Humstad et al. 2012). A geological longitudinal section map, as shown in Fig. 4, was created based on this mapping and the pre-construction investigations. The rock types mapped in the tunnel were sandstones, calcareous shale, black shale, nodular limestone and intrusions of rhomb-porphyry, diabase and syenite. The intrusive rock is of Carboniferous–Permian age and the folding is a result of the Caledonian orogeny. The Caledonian orogeny is found from Scotland to the Norwegian mainland and up to Svalbard. The folded rock was deposited during the Cambrian Period (Oftedahl 1981).

Monitoring and testing methodologies

In the following, the methodology and layout for testing and monitoring in the Løren tunnel will be described. It should be noted that the methodology, including the setup of the extensometer and RRS monitoring, was very similar to that used in the Bærum and Finnfast tunnels (Grimstad et al. 2008), as referred to in the Introduction.

Extensometers from the surface

Three Geokon multipoint borehole extensometers (MPBX), each with three groutable anchors, were installed from the surface by the NGI, which also provided the resulting monitoring data (see Fig. 5). At chainage 1220, one extensometer was installed above each tunnel tube, and at chainage 1030, one extensometer was installed above tube B. Table 1 shows the depths of the anchors. Anchor 1 was intended to be placed in the rock just beneath the soil/rock transition. Anchor 3 was placed just above the tunnel roof. As an example, the extensometer setup and the setup for rib measurement described in the next section are shown for B1220 in Fig. 6.

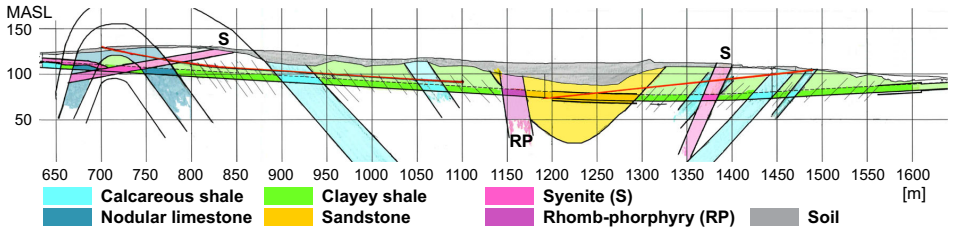

Fig. 4 Longitudinal profile illustrating the rock type distributions and structural geology (Iversen 2011)

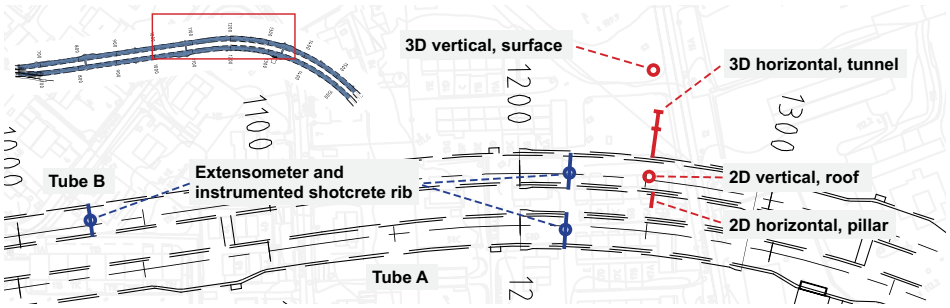

Fig. 5 Locations of extensometers, instrumented ribs of reinforced sprayed concrete (RRS) and rock stress measurements

At the surface, the extensometer had a metal head with three holes for measuring deformations. The measurements were conducted with a clock-gauge caliper, which was calibrated before and after each extensometer reading. Three measurements were performed for each anchor and an average of the three values was used in the resulting graphs.

Monitoring of the RRS

To measure the load on the ribs, instruments were mounted on the rebar before sprayed concrete was applied (see Fig. 7). The rebar in the rib was 20 mm in diameter and placed with a centre-to-centre (c/c) spacing of approximately 100 mm. One concrete strain meter and one rebar strain meter were placed in pairs at five locations along the tunnel profile, as illustrated in Fig. 6. Both instruments used vibrating wires to measure the strain and had a built-in gauge for temperature correction. The stresses for the steel were calculated from the monitored strain based on using a deformation modulus of 200 GPa.

In the Finnfast and Bærum tunnels, pressure cells were installed in an attempt to measure the support pressure and ring pressure in the RRS. This was discarded in this case because of the unreliable results experienced at Finnfast and Bærum (Grimstad et al. 2008) and problems with applying the sprayed concrete without creating cavities. If larger deformations and loads are expected and the cells are sprayed before the mounting of the rebars in the RRS, such instrumentation will likely provide very interesting data.

Table 1 Anchor depths (depth below surface) for the extensometers

	B1220	A1220	B1030
Soil/rock	22.5 m	26 m	7.5 m
Anchor 1	24 m	28 m	18 m
Anchor 2	29 m	32 m	23 m
Anchor 3	30 m	33 m	24 m

Rock stress measurements

In-situ stresses have been measured based on three principles: 2D doorstopper overcoring in the pillar and roof, 3D overcoring inside the tunnel and 3D overcoring from the surface. The locations of the different measurement holes are shown in Fig. 5.

Overcoring measurement is performed by drilling a hole, gluing strain gauges to its walls and then overcoring this first hole with the strain gauges inside. The strain from the expansion of the rock is then used, together with the material parameters, to calculate the stress to which the rock was originally exposed (Kim and Franklin 1987). The stress measurements from the surface were performed by Pöyry SwedPower

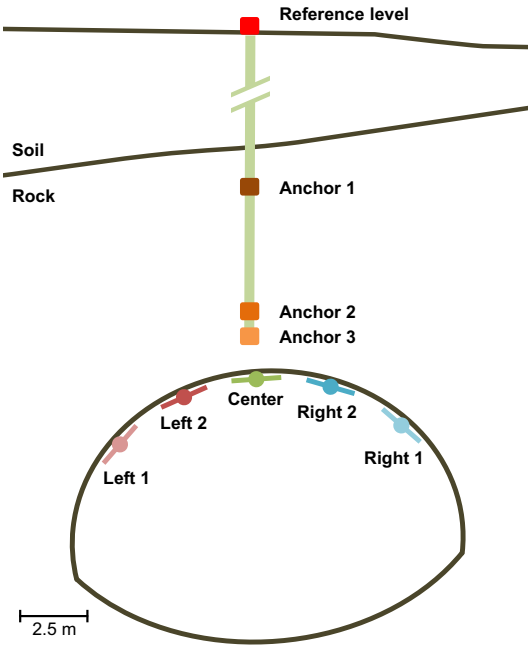

Fig. 6 Extensometer and strain measurement setup at chainage B1220

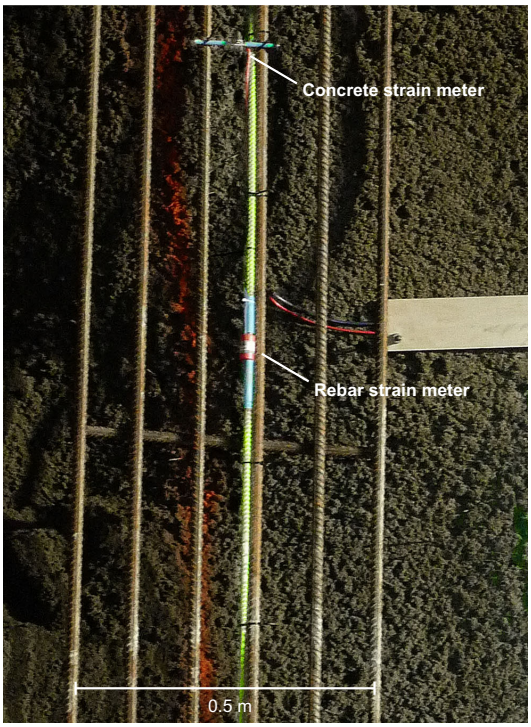

Fig. 7 Concrete and rebar strain meters mounted on the rib before the application of sprayed concrete

AB, and those from the tunnel were performed by SINTEF. For more information about the specific methods used, reference is made to Sjöberg and Klasson (2003) and Larsen and Trinh (2014), respectively.

For the surface measurement, an 86-m hole was drilled. An attempt was made to measure at depths of 58.9, 60.6 and 65.3 m, but due to there being too many joints, no measurements were successful.

The 3D measurements in the tunnel were performed between 12.5 and 18 m from the tunnel wall, and five of these measurements were successful. The software program DISO (Determination of In-situ Stress by Overcoring) was used to calculate the stress and validate the measurements (Larsen 2010).

The 2D doorstopper overcoring was also carried out by SINTEF. This method provides the stress for the plane perpendicular to the borehole and can be used for measurements up to 10 m from the tunnel contour. One measuring series usually consists of seven to ten measurements and requires about 1.5 days to complete (Larsen and Trinh 2014). Based on this method, five measurements were performed in the tunnel roof at 1–3.5 m into the borehole, and seven measurements were performed in the pillar at 0.8–4.1 m into the borehole (Larsen 2010).

Results of testing and monitoring during tunnelling

Rock mass properties

The rock mass parameters based on the testing of samples from holes for rock stress measurement and core drilling are presented in Table 2. There are generally four types of rock in the area: sandstone, syenite, rhomb-porphyry and diabase. Sandstone normally has a lower strength than the other rocks, which are intrusive. Considering the strength values and geological mapping, the 3D stress measurements were performed in syenite and the 2D measurements were performed in sandstone. The rock from the core hole is described in the core log (Haug et al. 2007) as sandstone for chainages 1010–1012 and shale for chainages 1217–1223.

For the cores related to 3D stress measurement, point load tests were also performed, indicating a compressive strength of 221 MPa and a tensile strength of 13 MPa. The large variations seen in some of the values in Table 2 may be due to anisotropy caused by testing parallel with the folded but still visible bedding planes (CH 1010–1012 and 2D hsm) and petrographic variations (3D sm).

Table 2 Material parameters for the rock from the core hole (CH), the hole for 3D stress measurement (3D sm), the hole for 2D horizontal stress measurement in the pillar (2D hsm) and the hole for 2D vertical stress measurement in the tunnel roof (2D vsm)

	Rock type	UCS (MPa)	No.	E-modulus (GPa)	No.	Poisson's ratio	No.	Density (kg/m^3)	No.
CH 1010–1012	Shale	na[b]	4	37.6	2	0.170	1	2741 ± 17.3	4
CH 1217–1223	Sandstone	80.6 ± 16.0	4	42.6 ± 17.2	4	0.155 ± 0.013	4	2753 ± 208.9	4
3D sm	Sandstone/syenite[a]	146.1 ± 45.89	4	56.0 ± 10.56	4	0.185 ± 0.051	4	2795 ± 161.8	4
2D hsm	Sandstone	62.2	2	44.8 ± 14.57	4	0.120	2	2682	2
2D vsm	Sandstone	29.0	2	37.0	2	0.210	1	2693	2

[a] Exact rock type not recorded

[b] Not given due to inconsistent testing values

Table 3 Rock mass quality from mapping during tunnel excavation. The rock type is sandstone with a thin diabase dyke crossing between chainages 1200 and 1215

From chainage	To chainage	Rock class	Q-value	RQD	J_n	J_r	J_a	J_w	SRF
A1204	A1208	D	1.2	50	6	1.5	4	1	2.5
A1208	A1211	D	3.1	62.5	6	1.5	2	1	2.5
A1210	A1215	D	1.2	50	6	1.5	4	1	2.5
A1215	A1219	E	0.56	45	12	1.5	4	1	2.5
A1219	A1222	D	2.5	50	6	1.5	2	1	2.5
A1222	A1225	D	3.1	62.5	6	1.5	2	1	2.5
A1225	A1228	D	1	60	12	1.5	3	1	2.5
A1228	A1208	E	0.83	50	12	1.5	3	1	2.5
B1203	B1210	D	1.6	70	6	1	3	1	2.5
B1210	B1214	C	4.1	82.5	6	1.5	2	1	2.5
B1214	B1219	C	7.8	62.5	4	1.5	2	1	1.5
B1219	B1222	D	1	62.5	12	1	2	1	2.5
B1222	B1226	E	0.16	37.5	12	0.5	4	1	2.5
B1226	B1229	E	0.62	50	12	1.5	4	1	2.5
B1229	B1232	E	0.42	50	12	1	4	1	2.5

The rock mass quality based on mapping during excavation and core logging is presented in Tables 3 and 4. As shown, the resulting Q-values range from fair (C) to very poor (E). The difference in RQD values between the tunnel mapping and the core mapping is likely primarily due to blast damage and the angle between the core hole and the joint sets. In the further use of these data in the numerical model, great emphasis has been placed on selecting values that are representative of the rock mass of the respective area as a whole.

Displacements monitored by extensometers

The results of the displacement monitoring are shown in Figs. 8, 9 and 10, with values above 0 (black font) indicating upward movement and values below 0 (red font in parentheses) indicating downward movement in millimetres. Because of an uplift of the terrain between 1 and 2 cm, which was caused by the rock mass grouting, the values had to be corrected for the movement of the head of the extensometer before identifying the deformations caused by the advancement of the tunnel faces. The displacement of the head in the figures is shown as the "Reference level".

In the charts, the distance from the MPBX is that from the far end of the holes. For B1220 and A1220, all grouting holes that may have influenced the rock mass in the area of the extensometers have a length of 15 m, with the packer placed 3 m into the hole, and a planned end pressure of 60 bar. For more details regarding the rock mass grouting, see Høien and Nilsen (2014).

MPBX B1220

Tunnelling past the extensometer took place between 04.03.2010 and 17.03.2010, and the four observations made during this period were probably not influenced by the rock mass grouting. The readings are presented in Fig. 8. On 04.03.2010, the face was at chainage B1221.

In this period, a small rise can be observed from the first observation to the second observation. From this highest point to the fourth point, anchor 3 has been lowered 2.39 mm. At the fourth point, the tunnel has passed the extensometer by 20 m. The relative expansion between anchors 1 and 3 during the period is 1.61 mm.

Table 4 Rock mass quality from the logging of cores from probe drilling (Iversen and Kveen 2007). The core hole is sub-horizontal, and the rock and soil cover is approximately 70 m at these chainages, which places it close to the sole of the tunnel. The rock type is sandstone

From chainage	To chainage	Rock class	Q-value	RQD	J_n	J_r	J_a	J_w	SRF
1217	1218	B	198	90	3	2	2	0.66	1
1218	1219	B	20.9	95	3	2	2	0.66	1
1219	1220	B	13.33	80	3	2	2	0.5	1
1220	1221	B	14.17	85	3	2	2	0.5	1
1221	1222	B	16.67	100	3	2	2	0.5	1
1222	1223	B	17.6	80	3	2	2	0.66	1
1223	1224	B	19.8	90	3	2	2	0.66	1

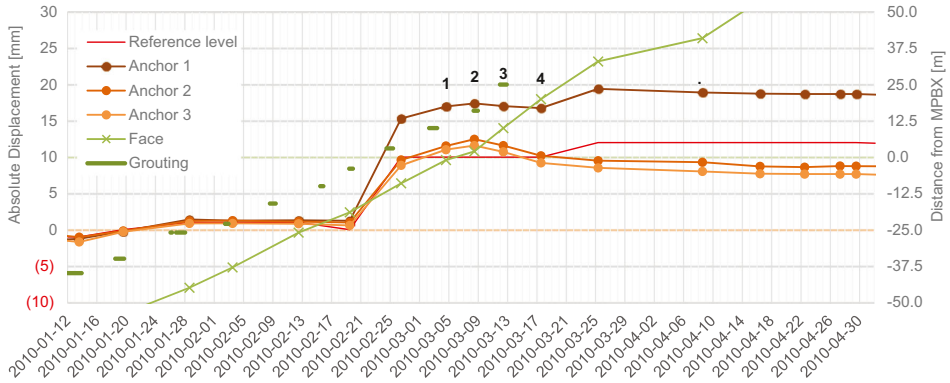

Fig. 8 Absolute displacement for the extensometer in tube B at chainage B1220. The numbers are the observations mentioned in the text

Between 17.03.2010 and 25.03.2010, for anchor 1, a lift of several millimetres can be observed. This corresponds to the dates for the rock mass grouting of tube A.

MPBX A1220

Tunnelling past the extensometer took place from 25.03.2010 to 22.04.2010. The first of the four observations during the period may have been influenced by the rock mass grouting performed on 26.03.2010. Two blast rounds were performed between the first and second observations and, because of this, there might have been a small peak if more measurements had been carried out.

From 08.04.2010 (observation 2) to 22.04.2010 (observation 4), there was a lowering of anchor 3 by 2.16 mm, and the face was 25 m past the extensometer. Note that the line for anchor 3 is above that for anchor 2 in the figure. The relative expansion between anchors 1 and 3 during this period was 2.07 mm.

MPBX B1030

Tunnelling past the extensometer, at chainages B1039 to B1011, was carried out from 01.07.2010 to 10.08.2010. During this period, there was a stop at A1030 for 3–4 weeks due to summer vacation. The excavation of chainages A1030 to A1027 was carried out on 03.08.2010. Before this blast round, an extra grouting cycle with 15-m holes was conducted. In addition, anchor 3 was exposed and broken during blasting. It is, therefore, not possible to determine whether any deformation occurred during the tunnelling towards the extensometer, and only minor deformations were recorded after the tunnel passed.

Strain measurements in the RRS

The strain measurements for the rebar are presented in Figs. 11, 12 and 13. In the figures, 100 μS is equal to 20 MPa in the steel, which, again, gives a load of 6.3 kN in the rebar.

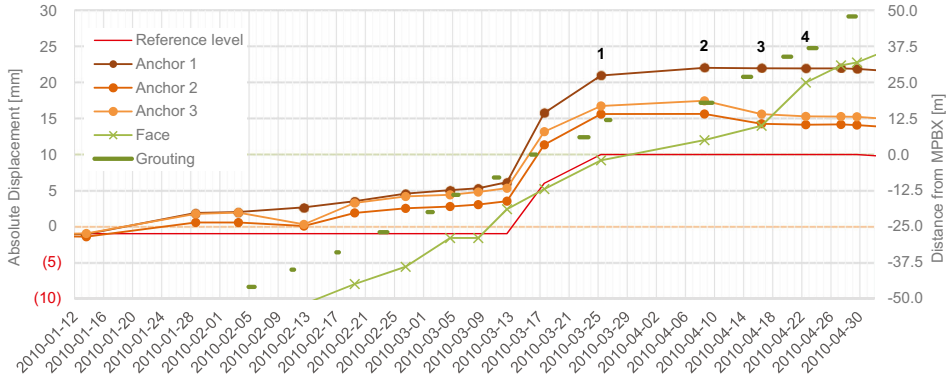

Fig. 9 Absolute displacement for the extensometer in tube A at chainage A1220. The numbers are the observations mentioned in the text

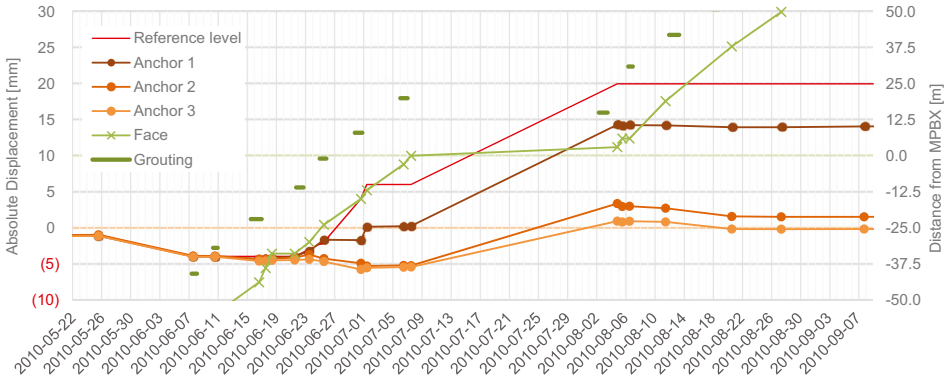

Fig. 10 Absolute displacement for the extensometer in tube B at chainage B1030. The numbers are observations mentioned in the text

Negative values are compression and positive values are tension. The rebar in the ribs is Ø20 mm B500NC, which has a yield strength of 500 MPa. The position of the strain gauges is shown in Fig. 6.

According to Pedersen et al. (2010), sprayed concrete has a drying shrinkage of 0.8–1.2 ‰. Related to Figs. 11, 12 and 13, this corresponds to − 800 to − 1200 µS. The drying shrinkage is time-dependent and dependent on the relative humidity (Standard Norge 2008). Due to uncertainty regarding the size of the shrinkage, the data in the figures are not corrected for this. For a tunnel with a width of 10 m, a drying shrinkage of 1.0 ‰ for an unrestrained arch will give a reduction in diameter of approximately 10 mm. Because the rebar is embedded in and coupled to the concrete through a chemical and mechanical bond, the stiffness of the rebar will create a force that counteracts the concrete shrinkage, which results in a strain in the rebar and the cracking of the concrete. Rebar strain from concrete shrinkage will be negative where it is embedded in concrete and positive in and close to the cracks (Gilbert 2001). Other restraints from, e.g. bolts and irregular rock surfaces will also reduce the drying shrinkage.

Rock stress measurements

The measured stresses are generally much higher than what is induced by gravity. This is, however, as expected in this region and, according to Myrvang (2001), this may be caused by folding of the rock, erosion of overlaying rock masses and/or plate tectonics. Myrvang also states that the cooling of igneous rock may create local compressive and tension stresses in the rock mass.

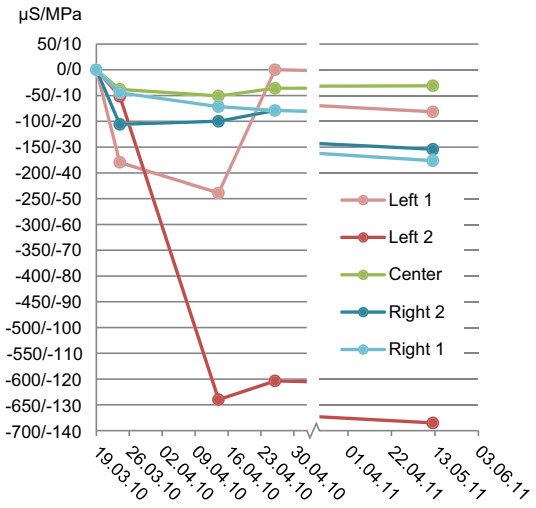

Fig. 11 Rebar strain in the RRS at B1220

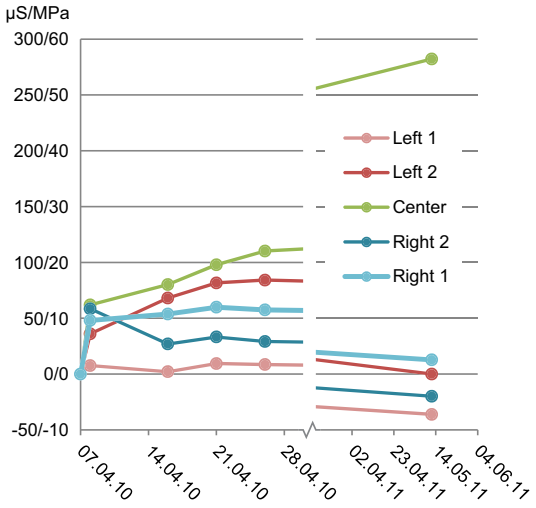

Fig. 12 Rebar strain in the RRS at A1220

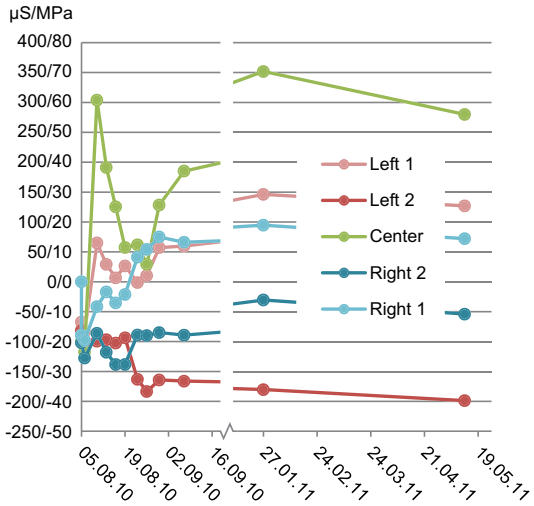

Fig. 13 Rebar strain in the RRS at B1028

3D overcoring

The results of the 3D overcoring carried out by SINTEF (Larsen 2010) show that the major principal stress is 13.6 MPa, horizontal and perpendicular to the tunnel axis. The minor principal stress is 2.2 MPa, with an orientation parallel to the tunnel axis and a 43° dip to the NW. Both have a margin of error of approximately ± 3 MPa. For more details, see Fig. 14 and Table 5. The test report states that there are substantial tectonic/geologic stresses in the area and that these stresses are at a level that may cause stress-induced cracks (Larsen 2010).

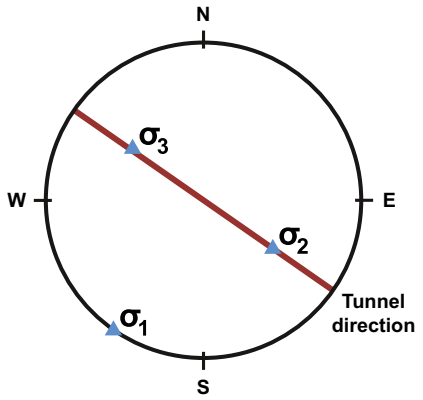

Fig. 14 Pole plot showing the directions of principal stresses based on 3D stress measurements in the tunnel wall (Larsen 2010). (Equal area projection, lower hemisphere)

2D overcoring

The stresses measured in the pillar and the tunnel roof are presented in Tables 6 and 7, respectively. Tunnel geometry control scanning showed that the width of the pillar in this area was slightly above 7 m.

The pillar hole was drilled halfway through and had a peak at about 3 m into the hole before beginning to decrease towards the middle. Theoretically, the stress should be highest at the pillar wall and decrease towards the middle. According to Myrvang (2001), fracturing from blasting in the pillar wall will move the stress peak towards the middle, as was observed in this case, and this is probably the reason for the discrepancy. As for the pillar hole, the roof hole showed increasing stresses from the contour.

As seen in Tables 6 and 7, the stresses vary quite a bit, which may be because the hole is perpendicular to the bedding.

Numerical modelling

To evaluate the measured data and the installed rock support, two-step numerical modelling has been performed. In the first step, the stress measurements are evaluated using two stress configurations (SC1 and SC2). As a second step, the most probable stresses found in the first step are used to investigate loads on and deformations of the RRS.

The 2D finite element software program RS^2 (also known as Phase2 9.0) was used (Rocscience Inc. 2016).

Model description

Numerical modelling was carried out for the cross-section at chainage 1220 (see Fig. 15). The geometry of the model is based on topographical data, borehole data, plan drawings and tunnel scanning. The tunnel profile has been extended by 1 m relative to the theoretical blasting profile to fit the real geometry as shown by the scanning data.

The boundary conditions are open at the top, restrained in the x direction at the sides and fixed at the bottom. Before the tunnel is "excavated", the model has a reference stage to zero out the deformations due to the settling of the model.

The constitutive models used are Mohr–Coulomb and Generalised Hoek–Brown for the soil and rock, respectively.

To simulate the blast damage zone, the model includes three 0.3-m-thick "rings" around the tunnel tubes, with an increasing amount of blast damage towards the tunnel periphery (see Table 9), resulting in a blast damage zone of 0.9 m.

Table 5 Stresses from 3D stress measurements performed in the tunnel wall (Larsen 2010)

	Stress (MPa)	Global direction	Direction relative to tunnel
σ1	13.6 ± 2.8	215.5/0	89.5
σ2	5.0 ± 1.3	124/47	359
σ3	2.2 ± 3.2	307/43	178
σv	3.70		
σh (min)	3.46	125.7	
σh (max)	13.54	35.7	
Tunnel		125	

Input parameters for rock mass and soil

As input parameters for the rock mass, data from core hole logging and continuous geological mapping during the tunnel excavation were used. All rock testing was performed according to the International Society for Rock Mechanics (ISRM) suggested methods (ISRM 2007). For the core drilling, data from chainages 1217–1223 and the 2D doorstopper stress measurement (see the rock mass properties section of Table 2) were used to calculate the mean. The Q-value parameters were determined mainly based on the tunnel mapping (see the rock mass properties section of Tables 3 and 4). These data were then used to calculate the rock mass properties in RocData (Rocscience Inc. 2015) by adjusting for rock mass quality based on the Geological Strength Index (GSI) and blast damage. The GSI was not systematically mapped in the tunnel (like Q-values) and, therefore, it has been calculated from RQD, J_r and J_a using the following equation (Hoek et al. 2013):

$$GSI = \frac{52\ J_r/J_a}{(1 + J_r/J_a)} + RQD/2 \quad (1)$$

Tunnel blasting was performed with a reduced charge at the perimeter and the second row, but substantial damage to the tunnel contour was still registered. To include the effect of blast damage on the rock, the material parameters for sandstone have been calculated with D-values of 0, 0.2, 0.4 and 0.6 (Hoek and Diederichs 2006).

The Q-value for the sandstone in the area is 1.4; (RQD/J_n) * (J_r/J_a) * (J_w/SRF) = (65/9) * (1.5/3) * (1/2.5)), which gives a GSI of 50 using Eq. 1. For the soil and sandstone, Poisson's ratios of 0.2 and 0.14 gives vertical/horizontal stress ratios of 0.25 and 0.16 for gravity-driven stresses, respectively.

For the soil, which consists of clay, silt and some sand, input parameters have been selected based on the log from the drilling of the holes for the extensometers.

The materials in the model are elastic, and the properties of the soil and sandstone are shown in Tables 8 and 9.

Table 6 Stress measurements in the pillar. σ_1 and σ_2 are the principal stresses in a vertical plane along the pillar

Hole depth (m)	σ_1 (MPa)	σ_2 (MPa)	Direction from vertical (°)
0.8	1.1	− 0.9	16
1	0.3	− 0.9	10
2.5	7.6	− 3.4	22
2.8	6.1	− 0.4	1
3.2	7.7	0.7	− 15
3.7	2	− 1.2	− 77
4.1	2	− 0.6	44

Rock stresses

As input for the in-situ stresses, two models were used based on the available data. Both include vertical and horizontal gravity-driven stresses, with the vertical component being based on soil and rock load, and the horizontal component being derived from applying the Poisson value to the vertical component. For the rock, an additional horizontal component is also included to simulate tectonic or other remnant stresses.

The first model, stress configuration 1 (SC1), is based on the results of the 3D stress measurements, where the additional horizontal stresses are set as the measured data, $\sigma_{h\ (max)}$ is 13.54 and $\sigma_{h\ (min)}$ is 3.46. The direction of the major horizontal stress corresponds to the in-plane stress, and the minor horizontal stress corresponds to the out-of-plane stress in the model.

In the second model, stress configuration 2 (SC2), the additional horizontal stress was varied between 1.00 and 2.75 MPa in steps of 0.25 MPa. The resulting stresses in the model corresponding to the 2D stress measurement boreholes were exported for each step and plotted in a graph, together with the measured data, to find the additional horizontal stress that best fits.

For both models, the gravitational stresses are given by the density of the material and Poisson's ratio. This provides horizontal/vertical stress ratios for the soil and sandstone of 0.25 and 0.16, respectively. The gravitational stress contribution is, thus, approximately 1.0 MPa vertically and 0.2 MPa horizontally at the height of the tunnel floor.

Loading effects on RRS

To analyse the loading from rock deformations on the rock support, the most likely rock stress distribution based on the first step of the analysis was used in a new model. The installation of the support took place at the same stage as the excavation of the tunnel, resulting in the concentration of the total load on the support. This will theoretically give a higher load

Table 7 Stress measurements in the tunnel roof. σ_1 and σ_2 are the principal stresses in a horizontal plane above the tunnel roof

Hole depth (m)	σ_1 (MPa)	σ_2 (MPa)	Global direction (°)	Direction relative to tunnel (°)
1	2.2	− 0.5	66	121
1.4	4.1	0.7	75	130
1.8	2	0.2	53	108
3	3.5	1.5	147	202
3.5	0.7	− 3	74	129

as compared to reality because some of the deformations will occur before installation (Hoek 1998).

The tunnels in the modelled area were supported with grouted and pre-stressed bolts (c/c 1.5 m), fibre-reinforced sprayed concrete (thickness 0.18 m), spiling bolts (c/c 0.3 m) and RRS (c/c 2.5 m) with six rebars that were 20 mm in diameter at a c/c of 0.1 m. The rebar was pre-bent and held in place by mounting bolts, not rock bolts, as are typically used, to follow the theoretical profile (see Fig. 16). The thickness of the ribs was between approximately 0.3 and 0.5 m, and their width was about 0.7 m. The sprayed concrete layer used to smooth out the blasted profile, where the ribs were used, was often considerably thicker than the prescribed 0.18 m due to overbreak.

In the numerical model, the support has been simplified by modelling the rib and sprayed concrete as reinforced cast concrete. The simplification involved the division of the number of rebars and the amount of concrete used in a rib by 2.5 (the c/c distance) to distribute it on the 1-m unit distance in the 2D model. Based on this, the rib and reinforced sprayed concrete were modelled as 0.3-m-thick double-reinforced cast concrete with Ø20 mm rebar at a 0.4-m spacing.

This "cast concrete" is modelled as fully bonded with the rock because the displacement measurements show only small movements, which should not detach the concrete from the rock. The rebar has a tensile strength of 400 MPa, and the concrete has a deformation modulus of 25,000 MPa and a compressive strength of 40 MPa. In addition, grouted and pre-stressed Ø20-mm bolts with a length of 4 m, a c/c of 1.5 m in and out of plane, and a strength of 157 kN were included in the analysis. A summary of the support is presented in Table 10.

Results of numerical modelling

Stress configuration 1 (SC1)

When applying the results from the 3D stress measurement, the model has an additional in-plane horizontal stress of

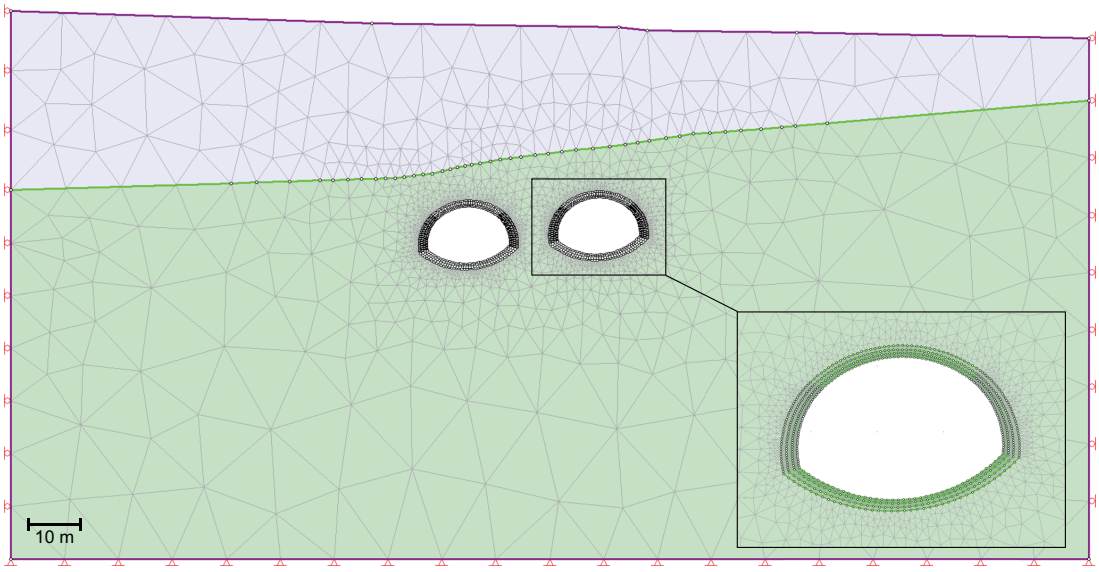

Fig. 15 Geometry of the numerical model for chainage 1220. Purple is soil and green is rock (sandstone)

Table 8 Material properties of the soil

Density (MN/m^3)	0.02
E-modulus (MPa)	30
Tensile strength (MPa)	0
Friction angle (°)	33
Cohesion (kPa)	1
Poisson's ratio	0.2

13.6 MPa. As seen in Fig. 17, this results in very high stresses (exceeding 25 MPa) in the roof and, as seen in Fig. 18, negative minor principal stresses in the walls.

Stress configuration 2 (SC2)

The major principal stresses (σ_1) exported from the models for the various additional horizontal stresses are presented, together with the results of the 2D measurement in the roof and pillar, in Figs. 19 and 20. The exported values correspond to the placement of the roof and pillar measurement holes. In the tunnel roof, the direction of σ_1 is tangential to the tunnel periphery and gradually begins to follow the soil/rock surface with decreasing depth, while in the pillar, this direction is vertical. By comparing the median values for the depth range of 1–3.5 m to the roof data, an additional horizontal stress of 1.50 MPa was found to give the best fit with the measurements. The distribution of the major and minor principal stresses for an additional horizontal stress of 1.50 MPa is presented in Figs. 21 and 22, respectively.

Performance of the RRS

As concluded above, the model providing the results that best correspond with the measured data is that with an additional horizontal stress of 1.50 MPa. This model is, therefore, selected for further analysis.

Table 9 Material properties of the sandstone

Blast damage (D)	0	0.2	0.4	0.6
Q-value	1.4	1.4	1.4	1.4
GSI	50	50	50	50
σ_c intact (MPa)	61	61	61	61
Intact E-modulus (GPa)	42	42	42	42
Poisson's ratio	0.14	0.14	0.14	0.14
mi	17	17	17	17
Density (MN/m^3)	0.027	0.027	0.027	0.027
Rock mass E-modulus (GPa)	12.9	9.7	7.2	5.3
mb	2.851	2.338	1.824	1.326
s	0.004	0.003	0.002	0.001
a	0.506	0.507	0.508	0.509

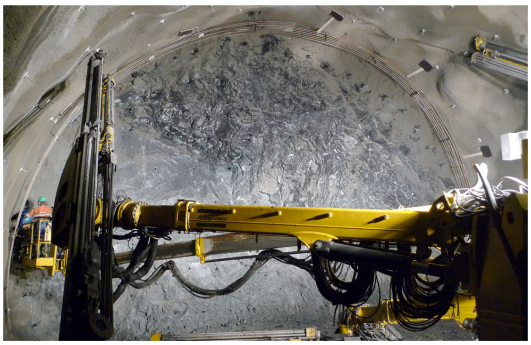

Fig. 16 Ready-mounted rebar for the application of sprayed concrete. The light and dark plywood plates serve as protection for the instrumentation wiring during sprayed concrete application. The tunnel width is 15.5 m (the tunnel profile was extended to make room for the RRS)

The deformations in the model are shown in Fig. 23. The deformation downward in the tunnel roof is about 1 mm, and the relative expansion in the rock body is 0.12 mm. The corresponding displacement in the MPBX at B1220 is 2.39 mm and the relative expansion is 1.61 mm.

Figure 24 shows the capacity plot of the support. It illustrates that the deformations from the excavation generate only minor loads in the support construction compared to its capacity, with a safety factor above 10. The compression load in the rebar is 8–22 kN, which, in μS, is − 130 to − 350. The capacity plots are based on Carranza-Torres and Diederichs's envelope principle (Carranza-Torres and Diederichs 2009), and show thrust versus moment and thrust versus shear plots for both the concrete and the reinforcement. Each beam (cast concrete) element along the tunnel periphery is plotted in the diagrams with its given values.

Discussion and conclusions

The measurement programme described in this paper was designed to obtain data on the rock deformations caused by tunnelling as a basis for evaluating what loads this would give on the rock support.

The rock mass grouting has, to a large degree, disturbed the extensometer deformation measurements. The least-affected extensometer, at B1220, registered a deformation of 3.07 mm, which is expected to be related to the tunnel. This deformation occurred during the excavation from 1 m before the extensometer to 20 m after. According to Hoek et al. (1997), deformation begins about half a tunnel diameter before the measurement point, and about one-third of the total deformation is expected to have taken place when the tunnel reaches the measuring point. All deformations are expected to have taken place when the excavation has passed the

Table 10 Actual and simplified/equivalent support for the area around chainage 1220 for use in the numerical model.
[a]Calculation: (RRS thickness * RRS width)/RRS distance + smoothing layer = (0.4* 0 .7)/ 2.5 + 0.18 ≈ 0.3

Actual support		Equivalent support	
RRS, c/c distance	2.5 m	Rebar spacing	0.4 m (Ø20 mm)
Rebar in RRS	6 x Ø20 mm	Rebar tensile strength	400 MPa
RRS thickness	0.3–0.5 m	Concrete thickness	0.3 m[a]
Sprayed concrete (smoothing layer)	0.18 m	Concrete compressive strength	40 MPa
Spiling bolts c/c dist.	0.3	Concrete E-modulus	25,000 MPa
Rock bolts	4 m (Ø20 mm) c/c 1.5 m	Rock bolts	4 m (Ø20 mm) c/c 1.5 m

measuring point by 1–1.5 tunnel diameters. Given this, the total deformation will be about 4 mm.

The rebar strain meters in the RRS showed quite low values. It is, therefore, difficult to determine whether the registered strain is due to actual rock displacement or drying shrinkage in the concrete because the expected values for both are a few hundred μS. Some small impacts on the strain meters at B1028 may be related to the passing excavation of tube

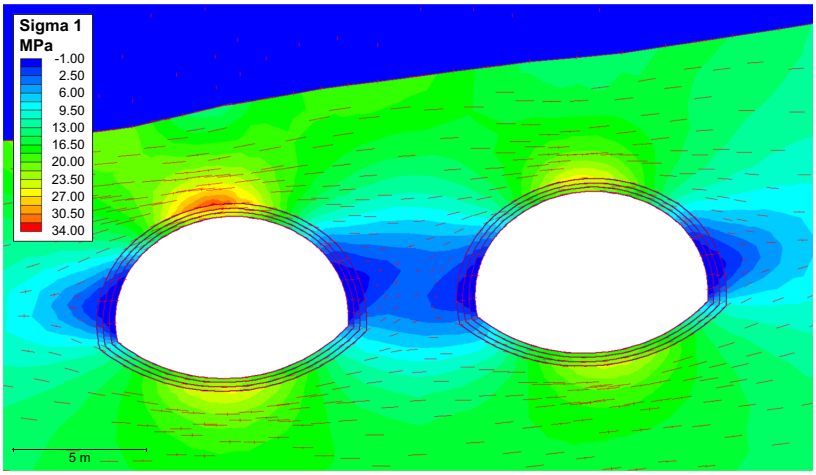

Fig. 17 Major principal stress with gravity-induced stress and an additional horizontal stress of 13.6 MPa

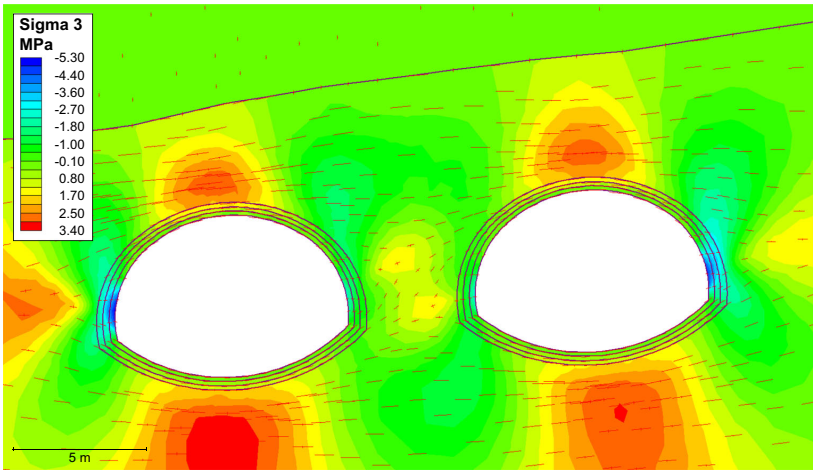

Fig. 18 Minor principal stress with gravity-induced stress and an additional horizontal stress of 13.6 MPa

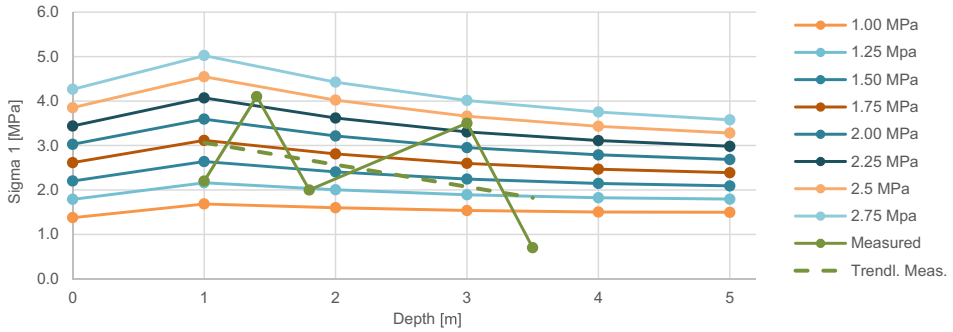

Fig. 19 σ_1 values from the roof in the model with various additional horizontal stresses

A. The readings of − 250 and − 650 μS for left 1 and left 2 at B1220 (see Fig. 11) may also be related to the passing excavation of tube A.

The numerical modelling shows that the 3D stress measurements that were performed some distance away from the tunnel do not correspond well with the 2D stress measurements performed close to the tunnel roof. If a rock mass with a high deformation modulus is near a rock mass with a lower deformation modulus, stresses will generally concentrate in the high deformation modulus rock mass. The syenite in the area has both a higher uniaxial compressive strength and a higher deformation modulus than the

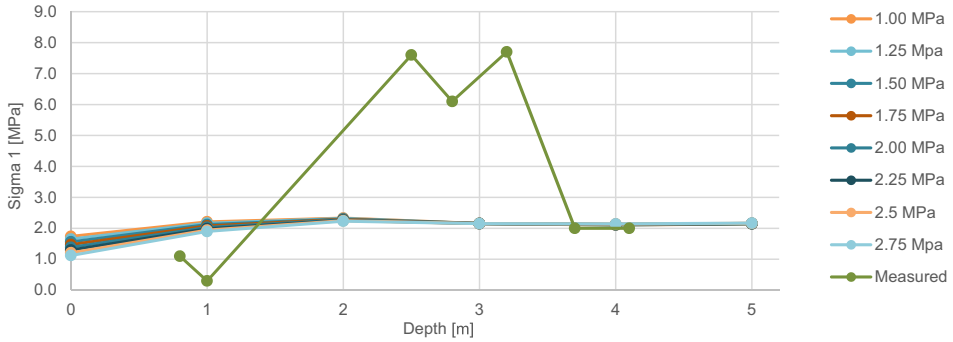

Fig. 20 σ_1 values from the pillar in the model with various additional horizontal stresses

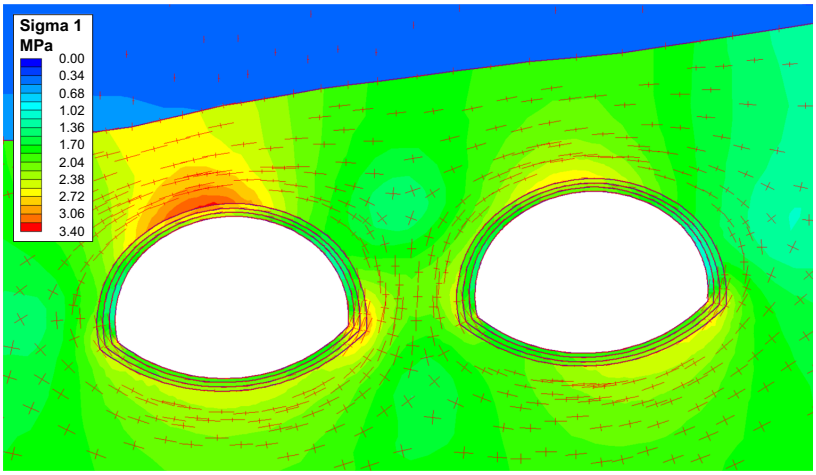

Fig. 21 Major principal stress with gravity-induced stress and an additional horizontal stress of 1.50 MPa in the rock mass

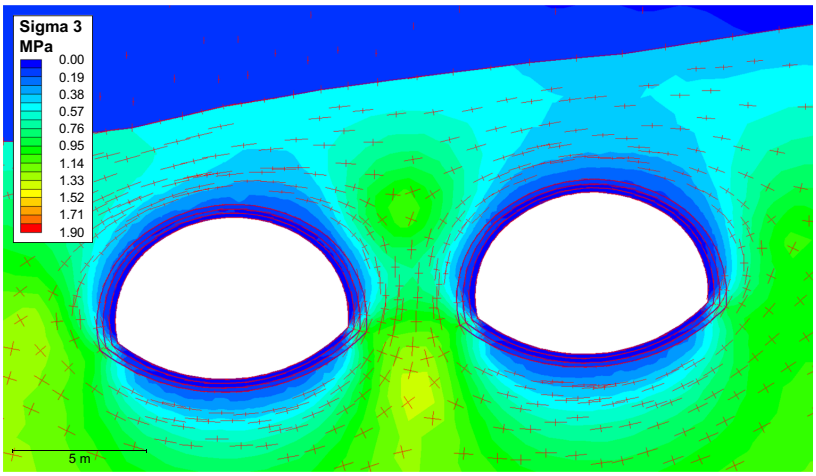

Fig. 22 Minor principal stress with gravity-induced stress and an additional horizontal stress of 1.50 MPa in the rock mass

surrounding rock. The stress measurements have a quite large margin of error, which may be due to this change in deformation modulus, possible recordings in different rock types and joints being close to the individual measurements. In addition, the cooling of intrusive rock may create residual stresses. Because SC1 (see Fig. 17) has a σ_1 of 20–25 MPa, the 2D measurements in the roof are of a different scale and there is a syenite intrusion in the area, it is likely that the 3D measurement has hit a local stress concentration. The quite high, negative, generally vertical minor principal stresses shown for SC1 in Fig. 18 are not likely occur in situ. This is because joints in the rock mass would release these stresses. The resulting stresses in the model from SC1 are considered implausible, and it is assumed that SC2, based on the 2D stress measurements, best fits the in-situ stresses. The negative subhorizontal stresses in the pillar may be caused by the ability of the rock to expand on two sides (normal to the σ_2 direction), creating tension in the σ_2 direction.

As shown by Fig. 19, the measured stresses do not follow the theoretical distribution, but have quite a considerable variation. This may be explained by the varying deformation modulus caused by the benching of the sandstone, local jointing and/or the local influence of high-pressure grouting. When considering the trend line in the same figure, it seems that the measured stress would match a field/additional horizontal stress of about 1.5 MPa. In this model, the total deformation in the roof is 1.18 mm and the relative deformation in the rock body is 0.16 mm, as compared to a deformation in the extensometer at B1220 of about 4 mm and a relative expansion between anchors 1 and 3 of 1.61 mm.

The rock overburden at B1220 is about 9 m and the measured relative deformation in excess of 1 mm can be

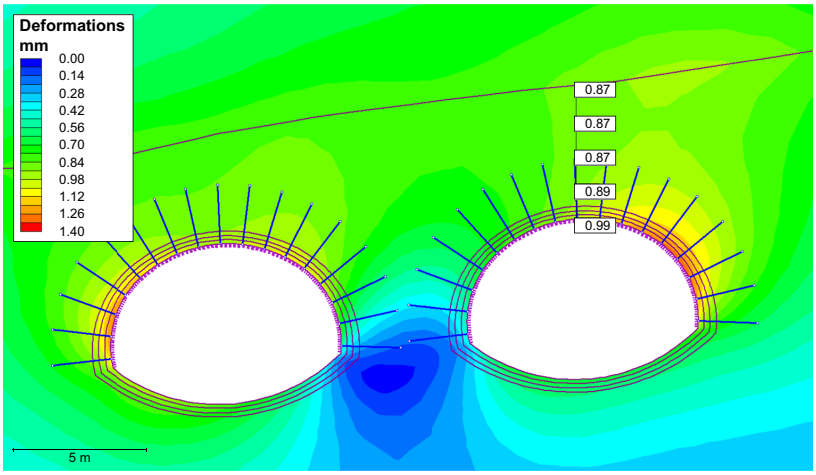

Fig. 23 Deformations with gravity-induced stress and an additional horizontal stress of 1.50 MPa in the rock

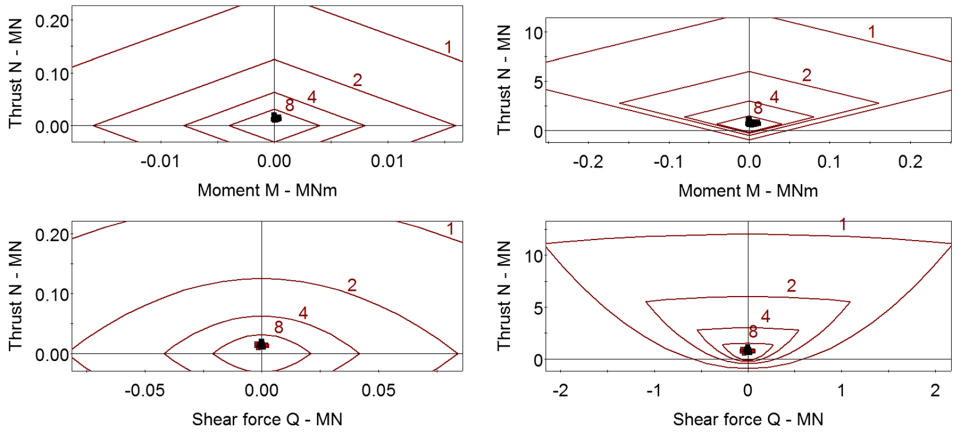

Fig. 24 Capacity plot for the cast concrete simulating the ribs. The burgundy lines are the safety envelopes for safety factors 1, 2, 4 and 8

considered close to zero for practical purposes. This deformation may be caused by the displacement in a single joint and it is, therefore, not likely that a numerical model would yield the same deformation as the measured data when the deformations are this small.

Regarding the loading on the rib, a deformation in the rock of about 2–3 mm is expected after the mounting. This is because the rib is placed about 1 m behind the face and some of the deformation would already have taken place. The numerical model shows strains at the same level as those recorded by the strain meters but, as mentioned above, drying shrinkage may also cause strains at this level. The supposed strains in the rib from drying shrinkage and from deformations in the rock are moving in the same direction and it is difficult to distinguish which strains come from which sources. In either case, the numerical model shows very small loads on the support construction, far from its capacity (see Fig. 24), with millimetre-scale deformations.

There are several uncertainties and assumptions in the analyses presented in this paper, but the results are still quite unambiguous because the deformations are very small. Both the measurements and the modelling show that the ribs have little or no load. This means that the ribs do not have a support function, as they were designed to, but more of a rock-reinforcing function. It also indicates that the rock mass is self-bearing, provided that the contour is kept intact. Hoek and Marinos (2000) state that, in weak heterogeneous rock masses, sprayed concrete and bolting are sufficient rock reinforcements up to a tunnel closure of 1%. In this case, this means a deformation in the crown of about 6 cm.

The Q-values mapped during excavation in the area indicate a recommended rock support according to the Q-method very close to the border for where to start using RRS. Because of a long stretch with a low overburden and uncertain rock mass quality, spiling bolts and RRS were still chosen to be used as an integrated part of the excavation process. The rock mass quality where one, according to the Q-method, should start to use RRS is based on empirical data. Considering the measured data, it seems that, with a rock mass quality at the border of requirement for RRS and probably also with quite worse rock mass, RRS is not required because of large stresses and deformations in the rock mass. The main function of the RRS is probably keeping the rock in place by locking blocks, increasing friction in the joints and preventing movement in larger filled joints. This goal can quite likely be obtained by an even leaner and more simply designed rib than the one used in this case.

References

Aksoy CO, Ogul K, Topal I, Ozer SC, Ozacar V, Posluk E (2012) Numerical modeling of non-deformable support in swelling and squeezing rock. Int J Rock Mech Min Sci 52:61–70. https://doi.org/10.1016/j.ijrmms.2012.02.008

Barla G, Bonini M, Semeraro M (2011) Analysis of the behaviour of a yield-control support system in squeezing rock. Tunn Undergr Space Technol 26(1):146–154. https://doi.org/10.1016/j.tust.2010.08.001

Carranza-Torres C, Diederichs M (2009) Mechanical analysis of circular liners with particular reference to composite supports. For example, liners consisting of shotcrete and steel sets. Tunn Undergr Space Technol 24(5):506–532. https://doi.org/10.1016/j.tust.2009.02.001

Gilbert RI (2001) Shrinkage, cracking and deflection—the serviceability of concrete structures. Electron J Struct Eng 1(1):15–37

Grimstad E, Kankes K, Bhasin R, Magnussen AW, Kaynia AM (2002) Rock mass quality Q used in designing reinforced ribs of sprayed concrete and energy absorption. Fjellsprengningsteknikk—bergmekanikk—geoteknikk, Oslo, November 21–22, 2008

Grimstad E, Tunbridge L, Bhasin R, Aarset A (2008) Measurements of deformation and forces in reinforced ribs of sprayed concrete. Why do we use cast concrete lining when ribs of sprayed concrete have a large margin? Fjellsprengningsteknikk—bergmekanikk—geoteknikk, Oslo, November 20–21, 2008

Hoek E (1998) Tunnel support in weak rock. Symposium of Sedimentary Rock Engineering, Taipei, Taiwan, November 20–22, 1998

Hoek E, Diederichs MS (2006) Empirical estimation of rock mass modulus. Int J Rock Mech Min Sci 43(2):203–215. https://doi.org/10.1016/j.ijrmms.2005.06.005

Hoek E, Marinos P (2000) Predicting tunnel squeezing problems in weak heterogeneous rock masses. Tunnels Tunn Int 32(11):45–51

Hoek E, Kaiser PK, Bawden WF (1997) Support of underground excavations in hard rock, 3rd edn. Balkema, Rotterdam

Hoek E, Carter TG, Diederichs MS (2013) Quantification of the geological strength index chart. 47th US Rock Mechanics/Geomechanics Symposium, San Francisco, June 23–26, 2013

Høien AH, Nilsen B (2014) Rock mass grouting in the Løren tunnel: case study with the main focus on the groutability and feasibility of drill parameter interpretation. Rock Mech Rock Eng 47(3):967–983. https://doi.org/10.1007/s00603-013-0386-7

Humstad T, Høien AH, Kveen A, Hoel JE (2012) Complete software overview of rock mass and support in Norwegian Road Tunnels, Eurock 2012. ISRM, Stockholm, Sweden.

International Society for Rock Mechanics (ISRM) (2007) The complete ISRM suggested methods for rock characterization, testing and monitoring: 1974–2006. ISRM Turkish National Group, Ankara

Iversen E (2011) Lørentunnelen - Longitudinal general geology section map

Iversen E, Kveen AT (2007) Rv. 150, Lørentunnelen, Geologisk rapport for konkurransegrunnlaget, Oppdrag A-37A, rapport nr. 3. Statens Vegvesen, Oslo

Kim K, Franklin JA (1987) Suggested methods for rock stress determination. Int J Rock Mech Min Sci Geomech Abstr 24(1):53–73

Larsen T (2010) 3-dimensjonal og 2-dimensjonal bergspenningsmålinger ved Lørentunnelen. SINTEF, Trondheim

Larsen T, Trinh NQ (2014) In-situ rock stress measurements and numerical modelling. SINTEF, Trondheim

Mao DW, Nilsen B, Lu M (2011) Analysis of loading effects on reinforced shotcrete ribs caused by weakness zone containing swelling clay. Tunn Undergr Space Technol 26(3):472–480. https://doi.org/10.1016/j.tust.2011.01.004

Myrvang A (2001) Bergmekanikk. Department of Geology and Mineral Resources Engineering, NTNU, Trondheim

Norsk Forening for Fjellsprengningsteknikk (NFF) (2008) Tung bergsikring i undergrunnsanlegg, vol 5. Håndbok. NFF, Oslo

Norwegian Geotechnical Institute (NGI) (2013) Using the Q-system—rock mass classification and support design. Handbook. NGI, Oslo

Oftedahl C (1981) Norges geologi/geology of Norway. Tapir, Trondheim

Pedersen KB, Kompen R, Kveen A (2010) Arbeider foran stuff og stabilitetssikring i vegtunneler. Teknologirapport. Norwegian Public Roads Administration, Oslo

Rocscience Inc. (2015) RocData, vol 5.006. Rocscience Inc., Toronto

Rocscience Inc. (2016) RS2, vol 9.011. Rocscience Inc., Toronto

Schwingenschloegl R, Lehmann C (2009) Swelling rock behaviour in a tunnel: NATM-support vs. Q-support—a comparison. Tunn Undergr Space Technol 24(3):356–362. https://doi.org/10.1016/j.tust.2008.08.007

Sjöberg J, Klasson H (2003) Stress measurements in deep boreholes using the Borre (SSPB) probe. Int J Rock Mech Min Sci 40(7–8):1205–1223. https://doi.org/10.1016/S1365-1609(03)00115-1

Standard Norge (2008) Eurocode 2: design of concrete structures. Part 1-1: general rules and rules for buildings. Standard Norge, Lysaker

Vianova Systems (2011) Novapoint Tunnel, 18th edn. Vianova Systems, Sandvika

Paper II

Main aspects of deformation and rock support in Norwegian road tunnels

Høien, A.H.[a]
Nilsen, B.[b]
Olsson, R.[c]

[a]Norwegian University of Science and Technology, Sem Sælands veg 1, 7491 Trondheim, Norway and Norwegian Public Roads Administration, Postboks 8142 Dep, 0033 Oslo, Norway, are.hoien@vegvesen.no, Phone: +47 918 57 071, ORCID 0000-0001-5478-6377

[b]Norwegian University of Science and Technology, Sem Sælands veg 1, 7491 Trondheim, Norway, bjorn.nilsen@ntnu.no

[c]Norwegian Geotechnical Institute, PO Box 3930 Ullevaal Stadion, 0806 Oslo, Norway, Roger.Olsson@ngi.no

Abstract
The general geology of Norway makes most of its tunnels to be constructed mainly in strong rock intersected by weakness zones of different sizes and characteristics. The Norwegian support tradition is, to the largest degree as possible, to reinforce the rock to make it self-bearing. In weak rock, this reinforcement has been accomplished by using bolts, sprayed concrete and ribs of reinforced concrete (RRS). RRS are normally designed with 6 rebars mounted on brackets that are attached to rock bolts with a c/c of 1.5 m covered in sprayed concrete. The spacing between the RRS in the tunnel direction is usually 1 to 3 m. In recent years, the application of RRS has gradually changed from following the blasted tunnel profile that formed unarched RRS that reinforced the rock to using RRS with an arched design that supports the rock. Following this development was an increase in the use of materials, as the amount of sprayed concrete used is now considerably larger and the rebar diameter changed from 16 to 20 mm. This change has also caused an abrupt increase in the support measures used for decreasing rock quality, from simple reinforcement by bolts and sprayed concrete to load-bearing arches. The authors believe that a more gradual transition is logical and this article will discuss and evaluate the current Norwegian support strategy by reviewing international theory, performing parameter analysis and presenting data from current and previous Norwegian road tunnels, with a focus on rock mass quality and deformations. Norwegian conditions comprise the basis for the discussion, but the problem at hand is also of general interest for hard rock tunnelling conditions.

Keywords
Rock support; deformations; road tunnels

1 Introduction

In Norwegian tunnelling, stability challenges are usually related to zones of weak rock. Typical challenges can include wide weakness zones in sub-sea fjord crossings 100 to 300 meters (m) below sea level, minor zones and jointed rock in urban areas with typically a 5- to 100-m overburden, overstressing of solid rock and weakness zones for tunnels under high mountains or along steep valley sides (up to a 1000-m overburden or more). Many weakness zones include the remains of Mesozoic weathering and may contain swelling minerals.

The Norwegian tradition is to take advantage of the self-bearing capacity of the rock mass as much as possible. When rock reinforcement requires more than bolts and sprayed concrete, a lean support construction is used to reinforce and keep the rock mass in place, rather than heavy support constructions, for example, fully casted lining. This lean support is usually comprised of reinforced ribs of sprayed concrete (RRS) (see Fig. 1). The RRS is combined with spiling bolts and sprayed concrete to keep the rock in place after blasting, before RRS installation. The spiling bolts are held in place in the rear end with either steel straps and radial rock bolts or RRS.

RRS typically consists of six rebars c/c 10 cm mounted to rock bolts c/c 1,5 m along the tunnel periphery and covered with sprayed concrete. Originally, the rebars were installed so that they strictly followed the blasted tunnel profile (unarched RRS; see Fig. 2 a), but in recent years the practice for road tunnels in Norway has been to form load-bearing arches (arched RRS, Fig. 2b) (Pedersen et al., 2010).

Fig. 1 Mounting of rebars for two RRS for permanent support (2). Further toward the face two (1) blast rounds are temporarily supported with spiling bolts held in place by steel straps and radial rock bolts. Finished RRS can be seen to the right (3).

The main purpose of this article is to discuss and evaluate the support strategies adapted for rock mass quality and deformations. The current support strategy involves a very considerable, abrupt increase in the support level at a certain drop in rock mass quality, from simple reinforcement with rock bolts and sprayed concrete to load-bearing constructions, such as arched RRS. It is believed that a more gradual transition from rock bolts and sprayed concrete to load-bearing support would be logical, and in this article the authors want to discuss this possibility. Among the main challenges posed by this alternative approach are gravitational problems related to weak rock masses and filled joints, minor weakness zones and moderate swelling problems under favourable stress conditions. As background for the discussion, a review will be conducted of international theories and experiences. Data on rock mass quality, rock support and deformation in Norwegian tunnels will be used to

illustrate the feasibility of the proposed alternative support strategy. Norwegian geological conditions are typical for hard rock tunnelling and it is assumed that the conclusions of this study will be applicable under these general conditions.

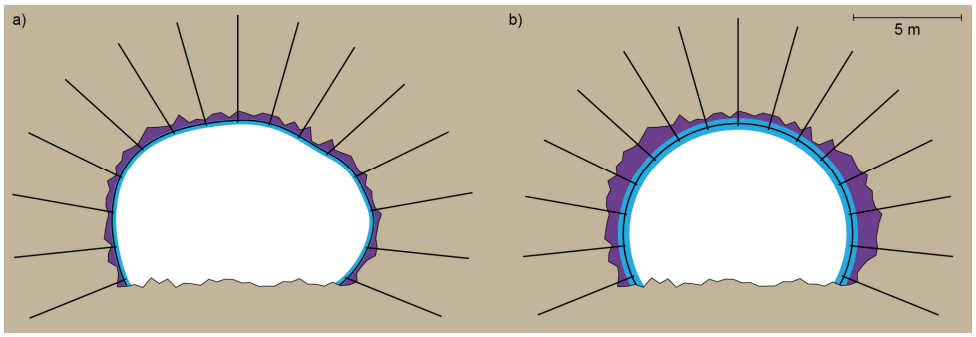

Fig. 2 Schematics of a) unarched RRS and b) arched RRS. The black lines are rebar and rock bolts. The purple area is sprayed concrete smoothing layer and the light blue area is the final layer covering the rebar. The rugged surface represents the blasted profile.

2 Basic characteristics of Norwegian bedrock

2.1 Brief geological overview

Geologically, Norway mainly consists of Precambrian and Cambro Silurian (Caledonian) bedrock (see Fig. 3). The Precambrian rocks are mainly gneisses and intrusive granite and gabbro of various degrees of metamorphism. The Caledonian rocks are mainly metamorphosed sedimentary and volcanic rocks. Permian volcanic and igneous rocks can be found in Southeast Norway i.e. the Oslo region. In the Mesozoic, there was a weathering of bedrock that eroded during glacial landscape formation in the Pleistocene. The bedrock today therefore mainly consists of hard rock intersected by weakness zones of different extents and character originating from tectonic activity and in some cases, Mesozoic weathering.

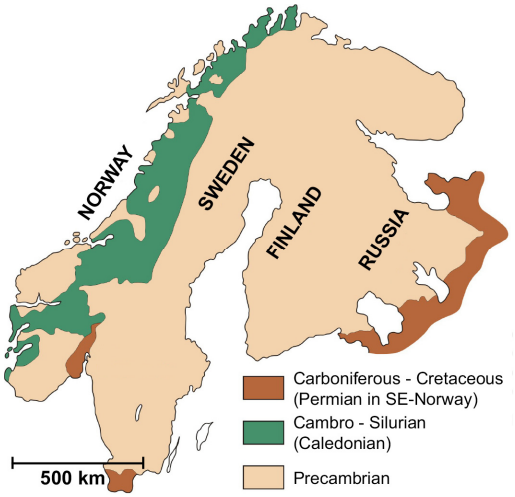

Fig. 3 Overview of regional geology.

2.2 Properties of intact rock

Box plots of uniaxial compressive strength (UCS) and E-modulus based on the SINTEF rock mechanical properties database (SINTEF, 2016) are shown in Fig. 4 and Fig. 5, respectively. The circles and stars are outliers and were not included in the distribution calculation. The dataset is based on testing about 3300 samples. There is considerable variation in both the UCS and the E-modulus but according to NBG (1985) classification, both the UCS and E-modulus values are large or very large.

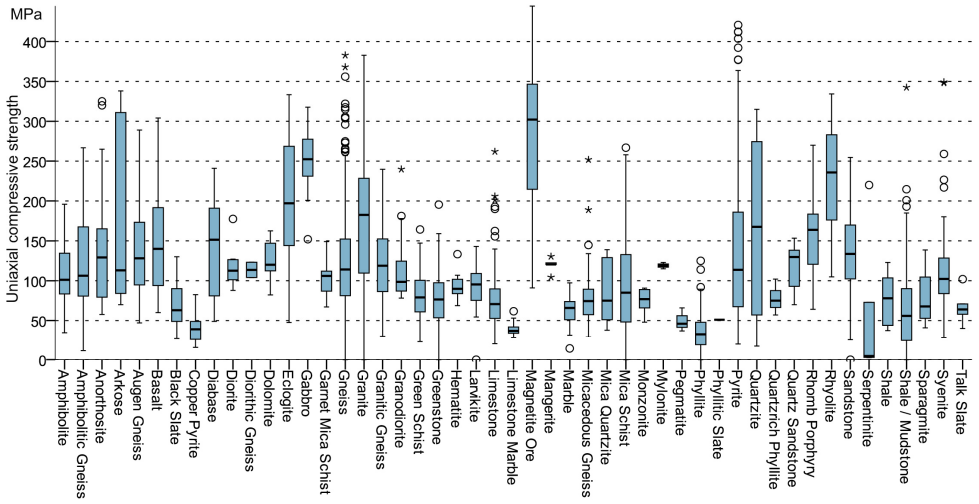

Fig. 4 Uniaxial compressive strength (UCS) in MPa for Norwegian rock types extracted from the SINTEF rock mechanical properties database (SINTEF, 2016).

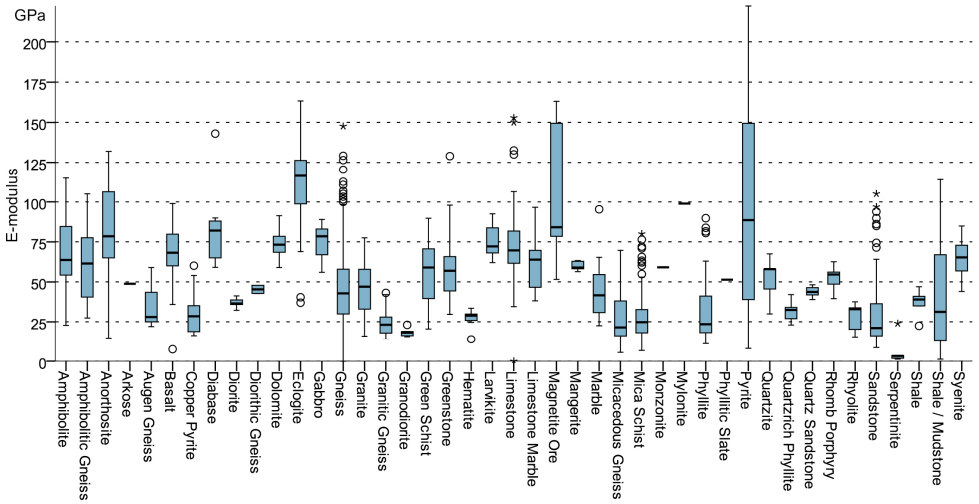

Fig. 5 E-modules in GPa for different Norwegian rock types extracted from the SINTEF rock mechanical properties database (SINTEF, 2016).

2.3 Rock stresses

As for many other regions in the world, the in-situ rock stresses in Norway vary considerably in magnitude as well as orientation. Myrvang (2001) stated that when measured, the horizontal stresses are usually much higher than the vertical component would indicate. He also stated that the vertical stress in most cases corresponds well to the overburden and is

normally the minor principal stress, at least down to 500 m. An overview map of Norwegian geology and horizontal stresses is shown in Fig. 6. According to Myrvang (1993), the overall tendency is that the principal stresses seems to be parallel the Caledonian mountain range.

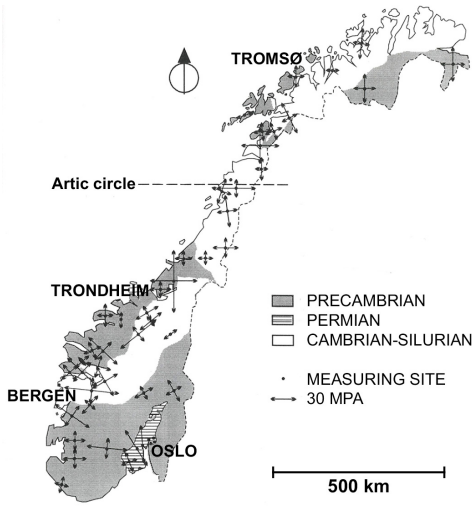

Fig. 6 Directions of horizontal stress in Norway (Myrvang, 1993).

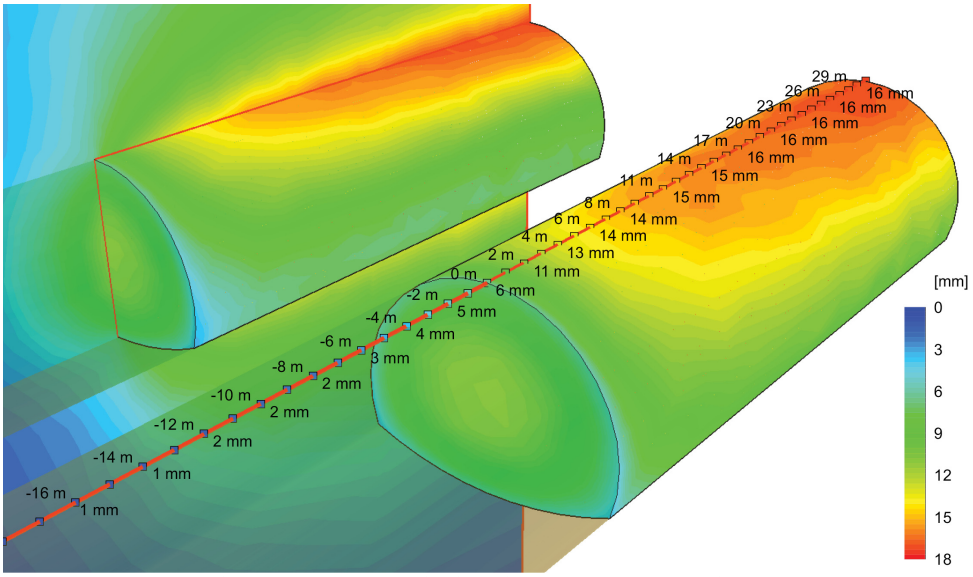

Fig. 7 Deformations around a typical two-tube tunnel (tube width is 10.5 m). Negative values are the meters in front of the face and positive values are the meters behind the face. The left tube has a vertical contour plane intersecting the centre of the tunnel.

3 Theoretical basis for evaluating tunnel deformation and rock support

In this section, the pertinent background material on tunnel deformation and rock support will be presented. This material will be used in the subsequent main sections to evaluate current practices in Norwegian road tunnelling.

3.1 Deformations from tunnel advancement

As the tunnel face advances, deformations take place in the rock mass. According to Hoek et al. (1997), the deformation starts about one-half of the tunnel diameter ahead of the face and at the face about one-third of the deformations have taken place. At about one to one and a half tunnel diameters behind the face, the deformations have reached their final value. This is confirmed by the results from RS3-modelling, based on the ideal conditions shown in Fig. 7. The model has the same conditions as the models described in Section 4, with 500 m overburden and the "GSI 50" material.

3.2 Critical strain

The critical strain concept was introduced by Sakurai (1981) and can be explained as the strain of a rock or rock mass at yield load. More specifically, the critical strain, ε_0, is:

$$\varepsilon_0 = \frac{\sigma_c}{E} \qquad (1)$$

Where σ_c is the UCS
E is the E-modulus.

For a linear elastic rock sample, critical strain would be the strain at maximum load during testing. Sakurai (1983) stated that the stability of tunnels can be assessed on the basis of strain in the rock mass surrounding the tunnel and showed how displacement measurements can be used in back-analysis to evaluate tunnel stability and initial stresses.

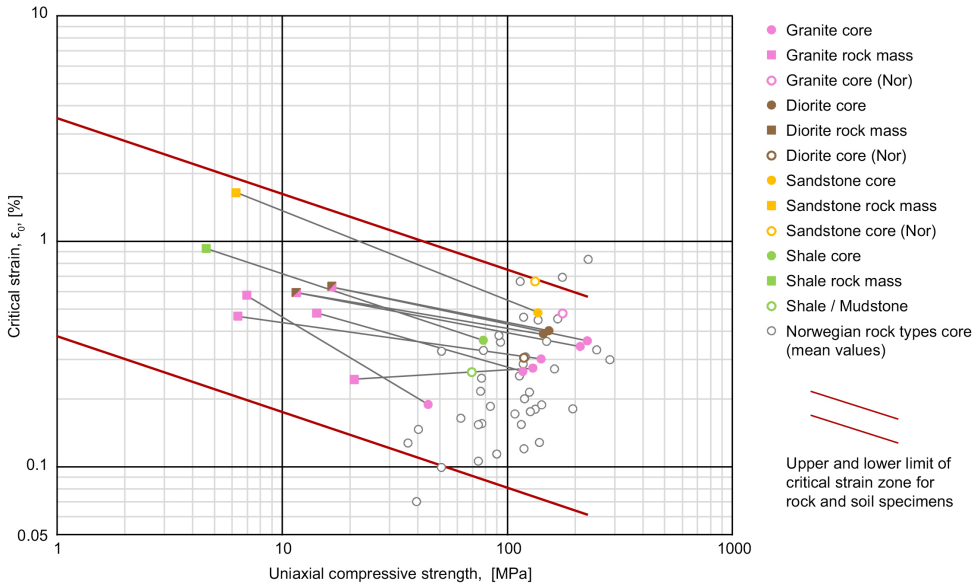

Fig. 8 Critical strains for rock cores and rock masses. The colour-filled symbols are data from Sakurai (1983), while the unfilled symbols are data from SINTEF (2016). The SINTEF values are the mean values for a certain rock type. The red lines are the envelope of an extensive number of tests on cores from Sakurai (1981).

In Fig. 8, Sakurai's relationship between critical strain and uniaxial strength is presented with data for Norwegian rocks based on the SINTEF rock mechanical properties database (SINTEF, 2016). The red lines in the figure envelope a large number of rock and soil core specimen tests, ranging from UCS 0.01 to 100 MPa, presented by Sakurai (1981). As illustrated, the critical strain tends to increase with the decrease of uniaxial compressive

strength and ranges, according to Sakurai (1983), from 0.1% to 1% for rocks and from 1% to 5% for soil.

Based on in-situ testing and back-calculations, the critical strains for the rock mass of different rock types were derived (Sakurai, 1983). In Fig. 8, these relationships are shown where the grey line connects the corresponding core and rock mass values. The mean values obtained from core testing of corresponding Norwegian rock types (SINTEF, 2016) are presented as unfilled symbols in the same colour as Sakurai's data. A box plot of critical strains for Norwegian rock samples, based on the SINTEF-database (SINTEF, 2016), is presented in Fig. 9. One can see that most rock types have quite low critical strains, but since they have high UCS values, they can be exposed to significant stresses without reaching their limit.

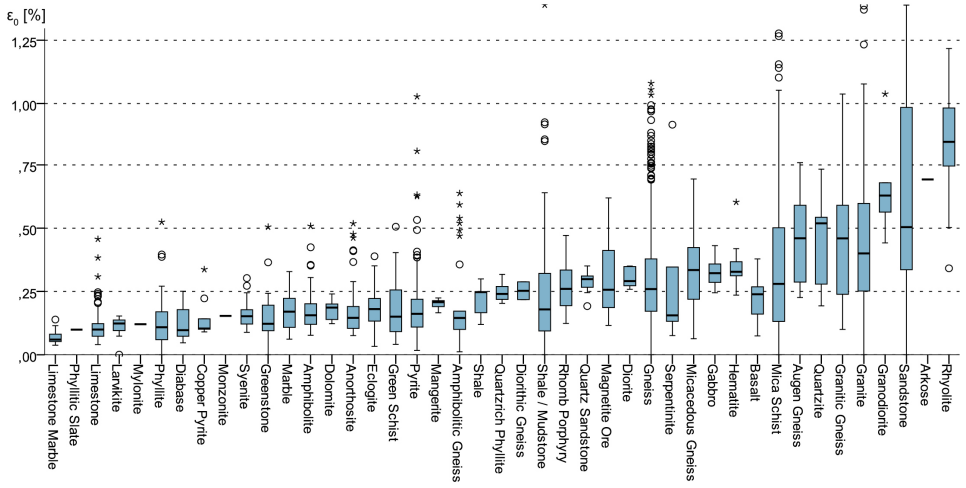

Fig. 9 Critical strains for Norwegian rock types (SINTEF, 2016).

3.3 Deformations related to rock mass strength and in-situ stress

In Hoek (1999), Hoek and Marinos (2000) and Hoek (2001), it is shown that strain and deformation can be predicted by the rock mass strength and in-situ stresses (see Fig. 10). Different classes are defined with a brief suggestion on how to reinforce or support rock, where the transition between typical rock reinforcement and rock support is between class A and B. The diagram is the result of a study on a closed formed analytical solution for a tunnel in a hydrostatic stress field, based on the theory of Duncan Fama (1993) and Carranza-Torres and Fairhurst (1999). A statistical simulation using the Monte Carlo method was conducted before a line fitting was performed on the data. The input values for the simulation were: in-situ stresses from 2 to 20 MPa (80 to 800 m depth), tunnel diameters from 4 to 16 m, uniaxial strength of intact rock from 1 to 30 MPa, Hoek-Brown constant m_i from of 5 to 12, Geological Strength Index (GSI) from 10 to 35 and, for the Carranza-Torres solution, a dilation angle of 0 to 10 (Hoek and Marinos, 2000).

Sakurai (1983) suggested that tunnel strain levels in excess of approximately 1% are associated with tunnel stability problems. This is supported by the plot in Fig. 11 (from Hoek (2001), where field observations of rock mass uniaxial strength are plotted against tunnel strain and observations are marked in red if they required special support considerations. The plot shows only one case of a stability problem below the 1% line and it can also be seen that there are cases with as high as a 4% strain with no stability problems.

For the different squeezing classes presented in Fig. 10, indications of the necessary support are provided: A) bolts and sprayed concrete, B) sometimes lattice girders or steel sets, C) heavy steel sets, D) fast installation and face support, and E) yielding support may be required.

According to Hoek (1999), it is reasonable to assume an isostatic stress field, as in the Monte Carlo simulation done for Fig. 10, for very weak rock, such as in a fault or shear zone, since this type of rock has undergone failure and is incapable of sustaining significant stress differences. Because of this, even if the far field stresses are anisotropic, the stresses within the fault zone are likely to be approximately isotropic.

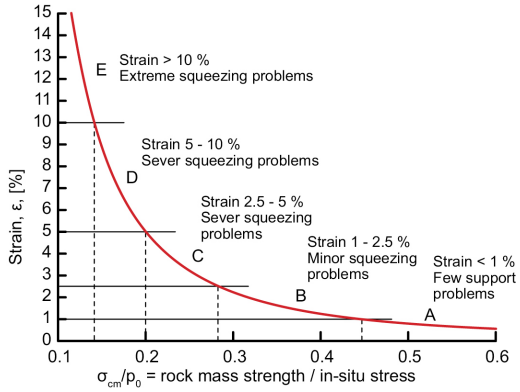

Fig. 10 The relationship between strain and rock mass strength and in-situ stress. The curve is for unsupported rock. Based on Hoek and Marinos (2000).

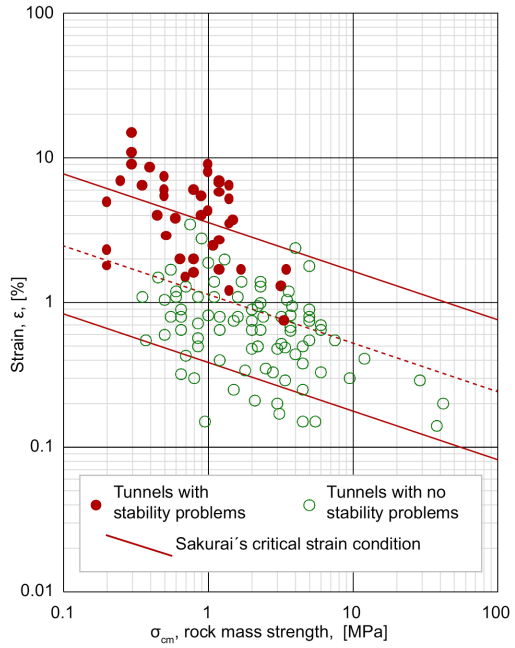

Fig. 11 Field observations from the Second Freeway, Pinglin and New Tienlun headrace tunnels in Taiwan, based on Hoek (2001), Hoek (1999) and Sakurai (1983).

3.4 Rock mass quality

In rock engineering, there are many tools for describing rock mass quality. These tools are often also used for designing support, evaluating alternative excavation methods or estimating input for rock engineering applications (Palmstrom and Stille, 2007). The tool that is used most by far in Norway is the Q-system. The Q-system is used for rock mass quality documentation and as a basis for support design, either with the "built-in" support chart (e.g. the rail authorities (Bane NOR, 2018) or a modified chart defined by the road authorities (Statens vegvesen, 2016b). For engineering applications, the GSI (Hoek, 1994) is usually used with the Hoek-Brown failure criterion and the rock mass E-modulus estimation (Hoek, 2006).

3.4.1 The Q-system

The Q-value is calculated from six parameters, as shown in Eq. 2 (Barton et al., 1974). The values for each parameter are extracted from tables, charts and/or equations based on mapping in the field or on cores. To visualize variations, one can take the minimum, maximum and mean value for each parameter and calculate Q-values. The Q-value is logarithmic and spans from 0.001 (exceptionally poor) to 1000 (exceptionally good).

$$Q = \frac{RQD}{J_n} \times \frac{J_r}{J_a} \times \frac{J_w}{SRF} \qquad (2)$$

Where *RQD* is the Rock Quality Designation
J_n is the joint set number
J_r is the joint roughness number
J_a is the joint alteration number
J_w is the joint water reduction factor
SRF is the stress reduction factor

RQD/J_n represents a description of block size, J_r/J_a represents the inter-block shear strength and J_w/SRF represents the active stress.

3.4.2 GSI

The Geological Strength Index was introduced in the mid-1990s by Hoek and co-authors Kaizer and Bawden. The system provides a number that, when combined with the intact rock properties, can be used to estimate the reduction in rock mass strength for different geological conditions (Hoek, 2006).

The GSI can be estimated in-situ by using diagrams describing the structure and joint surface conditions. There are two alternative diagrams, one for blocky rock masses and one for heterogeneous rock masses. To obtain the GSI value or a range describing the rock mass, the rock structure and the surface of the discontinuities are combined in the appropriate diagram. The GSI value ranges from 0 to 100, where the higher value is the better rock mass.

One of the most recent contributions from the people behind the GSI is a quantification of the two sides of the GSI chart that makes it possible to calculate GSI values from parameter values registered with the Rock Mass Rating- (RMR) and Q-system. The structure (jointing) side of the diagram is replaced with *RQD* and the surface condition side is replaced with $JCond_{89}$ or the J_r/J_a from the Q-system. $JCond_{89}$ is a parameter from the RMR-system describing the surface conditions. See Eq. 3 and Eq. 4 respectively for the two estimates (Hoek et al., 2013). An important aspect regarding these formulas is that they do not convert

from one rock mass classification system to another directly as conversions have done before, but are based on using corresponding parameter registrations of the systems to calculate a GSI value as an alternative or supplement to using the charts.

$$GSI = JCond_{89} + RQD/2 \quad (3)$$

$$GSI = \frac{52\ J_r/J_a}{(1 + J_r/J_a)} + RQD/2 \quad (4)$$

3.5 The elastic properties of rock mass and weak rock

To estimate the E-modulus of the rock mass (E_{rm}), at least 15 different formulas have been proposed by different authors based on input of different rock mass quality parameters, such as Q, RMR and GSI (Aksoy et al. 2012; Palmström and Singh 2001; Hoek and Diederichs 2006). Most of these estimates are based on a limited amount of data (Hoek and Diederichs, 2006).

Hoek and Diederichs (2006) have proposed two equations that can be used with the GSI, based on a new dataset of almost 500 tests. In addition to an equation proposed earlier (Hoek et al., 2002), these equations are probably the most commonly used today because they are well documented and easy to use based on computer software. The three respective equations of E_{rm} have slightly different input parameters to suit different premises:

- *Generalized Hoek & Diederichs (2006)*, which considers the elasticity of intact rock (E_i), blast damage (D) and GSI;
- *Simplified Hoek & Diederichs (2006)*, which considers D and GSI; and
- *Hoek, Carranza-Torres, Corkum (2002)*, which considers the strength of intact rock (σ_{ci}), D and GSI.

Elastic strain can be calculated based on Hooke's law. To illustrate the relation between the three parameters, different probable values of stress, strain and E-modulus have been plotted in Fig. 12. Vertical stresses representing overburdens from 25 to 1000 m is used, where 0.7 MPa represents the gravitational stress at 25 m, 2.6 MPa for 100 meter and the following stresses represent each subsequent even 100 m. The E-modulus ranges from 40 000 MPa to 313 MPa, where the high value represents e.g. a massive gneiss and the lowest value represents e.g. a crushed, clayey weakness zone material. The plot merely shows the sensitivity of the deformation with respect to the E-modulus in different relevant stress states and must not be confused with actual strain in the tunnel.

As shown in Fig. 12, the E-modulus and stress have a far greater impact on strain on the right side of the plot, where the rock is weak with low E-values, than on middle and high E-values. At the same time, the strain for low stresses that represents shallow tunnels is very small, even with low E-values.

According to ISRM (1978), a rock is weak when the uniaxial compressive strength is below 25 MPa. Hoek (1999) had a bit more complex definition based on including the in-situ stress as well. He suggested that a rock is weak when the uniaxial strength is about one-third of the in-situ stress acting upon the rock mass. The value (one-third) is related to point 0.3 on the x-axis in Fig. 10, where the plot shows a sudden increase in convergence at about this point. This approach implies that the "weakness" of the rock is not only defined by the rock

mass strength, but also by the stress conditions of the rock mass in which the tunnel is excavated.

As the weakness of rock also depends on the stress state, an upper limit of the E-modulus of weak rock is hard to define, but it may be easier to define a lower limit. One reasonable assumption might be that rock mass with E_{rm} close to soil should be considered weak rock. As an indication of what this lower limit may be, Bowles (1997) and Zhu (2012) have found E-values of about 50-200 MPa for dense clays and sands.

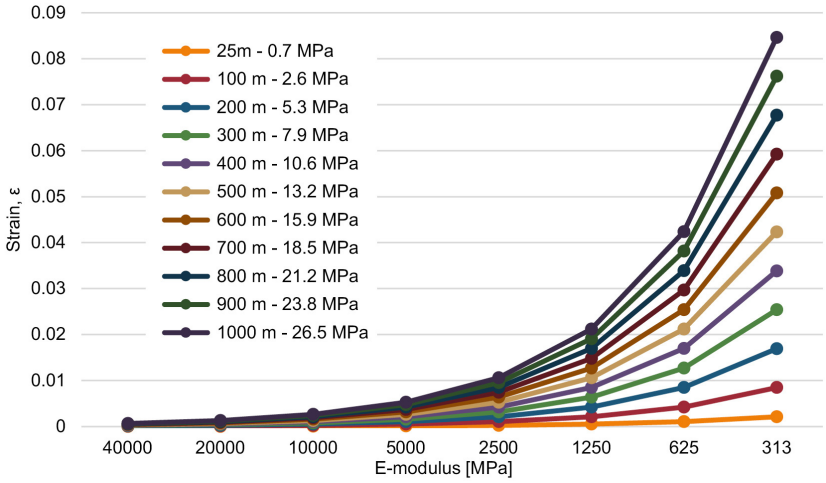

Fig. 12 Strain vs. E-modulus calculated based on Hooke's law for different (vertical) stresses.

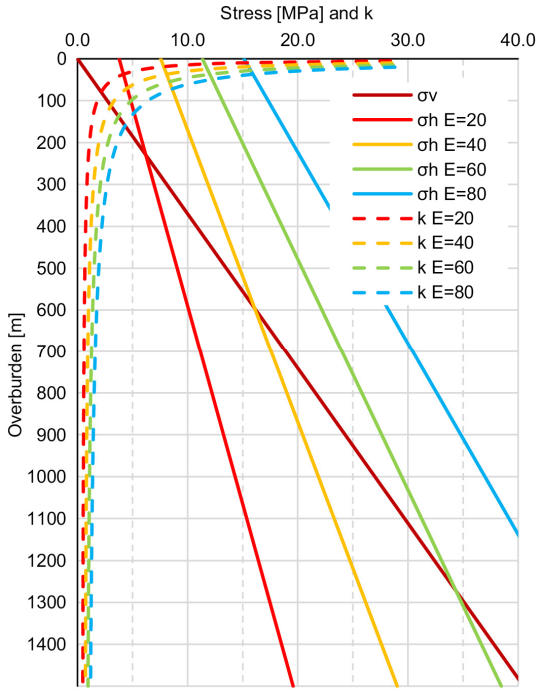

Fig. 13 The ratio *k* and calculated stresses toward depth, based on Sheorey (1994).

3.6 Rock stress

The in-situ stresses in the rock mass are usually defined by a gravity-driven vertical stress and a horizontal stress that is a ratio of the vertical, as shown in Eq. 5 and 6.

$$\sigma_v = \gamma z \tag{5}$$

$$\sigma_h = k\sigma_v \tag{6}$$

Hoek (2006) referred to a large number of in-situ measurements which have shown that the ratio *k* tends to be high at a shallow depth and that it decreases with depth. Sheorey (1994) proposed an equation for *k* (see Eq. 7) that is plotted in Fig. 13 for a selection of E-modules with the resulting stresses. The model is based on an elasto-static stress model of the earth and considers the elastic constants of the crust, density and thermal expansion. According to Hoek (2006), the estimated curves for *k* by Sheorey (1994) are similar to measured stresses published by Brown and Hoek (1978), Herget (1988) and others, and are therefore considered a reasonable basis for estimating the value of *k*.

$$k = 0.25 + 7E\left(0.001 + \frac{1}{H}\right) \tag{7}$$

4 Numerical parameter analysis of a typical two tube tunnel

The degree of deformation is essential when selecting support, especially when the deformations are large. Two parameter studies with the aim to illustrate the deformations that can be expected with different stresses and rock qualities, and the effect of the zone width, have therefore been conducted.

4.1 Influence of rock mass quality and stress on deformations

To investigate the relationship between stress and rock quality, numerical modelling was performed by using RS2 software (Rocscience Inc., 2017a). The model has two 10.5-m wide and 8-m high tunnels with 9.5-m rock between them, as shown in Fig. 12. Analysis was performed for 11 different overburdens, ranging from 35 to 1000 m. For 35-, 100- and 200-m depths, the horizontal and vertical stresses were applied as suggested by Sheorey (1994) for rock mass with E-modulus 20 GPa, as this was the most applicable model. From 300 m and further down, the horizontal stress was set equal to the vertical stress, which was gravitational, to avoid a horizontal stress that was lower than the horizontal. Stresses $\sigma_v=\sigma_h$ were input as suggested by Hoek (1999) for very weak rock, which is also of most interest in the study and has the most impact on deformations. This also conforms to the line drawn by Myrvang (1993) when he stated that vertical stress coincides well with overburden stress and is, at least at a depth down to 500 m, often the minor principal stress. The model is 1000 m wide with restraints in the x-direction of the vertical boundaries, restraints in the x- as well as y-direction at the bottom and no restrictions at the top. The tunnels were placed 37 m from the bottom of the model for all depths.

Parameters representative of quite a strong rock type, σ_{ci} = 125 MPa, E_i = 20 GPa and m_i = 28, were used as a basis for the rock mass parameter calculations. The rock parameters were adjusted for GSI values between 80 and 10, in intervals of 10, using the RocData software (Rocscience Inc., 2015a). *Generalized Hoek-Brown* was used as the strength criterion and *Generalized Hoek-Diederichs (2006)* was used for rock mass E-modulus (E_{rm}) estimation. The values for E_{rm} and in-situ rock stress used in the parameter study are shown in Table 1 and Table 2.

A plastic analysis was performed based on an ideally elastic-plastic material. Generalized Hoek-Brown was used as a failure criterion. The model had two stages, "initial" and "excavation", and the displacements were set to zero before "excavation" to ensure that only displacements from the excavation were registered.

Table 1 Main material properties for numerical modelling

GSI	E_{rm} [Mpa]	m_b
80	17607	13.7
70	14656	9.6
60	10400	6.7
50	6144	4.7
40	3193	3.3
30	1628	2.3
20	913	1.6
10	610	1.1

Table 2 Vertical and horizontal rock stresses at tunnel depth in the different models

Overburden [m]	σ_v [Mpa]	σ_h [Mpa]
35	0.9	4.1
100	2.7	4.8
200	5.4	5.9
300	8.1	8.1
400	10.8	10.8
500	13.5	13.5
600	16.2	16.2
700	18.9	18.9
800	21.6	21.6
900	24.3	24.3
1000	27.0	27.0

In Fig. 14, results for the model with a 500-m overburden and the GSI 20 material from the parameter study are shown as an example. The reported displacement values from all models are the maximum value in the left tube, marked in the example with a "+". The small difference between the tubes is due to the graded asymmetrical mesh.

Fig. 15 shows the results of the parameter study. The colours in the figure represent the different squeezing classes (Hoek, 2001), shown in Fig. 10:

- Green area represents no squeezing, sprayed concrete and rock bolts are described for support
- Orange represents minor squeezing, where you may need to add light lattice girders
- Red represents severe squeezing, where steel sets are recommended and you need to start to support the face
- Purple represents very severe squeezing, where forepoling, face reinforcement and steel sets are usually necessary

The results from the parameter study show that even very weak rock mass can be self-bearing using bolts and sprayed concrete for reinforcement, if the stresses are not too high. In the next section, which considers the impact of zone width, this tendency is shown to be even more distinctive for weakness zones with a potentially large reduction of deformations.

Basarir (2008) has done a similar study based on the Rock mass rating system (RMR) for a circular tunnel with overburdens from 100 to 500 m and rock support. The deformations from this study are generally comparable to the results shown in Fig. 15. In addition, simple

simulations using RocSupport software (Rocscience Inc., 2015b) that uses an analytical approach yielded comparable values.

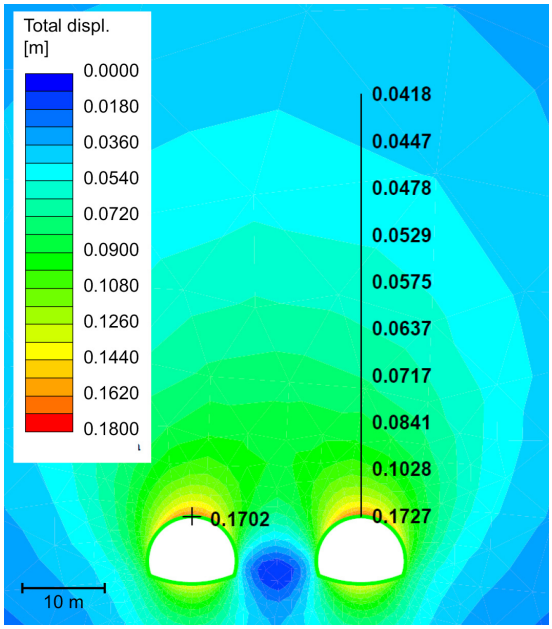

Fig. 14 Calculated deformations for a section of the model with a 500-m overburden and GSI 20. The deformations propagate far into the rock mass and the top displacement value is 50 m above the tunnel roof.

Overburden [m] \ GSI	80	70	60	50	40	30	20	10
35	2	2	3	6	11	23	43	74
100	2	2	3	6	11	22	40	69
200	3	3	5	8	15	31	60	106
300	4	5	7	12	23	48	92	170
400	6	7	9	16	32	66	131	249
500	7	8	12	21	40	85	170	340
600	8	10	14	25	50	106	227	451
700	10	12	17	30	60	130	271	585
800	11	13	19	34	69	148	315	696
900	13	15	22	39	80	174	370	857
1000	14	17	25	43	90	200	422	1030

Fig. 15 Displacement in mm of a 10.5-m wide tunnel with different overburdens and rock mass qualities. Green is strain under 1%, orange between 1 and 2.5%, red between 2.5 and 5% and purple above 5%. Fields with white text are the cases considered in the 3D model shown in Fig. 16 to Fig. 18.

4.2 Influence of zone width on deformations

A 2D model like the one used in the parameter study above calculated as if the material extends infinitely in and out of the screen/paper-plane. In Fig. 14, where the displacements for the model with 500 m overburden and GSI 20 are shown, one can see that the displacement propagates far into the rock mass. In that case, when one is interested in the behaviour of weak rock that appears as faults/weakness zones, one loses the possible restraint from stronger rock when the displacement extends further than where the stronger rock is probably present.

To show the effect of weakness zone width, two main models with 100- and 500-m overburden, and the same tunnel geometry as the 2D models, were created in the 3D numerical software RS3 (Rocscience Inc., 2017b). The models are 150 m in the tunnel direction and 500 m wide. In the middle of the models, a material with weaker rock mass properties than the surrounding rock is used as a weakness zone. The weakness zone is perpendicular to the tunnel direction and different models with zone widths of 50, 25, 10, 5, 2.5 and 1 m were made. See Fig. 16 a) for an example of the model. The materials were copied from the 2D model, where the surrounding rock is the material properties for GSI 80 and the weakness zone GSI 20 (see Table 1). In addition, the restraints, failure criterion, stresses, etc were the same as for the 2D model.

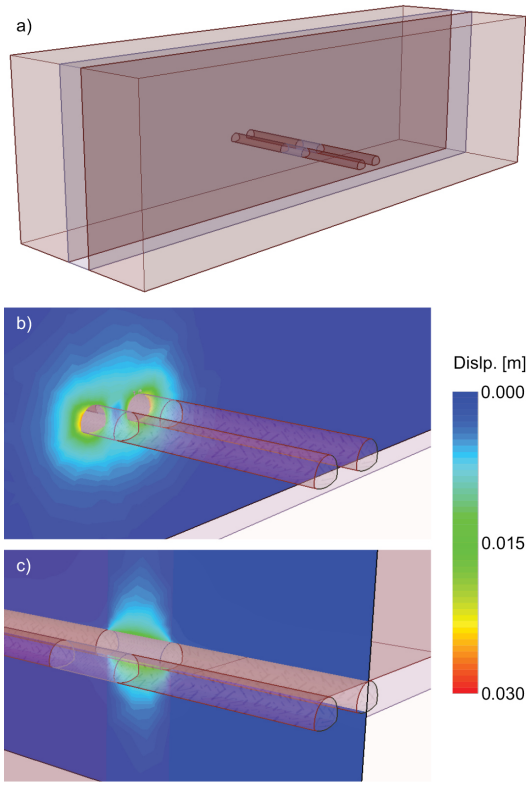

Fig. 16 3D model with an overburden of 100 m and a weakness zone width of 25 m. a) Model overview, b) Profile section in the middle of the zone, and c) Longitudinal section in the middle of the right tube.

To illustrate the distribution of displacement, a profile section of the middle of the zone and a longitudinal section along a tunnel tube for the 100-m overburden and 25-m zone width is shown in Fig. 16 b) and c). The zone width results are presented in Fig. 17 and Fig. 18, which show that displacement is strongly affected by zone width. The measurements are done high in the left wall (max. displacement) for the 100-m overburden and in the crown for the 500-m overburden. As the curves in the two figures have an almost identical distribution, it seems that the deformation for a certain zone width is strongly correlated to the deformation for a certain material/overburden combination (displacement values presented in Fig. 15). In looking at the 100-m overburden data, one can see that for the 2D data, representing an infinite zone width, the displacement is 40 mm (Fig. 15, overburden 100 and GSI 20), while for the 3D data and zone width of 1 m, the maximum displacement is 4 mm. For the 500-m overburden data, the 2D model yields a displacement of 170 mm,

while the 3D data for a 1-m zone width is 17 mm and the 3D data for a 5-m zone width is 39 mm. This means that when the zone becomes smaller than approximately 5 m, the deformations have moved from the severe squeezing class to the no squeezing class.

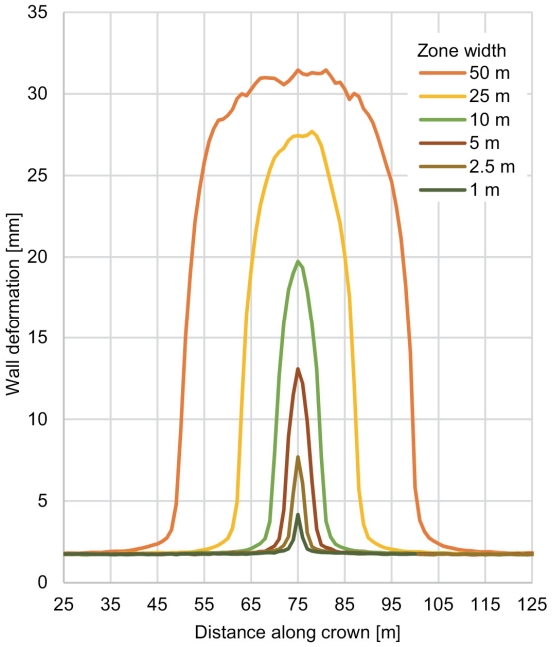

Fig. 17 Maximum displacement along a 150-m long tunnel section with different zone widths, for an overburden of 100 m. The centre of the zone is at 75 m.

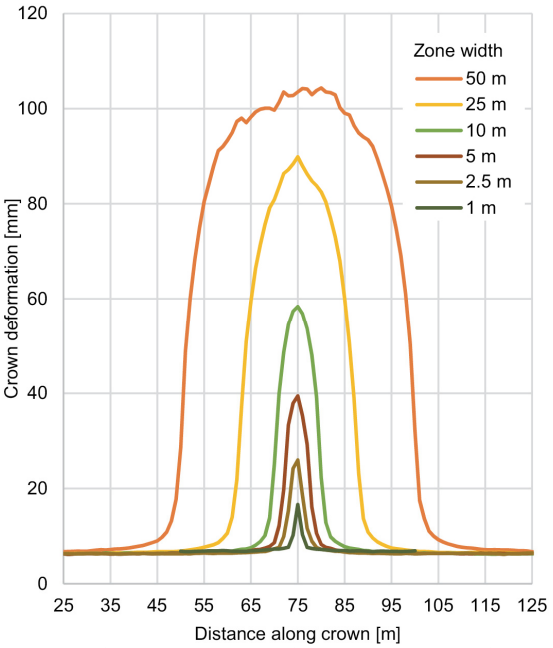

Fig. 18 Displacement at the crown along a 150-m long tunnel section, with different zone widths, for an overburden of 500 m. The centre of the zone is at 75 m.

5 Current support strategy for Norwegian road tunnels

As stated in Section 3.4, the Q-value is used for rock mass classification for road and railway tunnels in Norway. The rock support chart developed by the road authorities is largely based on the rock support chart in the Q-system (Pedersen et al., 2010) and the Q-system support chart is therefore also presented even if it is not directly used. The support strategy is subject to European design standards and the main principles from this standard are presented. In the discussion section, the current Norwegian support strategy will be debated and some possible changes will be suggested.

5.1 Rock support according to the Q-system

The Q-system support chart (see Fig. 19) is empirical when it comes to bolts and sprayed concrete, and mainly analytical regarding RRS. The support chart has been updated two times with about 2000 rock support/Q-value cases since the original publication in 1974 (NGI, 2015). The background for the RRS dimensioning is given in Grimstad et al. (2002), and is based on arched RRS.

For estimation of rock support using the support chart a parameter called "Equivalent dimension" is introduced, which is the span or height of the tunnel divided by the Excavation Support Ratio (ESR). The ESR expresses the safety requirements and is used to adjust for different rock support needs e.g. for a temporary mine opening versus a road tunnel.

In the handbook (NGI, 2015) on using the Q-system, it is stated that spiling should be used for Q-values lower than 0.6 to 0.1 and that at a Q_m (mean value) of the Q-value can be used for support of narrow weakness zones. The handbook also pointed out that one should be aware of discontinuities that form wedges in the crown and walls, and that the direction and placement of the bolts must be considered according to these discontinuities.

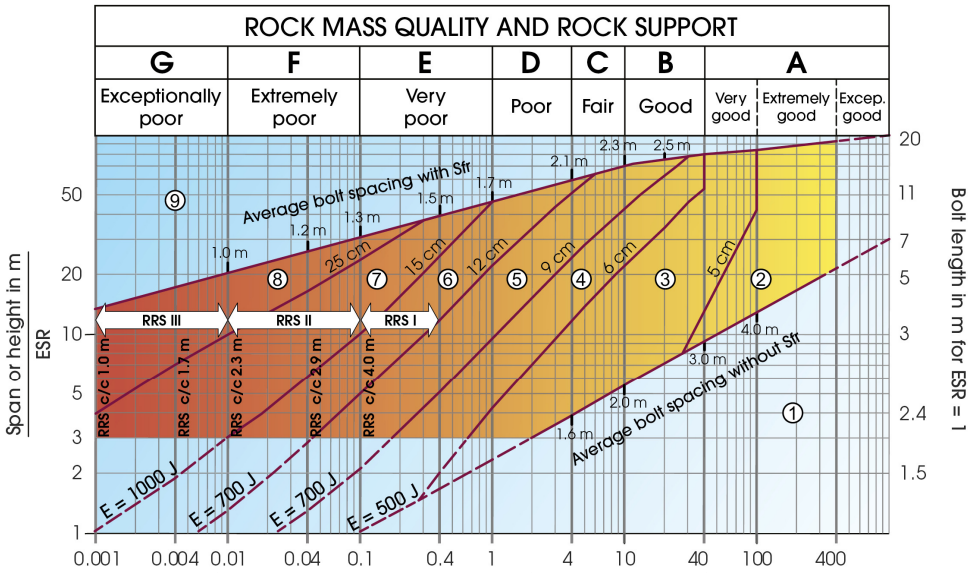

Fig. 19 The Q-systems rock support chart (NGI, 2015). For RRS dimensioning, see Table 3.

Table 3 RRS-classes in the Q system. Ex. D45/6+2 Ø16-20, Si = single rebar layer, D = double rebar layer, 45 = thickness in cm, 6+2 = 6 rebar in first layer, 2 in second, Ø16-20 = rebar diameter in mm. (NGI, 2015)

RRS class	5-m span	10-m span	20-m span
I		Si30/6 Ø16 - Ø20	D40/6+2 Ø16-20
II	Si35/6 Ø16-20	D45/6+2 Ø16-20	D55/6+4 Ø20
III	D40/6+4 Ø16-20	D55/6+4 Ø20	Special consideration

Table 4 Support table for Norwegian road tunnels developed by the NPRA (Pedersen et al., 2010; Statens vegvesen, 2016b)

Rock mass class	Rock conditions Q-value	Support class Permanent support
A/B	Weakly jointed rock mass Average joint spacing > 1 m. Q = 100 – 10	Support class I - Scattered bolting - Sprayed concrete B35 E700, thickness 80 mm
C	Moderate jointed rock mass Average joint spacing 0.3 – 1 m. Q = 10 – 4	Support class II - Systematic bolting, c/c 2 m - Sprayed concrete B35 E700, thickness 80 mm
D	Strongly jointed rock mass or bedded schistose rock Average joint spacing < 0.3 m. Q = 4 – 1	Support class III - Sprayed concrete B35 E1000, thickness 100 mm - Systematic bolting, c/c 1.75 m
E	Very poor rock mass. Q = 1 – 0.2 ---------- Q = 0.2 – 0.1	Support class IV - Systematic bolting, c/c 1.5 m - Sprayed concrete B35 E1000, thickness 150 mm ---------- - Systematic bolting, c/c 1.5 m - Sprayed concrete B35 E1000, thickness 150 mm - RRS: Rib dimension E30/6 Ø20 mm, c/c 2 – 3 m, Bolting along arch c/c 1.5 m, length 3 – 4 m - Invert cast concrete must be evaluated
F	Extremely poor rock mass. Q = 0.01 – 0.1	Support class V - Systematic bolting, c/c 1.0 – 1.5 m - Sprayed concrete B35 E1000, thickness 150 – 250 mm - RRS: Rib dimension D30/6+4 Ø20 mm, c/c 1.5 – 2 m Bolting along arch c/c 1.0 m, length 3 – 6 m Can be replaced with lattice girders - Invert cast concrete, pitch min. 10 % of tunnel width
G	Exceptionally poor rock mass Q < 0.01	Support class VI - Excavation and support design to be evaluated for each case

5.2 Rock support for Norwegian road and railway tunnels

The Norwegian Public Roads Administration (NPRA) has developed its own support table specially fitted to road tunnels safety levels, tunnel dimensions and durability requirements, as shown in Table 4. It was implemented in 2010 and incorporated into NPRA regulations N500 road tunnels (Statens vegvesen, 2016b), with more extensive descriptions in the V520 Road tunnels manual (Statens vegvesen, 2016a).

The NPRA requires the application of the Q-system for mapping Q-value and has defined support classes that are related to the NGI rock mass classes. In the NPRA regulations, general requirements regarding pre-investigations, rock mass classification and mapping during construction are described. Excavation and support toward and through weakness zones, support effect, design and execution of RRS (arched) are also described. The recommended support is integrated with the drilling and blasting excavation cycle and the dimensioning is largely based on the Q-system support chart.

5.3 Design according to Eurocode 7

According to EU rules, geotechnical design shall be done according to NS-EN 1997-1 Eurocode 7: Geotechnical design (Standard Norge, 2008), which Norway is also required to follow as an EEA member. There are generally four different approaches described for designing and dimensioning:

- Design by calculation
- Design by prescriptive measures
- Load tests and tests on experimental models
- Observational method

The most relevant approaches for Norwegian tunneling are prescriptive measures and the observational method. Prescriptive measures can be used e.g. if calculation models are not available. The measures should involve conventional and generally conservative rules in the design, and the strategies described in the two previous sections are usually associated with this approach.

The observational method is to be used e.g. if the prediction of the geotechnical behaviour is difficult. The main principle of this approach is to monitor, control and, if required, review or modify the design during construction. A typical approach is to have a monitoring strategy and a plan with established limits of behaviour and actions if the limits are exceeded.

The observational method is typically an alternative if one expects rock mass qualities of e.g. class G in Table 4, where an evaluation for each case is described. In the Frøya Tunnel, a case which will be discussed in some detail in Section 6.3, this principle was applied. The observational approach is also to a certain extent the basis for the New Austrian Tunneling Method (NATM), which is based on qualitative ground condition descriptions associated with excavation techniques and standard rock support requirements, with the rock as the essential load-bearing element. During and after excavation, the deformations are monitored to assess the stability of the tunnel (Maidl et al., 2013; Palmstrom and Stille, 2007).

Numerical modelling is commonly used as a tool for investigating the deformations, stresses and effects of rock support in more complex rock engineering conditions. The quality of input parameters is of great importance and if numerical modelling is used in the design of a specific case, one should always perform measurements during construction to verify the calculations.

6 Characteristics of rock mass quality, support and deformations in Norwegian road tunnels

In the following three sub-sections, data on the rock mass and support of present tunnels and deformation measurements performed in Norwegian tunnels will be presented. In addition, a case example of Norwegian road tunnel support from before the implementation of the NPRA support chart will be provided.

6.1 Rock cover, GSI and rock support

Since 2010, continuous registration of geology and rock support during excavations of Norwegian road tunnels has been mandatory, and the data have to be registered in a system called Novapoint Tunnel. After an excavation is completed, the data are stored in a national

tunnel database. In addition, the tunnel geometry and terrain surface are stored in the system making it possible to connect rock mass quality and overburden by chainage numbers. Currently there are data for 38 tunnels in the database.

Overburden [m] \ GSI	90	80	70	60	50	40	30	20	10
0-35	52	1805	3156	5172	4884	2391	815	78	22
35-100	33	2654	4627	4932	4491	1999	444	146	0
100-200	25	2098	5559	4867	1929	546	98	38	0
200-300	0	1152	2862	2721	1148	155	16	24	0
300-400	0	962	2265	2766	839	284	72	23	22
400-500	11	1027	1528	1858	517	84	47	23	0
500-600	10	1016	1291	566	237	104	13	15	0
600-700	0	415	222	101	50	5	0	0	0
700-800	0	562	97	41	0	0	0	0	0
800-900	31	1318	160	0	0	0	0	0	0
900-	0	0	0	0	0	0	0	0	0

Tunnel m
>2500
2500-250
250-50
<50

Fig. 20 Total tunnel meters excavated for 38 Norwegian road tunnels sorted according to GSI values and overburden. The green line marks the transition where the deformation according to Fig. 15 exceeds 1 %, with >1 % to the right of the line.

Overburden [m] \ GSI	90	80	70	60	50	40	30	20	10
0-35					15	50	206 / 20	15 / 35	22
35-100					5	13	40 / 5	83 / 30	
100-200						3	38	2	
200-300							10	24	
300-400								4	6 / 16
400-500						11	5	23	
500-600								15	
600-700									
700-800									
800-900									
900-									

Support classes
IVb
V
VI

Fig. 21 Tunnel meters supported with arched RRS for different GSI values and overburden for the same data set as in Fig. 20. The green line marks the transition where the deformation according to Fig. 15 exceeds 1 %, with >1 % to the right of the line.

For each blasting round during excavation, the Q-value and its six parameters are registered. These Q-values have been exported to Excel for all tunnels registered in the database. In addition the overburdens for the same tunnels have been exported and combined with the rock mass properties of each tunnel in Excel. All tunnels have then been imported into the statistics software SPSS (IBM Corp., 2013), resulting in a data set with about 14 000 cases, with each representing a Q-value/blast round and yielding a tunnel length of 85 km all together.

A GSI value has been calculated for each blasting round based on Eq.4. In Fig. 20 the tunnel lengths for different GSI values and overburden combinations are combined. As shown in the chart, the main weight is on relatively high GSI values (97.6% of the tunnel length is GSI 40 or above). Few cases have both low GSI value and high overburden.

Since the support class (shown in Table 4) corresponds to a certain Q-value interval for these tunnels, it is possible to sum up the length for a certain type of support. In Fig. 21, the use of arched RRS (classes IVb, V and VI) is shown for different combination of GSI and overburden. In Fig. 22, the total length for all support classes in the data set is shown. For example, one can see from Fig. 20 that 78 m of tunnel have been excavated in GSI 20 and with 0-35 m overburden, and from Fig. 21, that of these 78 m, 15 m have been supported with support class IVb and 35 m with V.

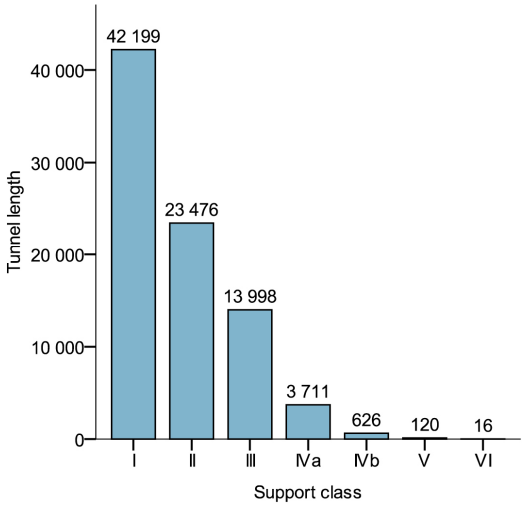

Fig. 22 Tunnel length and support measures for each class shown in Table 4.

6.2 Deformation monitoring

It is not very common to monitor deformations during tunnel excavations in Norway. In Table 5, however, deformation measurements from six different tunnels are presented. For all tunnels except the Frøya tunnel, the measured sections are supported with arched RRS. For the Frøya tunnel, which is discussed in more detail in Section 6.3, the measurements were used to evaluate the need for permanent support and the selection of different support measures. For the Rå and Sørås tunnels, very high swelling pressures were the main motivation factor for displacement surveillance.

As seen in the table, most deformations are very small with values lower than 1 mm. The largest values are approximately 20 mm. In considering the data, one must bear in mind that most measurements were done well behind the face and that rock reinforcement or support were already installed. The data will be further analysed in the discussion chapter.

Table 5 Displacement measurement data from Norwegian road and railway tunnels. Positive values are inward movement in mm. GSI values are calculated based on Eq. 4. In the horizontal or vertical displacement column, measurements done with an extensometer are vertical while the rest are horizontal. The diagonal displacement columns are measured from the wall on one side of the tunnel to the spring line on the other side.

Tunnel	Year	Method	Chainage	Hor or vert displ.	Diagonal displ. 1	Diagonal displ. 2	Instrument installation	Water/soil overburden	Rock overburden	Q-value	GSI
Finnfast subsea road tunnel	2008	Extensometer		1.1			At face	50	90	0.010	10
Bærum railway tunnel	2007	Extensometer	12782.5	0.3			Before pass	3.5	4.5	0.44	49
Løren road tunnel (TA)	2010	Extensometer	1220	2.16			Before pass	26	7	2.5	47
Løren road tunnel (TB)	2010	Extensometer	1220	2.39			Before pass	23	7	1.0	49
Sørås road tunnel (T51)	2016	Conv., tot. stat.	13171	1.2			face at 13177		32	0.25	34
Sørås road tunnel (T51)	2016	Conv., tot. stat.	13177	4.7	-2.6		at face		32	0.25	34
Rå road tunnel (T52)	2016	Conv., tot. stat.	13250	0.6			face at 13294		35	0.35	49
Rå road tunnel (T52)	2016	Conv., tot. stat.	13532	0.6			face at 13607		33	0.35	40
Rå road tunnel (T52)	2016	Conv., tot. stat.	13602	2.3			face at 13616		27	0.15	27
Frøya subsea road tunnel	1999	Convergence, tape	3440	13.50	0.65		30-60 m behind face		44	0.25	23
Frøya subsea road tunnel	1999	Convergence, tape	3992	0.70	4.40		30-60 m behind face	34	52	0.008	8
Frøya subsea road tunnel	1999	Convergence, tape	4003	0.45	1.68		30-60 m behind face	34	53	0.008	8
Frøya subsea road tunnel	1999	Convergence, tape	4012	0.75	3.09		30-60 m behind face	33	54	0.003	8
Frøya subsea road tunnel	1999	Convergence, tape	4820	0.39	-0.53		30-60 m behind face	25	121	0.19	23
Frøya subsea road tunnel	1999	Convergence, tape	5033	0.50	0.48		30-60 m behind face	34	114	0.13	18
Frøya subsea road tunnel	1999	Convergence, tape	5060	0.44	0.14		30-60 m behind face	32	117	0.19	23
Frøya subsea road tunnel	1999	Convergence, tape	5283	2.00	0.15		30-60 m behind face	31	120	0.18	24
Frøya subsea road tunnel	1999	Convergence, tape	5419	0.24	0.24		30-60 m behind face	41	112	0.13	25
Frøya subsea road tunnel	1999	Convergence, tape	5556	12.68	6.05	11.62	30-60 m behind face	50	104	0.20	27
Frøya subsea road tunnel	1999	Convergence, tape	5585	10.88	13.04	3.47	30-60 m behind face	55	101	0.15	23
Frøya subsea road tunnel	1999	Convergence, tape	6480	21.50			30-60 m behind face	36	100	0.025	13
Frøya subsea road tunnel	1999	Convergence, tape	6495	11.10	2.65	14.50	30-60 m behind face	36	100	0.017	11
Frøya subsea road tunnel	1999	Convergence, tape	6620	0.40	0.05		30-60 m behind face	24	104	0.10	18
Frøya subsea road tunnel	1999	Convergence, tape	6630	0.27			30-60 m behind face	24	103	0.050	21
Frøya subsea road tunnel	1999	Convergence, tape	6700	8.50	0.90		30-60 m behind face	24	101	0.11	24
Frøya subsea road tunnel	1999	Convergence, tape	6730	1.65	0.27		30-60 m behind face	24	100	0.042	16
Frøya subsea road tunnel	1999	Convergence, tape	6778	4.65	1.20		30-60 m behind face	24	98	0.33	28
Frøya subsea road tunnel	1999	Convergence, tape	6880	0.20	1.05		30-60 m behind face	25	91	0.027	15
Frøya subsea road tunnel	1999	Convergence, tape	6920	3.30	2.76	4.52	30-60 m behind face	25	88	0.013	10
Frøya subsea road tunnel	1999	Convergence, tape	6938	12.00	8.45	1.95	30-60 m behind face	25	88	0.050	17
Frøya subsea road tunnel	1999	Convergence, tape	7370	22.75	12.22		30-60 m behind face	22	61	0.022	16
Frøya subsea road tunnel	1999	Convergence, tape	7425	4.15	3.85		30-60 m behind face	21	57	0.008	8
Frøya subsea road tunnel	1999	Convergence, tape	7920	11.10	10.00		30-60 m behind face	.	31	0.015	10
Frøya subsea road tunnel	1999	Convergence, tape	8134	5.50	2.99		30-60 m behind face	.	19	0.15	29
Frøya subsea road tunnel	1999	Convergence, tape	8180	7.60	8.81		30-60 m behind face	.	16	0.25	28
Frøya subsea road tunnel	1999	Convergence, tape	8240	20.90	6.20		30-60 m behind face	.	11	0.13	23

6.3 Case example: The Frøya tunnel

The Frøya tunnel is a subsea road tunnel situated in Central Norway. The tunnel, which opened in the year 2000, has two lanes, a total length of 5300 m and its lowest point is 165 m below sea level. Geological pre-construction investigations indicated sections with very difficult rock conditions. An extensive follow-up arrangement was therefore designed, including continuous probe drilling, geological mapping, detailed registration of Q-values, deformation measurements and training for cave-in scenario. The mapped Q-values show that 1160 m of the tunnel were excavated in rock mass class E, 480 m were excavated in rock mass class F and 95 m were excavated in rock mass class G. As shown in Table 5, considerable time-dependent deformations were recorded during construction. According to the construction documentation, a large number of clay-rich weakness zones containing swelling clay were encountered (Statens vegvesen, 2000).

The Q-system rock support chart was not directly utilised during excavation, but comparisons between actual rock support and recommended support based on Q-values were conducted during excavation. Where large deformations could be expected, the deformations were measured using tape extensometers, and the recorded deformations were used as a basis to decide the final support.

Based on the recorded Q-values and rock support registered in Excel and as maps during construction, a dataset was produced in SPSS (IBM Corp., 2013) for this paper, systemizing the rock mass quality and the support for each tunnel meter.

To make the data more presentable, some categorizing was performed. For the plots in Fig. 23, the most extensive support for a tunnel meter determined the category. This means e.g. that a tunnel meter presented as RRS or cast concrete may also be supported with spiling. Some registrations in the transition between competent and weak rock have been omitted where heavy support has been used on a rock that was obviously too competent for this support. Invert cast concrete was used with all heavy support and excluded, as including it would double the number of categories.

An important point is that the RRS used in this project do not necessarily form a perfect arch but follow the blasted tunnel profile (unarched RRS). This means that only the cast concrete can be regarded as rock support in the sense that it will be load-bearing; the rest must be considered rock reinforcement. A few lattice girders were used in the Frøya tunnel and registered in this study as cast concrete. For more details regarding the support, excavation methods and measurements, reference is made to Holmøy and Aagaard (2002).

In Fig. 23, the different support measures are plotted with respect to rock mass quality. An important point to keep in mind while reading these diagrams is that consequences regarding the choice of support only can be observed with too little support, not too much. This means for instance that the use of cast concrete in the better part of the scale may not have been necessary, but the use of spiling in the poorer part of the scale actually worked. Some sections may also be over-supported in the transition between a “good” and “fair” rock and add the length of a more extensive support than necessary for the “good” rock.

As can be seen from the diagrams in Fig. 23, the weights of different support measures are arrayed in a reasonable order from light to heavy, with decreasing rock mass quality. It can also be observed that a considerable amount of bolt/sprayed concrete, spiling and RRS have been used as support in more or less all rock qualities. This indicates there may be factors

that are not identified by the input parameter, but have a significant impact on the required support.

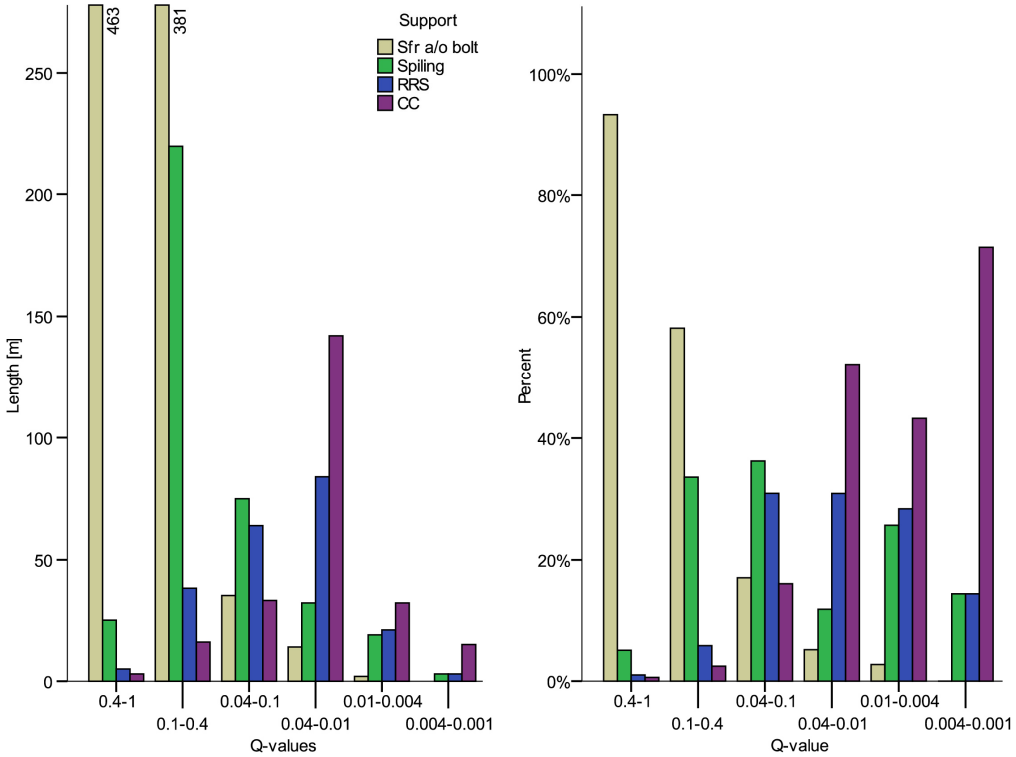

Fig. 23 Distribution of types of permanent support in weak rock in the Frøya tunnel. The diagram to the left shows the actual tunnel length supported with the different support measures and the diagram to the right shows the same information in percentages.

7 Discussion and conclusion

In the following section, the theory and data presented in previous sections will be discussed to consider the present use and possible changes in rock support for Norwegian tunnels, with a focus on deformations.

According to the critical strain concept, Norwegian hard rocks will have small deformations when they fail, and since they have high uniaxial compressive strength, they can withstand high rock stresses before that happens. The critical strain increases when considering rock mass compared to rock/cores, as shown by Sakurai (1983). Considering the reduction of E-modulus and uniaxial compressive strength for rock masses compared to rock mass quality, according to Hoek and Diederichs (2006) and Hoek et al. (2002), one can assume that the reduction in critical strain is also dependent on rock mass quality.

A relationship between rock mass strength and in-situ stress and the expected deformation of the tunnel was established by Hoek and Marinos (2000), as shown in Fig. 10. Based on their own and Sakurai's (1983) work, they stated that it seems a tunnel closure of 1% is a limit for where one needs to consider supporting the rock with more than bolts and sprayed concrete. Further, they stated that bolts and sprayed concrete may be sufficient even at up to 2.5% tunnel closure.

One subject which is not closely considered in the before mentioned method is the presence of swelling rock mass. While squeezing, according to Einstein (1996), is time-dependent shearing of the ground, swelling is time-dependent volume increase. Swelling in the Norwegian geological conditions will either originate from negative pore pressure due to stress changes or from the hydration and osmosis of minerals of the smectite-group. Consolidation with the exertion of water may also occur for some stress states. Einstein (1996) indicated that swelling and squeezing are closely connected and that shear failure occurs simultaneously with swelling. He also indicated that much of the deformation is probably due to shear failure and not due to swelling.

Fig. 12 indicates how deformations, according to Hooke's law, will occur for E-modulus and stress values related to tunnelling. The plot shows that if large deformations are to be expected, both quite low E-modulus and high stresses are needed, and that even rock with a very low E-modulus does not necessary deform much if the stresses are reasonable low. It also shows that for rock masses with a low E-modulus, only a small change has a large impact on the strain, making models with such rocks very sensitive to the input values compared to models with high E-modulus.

The same pattern can be recognised in the parameter study presented in Fig. 15. It shows that both quite a large overburden and a weak rock mass must be present to cause deformations that required more than bolts and sprayed concrete for rock support, according to the limits suggested by Hoek and Marinos (2000). The deformations presented from the parameter study suppose that the material parameters are constant along the tunnel axis. When the deformations are large, they propagate quite far out from the tunnel periphery. To show how a side rock of a better quality would affect the deformations, models with 100 and 500 m overburden were created in 3D, simulating a perpendicular weakness zone with GSI 20 of different widths with side rock of GSI 80 material. As shown in Fig. 17 and Fig. 18, the zone width has a substantial effect on the deformations, wherein a 10- and a 2.5-m wide zone at maximum only have about 60% and 25% of the deformation of the 50-m zone.

The before mentioned work by Hoek and Marinos (2000) is based on a circular tunnel profile. An important point regarding this work is that the tunnel profile does not seem to have a substantial effect on deformations when it is semi-circular, as in this case, since calculations in RocSupport and the study done by Basarir (2008), both based on a circular tunnel profile, show similar results. A probable reason is that the deformations distribute far into the rock and effects from the actual tunnel profile are redistributed.

In Table 5, deformation measurements from some Norwegian tunnels are presented. The values are generally a few mm and the largest deformations are from the Frøya tunnel, with maximum values of approximately 20 mm. For the Frøya tunnel, measurements were done well behind the face and therefore only the "tail" of the total deformation was registered. Since the tunnel face was at least 30 to 60 m away from the measurement point, it is not probable that the tunnel advance was causing the deformations, but rather time-dependent squeezing/creep/swelling and stress redistribution. Practically all the zones in the tunnel contained swelling clay.

The rock in Norway, as shown in Fig. 4 and Fig. 5, is mainly strong (50-100 MPa) and very strong (100-250 MPa) and has E-modulus in the range of 25 to 50 GPa. The rock mass is usually of a quality that is easy to support, meaning bolts and sprayed concrete are sufficient. Of the total tunnel length of 84 100 m in the Norwegian tunnel database, only 760 m (<1%) had a Q-value lower than 0.2, which implies the use of arched RRS (see Fig. 22). As a

comparison, the Frøya tunnel had 1230 m with Q-values lower than 0.2 of a total length of 5300 m and must be considered an extraordinary case.

The distribution of rock mass quality and overburden of recently opened tunnels in Norway is presented in Fig. 20. The axis of this figure has the same designation as Fig. 15. In considering the data in these figures, one can see that far most of the excavated tunnel length are in the green area where only small deformations are expected. If one in addition considers Fig. 15 one can see that most of the RRS is used in conditions that the parameter study suggests only reinforcement of the rock, not support. One should also have in mind that most of the weak rock appears in zones with the possible reduction that may give on the deformations.

Looking at the support data from the Frøya tunnel (see Fig. 23), where the Q-system support chart was not directly used, one can see that the different types of support overlap considerably in the different Q-value intervals. However, it seems that the support methods for each rock mass quality come in a reasonable order, ranging from lighter to heavier. But still, they do not effectively distinguish what type of support is needed for a certain value and it seems there must be processes that are not included by the input parameters in the Q-system but impact the necessary support, or that the parameter values are not weighted properly. To summarize, the rock mass that requires support for large deformations is not well distinguished from the rock mass that only requires reinforcement.

As shown in the parameter study, stress has a great influence on the expected amount of deformation and 3D analysis demonstrated that when a weak rock mass occured in a zone surrounded by more solid rock, the zone width had a significant impact on the deformation. The Q-value is supposed to consider this through the SRF parameter, which is split into four categories: weakness zones (values 2.5-10), squeezing (values 5-20), swelling (5-15) and competent rock, including rock burst. A main issue is the value ranges. As seen in the parameter study and in Hoek and Marinos (2007) squeezing classes, the problems caused by deformations exist within a larger range than these values take into account. The SRF parameter considers input on both rock mass and stress, which is not favourable when used for support analysis, since it seems rock mass and stress should be handled separately in the more extreme cases.

Both the support chart for the Q-system (see Fig. 19) and the NPRA support table (see Table 4) describe arched RRS for the support of all weak rock mass from Q=0.4 and Q= 0.2, respectively. This is also the limit where it is recommended that one start to use spiling bolts to keep the rock in place after blasting. For the Q-system, this limit is partly based on the data from the Frøya tunnel and one can see in Fig. 23 that they started to use spiling in the Q-value interval 0.4 to 0.1. As described for the Frøya tunnel above, spiling and non-arched RRS are used for all rock classes. On the basis of the parameter studies and the Frøya tunnel data, one can assume that these reinforcement measures are sturdy enough to avoid gravitational collapses due to cracked rock and unstable wedges, and also, to a certain degree, weakness zones containing swelling clay for cases with stresses expected reasonable near the surface.

Holmøy and Aagaard (2002) recommended that cast concrete should replace unarched RRS for block falls, inadequate hold for radial bolts in the RRS, clay in combination with water and when the deformation did not stop. The current practice is that cast concrete is practically never used but is replaced with arched RRS. Their reason not to use RRS for block falls is that it is expensive to fill the cavity with sprayed concrete, which is the common practice today if more than bolts and concrete are needed. To update their

recommendation to current practices would then be to advise the use of arched RRS when the hold for radial bolts is inadequate and when deformations do not stop.

As discussed in the section above, the deformations in Norwegian tunnels are generally very small. This also applies for weak rock mass that is not too far below the surface. For large deformations requiring load-bearing support to occur, an unfavourable combination of weak rock and stresses is required. Since it seems that the deformations propagate far into the rock mass, the extent of the weak rock is also of significance for the actual deformations.

The literature suggests that a strain between 1 and 2.5% is the limit between the rock mass being reinforced and self-bearing to requiring support by load-bearing constructions. The currently most used system for rock mass classification and support decision making in Norwegian tunnelling does not seem to distinguish well between these two different concepts and describes load-bearing support for all weak rock, while it seems that for weak rock with reasonable stresses, reinforcement would be sufficient. The data showing rock mass quality with the overburden suggest that most of the constructed tunnel length by far belongs to the category where only reinforcement (bolts, sprayed concrete, spiling and unarched RRS) is required.

Through the introduction of RRS in the Q-value support chart and in the NPRA support table, a considerable increase in support has occurred. If an effort had been made to identify under what conditions weak rock needs load-bearing support and under what conditions reinforcement is sufficient, a downscaling of heavy support for many tunnelling conditions would very likely be possible. A solution could be that for instance when the Q-value is below 0.4, one should also map the GSI. The GSI value could be considered with stresses and zone properties, such as width, heterogeneity and tunnel axis angle, to evaluate if a load-bearing construction is necessary and convergence measurements could be used to confirm support design.

The Frøya, Rå and Sørås are tunnels where large deformations were expected and/or one wanted to ensure the stability. These tunnels, especially the Frøya tunnel, are examples of cases in Norwegian tunnelling where a more NATM-like approach was applied, using measurements for design and confirmation of design. With the use of total stations for convergence measurement, instead of the old tape extensometers, one could quite easily conduct more measurements than usual for Norwegian tunnelling to confirm stability. A systematic registration of measurements and rock mass properties could be used as background data for a potential new support dimensioning in weak rock.

Considering the current dimensioning in Norwegian road tunnelling and bearing the previous information in mind, it seems that support with arched RRS for all conditions below Q-value 0.2 is not necessary and a system that is more adapted to the actual deformation conditions should be considered.

References

Bane NOR, 2018. Technical regulations. https://trv.jbv.no/wiki/Forside. Accessed 30.01.2018

Barton, N., Lien, R., Lunde, J., 1974. Engineering classification of rock masses for the design of tunnel support. Rock mechanics 6, 189-236. doi:https://dx.doi.org/10.1007/bf01239496

Basarir, H., 2008. Analysis of rock–support interaction using numerical and multiple regression modeling. Canadian Geotechnical Journal 45, 1-13. doi:https://doi.org/10.1139/t07-053

Bowles, J.E., 1997. Foundation analysis and design, 5 ed. McGraw-Hill, Auckland.

Brown, E.T., Hoek, E., 1978. Trends in relationships between measured in-situ stresses and depth. Int J Rock Mech Min 15, 211-215. doi:https://doi.org/10.1016/0148-9062(78)91227-5

Carranza-Torres, C., Fairhurst, C., 1999. General formulation of the elasto-plastic response of openings in rock using the Hoek-Brown failure criterion. International Journal of Rock Mechanics and Mining Sciences 36, 777-809

Duncan Fama, M., 1993. Numerical modelling of yield zones in weak rocks., in: Hudson, J.A. (Ed.), Comprehensive rock engineering. Pergamon, Oxford, pp. 49-75.

Einstein, H.H., 1996. Tunnelling in difficult ground - Swelling behaviour and identification of swelling rocks. Rock Mech Rock Eng 29, 113-124. doi:https://doi.org/10.1007/bf01032649

Grimstad, E., Kankes, K., Bhasin, R., Magnussen, A.W., Kaynia, A.M., 2002. Rock mass quality used in designing reinforced ribs of sprayed concrete and energy absorption, Bergmekanikkdagen. NFF, NBG, NGF, Oslo, pp. 39.31 - 39.19.

Herget, G., 1988. Stresses in rock. Balkema, Rotterdam.

Hoek, E., 1994. Strength of rock and rock masses. ISRM News Journal 2, 12

Hoek, E., 1999. Support for very weak rock associated with faults and shear zones, International Symposium on Rock Support and Reinforcement Practice in Mining, Kalgoorlie, Australia.

Hoek, E., 2001. Big tunnels in bad rock. J Geotech Geoenviron 127, 726-740. doi:https://doi.org/10.1061/(ASCE)1090-0241(2001)127:9(726)

Hoek, E., 2006. Practical Rock Engineering, www.rocscience.com.

Hoek, E., Carranza-Torres, C., Corkum, B., 2002. Hoek-Brown Failure Criterion – 2002 Edition NARMS-TAC Conference, Toronto, pp. 267-273.

Hoek, E., Carter, T., Diederichs, M., 2013. Quantification of the Geological Strength Index Chart, 47th US Rock Mechanics / Geomechanics Symposium. ARMA, San Francisco.

Hoek, E., Diederichs, M.S., 2006. Empirical estimation of rock mass modulus. International Journal of Rock Mechanics and Mining Sciences 43, 203-215. doi:http://doi.org/10.1016/j.ijrmms.2005.06.005

Hoek, E., Kaiser, P.K., Bawden, W.F., 1997. Support of underground excavations in hard rock, 3rd ed. A.A. Balkema, Rotterdam.

Hoek, E., Marinos, P., 2000. Predicting tunnel squeezing problems in weak heterogeneous rock masses, Tunnels & Tunnelling International Polygon Media Ltd, London.

Hoek, E., Marinos, P., 2007. A brief history of the development of the Hoek-Brown failure criterion. Soils and Rocks 30

Holmøy, K.H., Aagaard, B., 2002. Spiling bolts and reinforced ribs of sprayed concrete replace concrete lining. Tunnelling and Underground Space Technology 17, 403-413. doi:https://doi.org/10.1016/S0886-7798(02)00065-2

IBM Corp., 2013. IBM SPSS Statistics for Windows, 22 ed. IBM Corp., Armonk, NY.

ISRM, 1978. Suggested methods for the quantitative description of discontinuities in rock masses. Int J Rock Mech Min 15, 319-368. doi:https://doi.org/10.1016/0148-9062(78)91472-9

Maidl, B., Thewes, M., Maidl, U., Sturge, D.S., 2013. Handbook of Tunnel Engineering I : Structures and Methods. Wiley, Hoboken.

Myrvang, A.M., 1993. Rock Stress and Rock Stress Problems in Norway, in: HUDSON, J.A. (Ed.), Rock Testing and Site Characterization. Pergamon, Oxford, pp. 461-471.

Myrvang, A.M., 2001. Bergmekanikk. Norwegian University of Science and Technology, Department of Geology and Mineral Resources Engineering, Trondheim.

NBG, 1985. Ingeniørgeologi Berg. Tapir, Trondheim.

NGI, 2015. Using the Q-system - Rock mass classification and support design. Norwegian Geotechnical Institute, Oslo.
Palmstrom, A., Stille, H., 2007. Ground behaviour and rock engineering tools for underground excavations. Tunnelling and Underground Space Technology 22, 363-376. doi:https://doi.org/10.1016/j.tust.2006.03.006
Pedersen, K.B., Kompen, R., Kveen, A.T., 2010. Arbeider foran stuff og stabilitetssikring i vegtunneler, Teknologirapport. Norwegian Public Roads Administration, Oslo.
Rocscience Inc., 2015a. RocData, 5.006 ed. Rocscience Inc., Toronto.
Rocscience Inc., 2015b. RocSupport. Rocscience Inc, Toronto.
Rocscience Inc., 2017a. RS2, 9.025 ed. Rocscience Inc, Toronto.
Rocscience Inc., 2017b. RS3, 2.008 ed. Rocscience Inc, Toronto.
Sakurai, S., 1981. Direct Strain Evaluation Technique In Construction Of Underground Opening, The 22nd U.S. Symposium on Rock Mechanics (USRMS). American Rock Mechanics Association, Cambridge, Massachusetts.
Sakurai, S., 1983. Displacement Measurements Associated With The Design Of Underground Openings, International Symposium on Field Measurements in Geomechanics, Zurich, pp. 1163-1178.
Sheorey, P.R., 1994. A theory for In Situ stresses in isotropic and transverseley isotropic rock. Int J Rock Mech Min 31, 23-34. doi:https://doi.org/10.1016/0148-9062(94)92312-4
SINTEF, 2016. Rock mechanic properties of rocks tested in Sintef Rock mechanics laboratory, in: Infrastructure, S.B.a. (Ed.).
Standard Norge, 2008. Eurocode 7: Geotechnical design. Part 1: General rules, Eurocode 7: Geotechnical design. Part 1: General rules. Standard Norge Standard online, Lysaker.
Statens vegvesen, 2000. Sluttrapport for fastlandsforbindelsen Hitra Frøya. Statens vegvesen.
Statens vegvesen, 2016a. Tunnelveiledning, in: vegvesen, S. (Ed.), V520, Oslo.
Statens vegvesen, 2016b. Vegtunneler, in: vegvesen, S. (Ed.), N500, Oslo.
Zhu, T., 2012. Some Useful Numbers on the Engineering Properties of Materials. Department of Geophysics, Stanford University, California.

Paper III

Høien, Are Håvard[a]
Nilsen, Bjørn[b]
Vistnes, Gunnar[b]
Olsson, Roger[c]

Experimental triaxial testing of swelling gouge materials

[a] Norwegian University of Science and Technology, Sem Sælands veg 1, 7491 Trondheim, Norway and Norwegian Public Roads Administration, Postboks 8142 Dep, 0033 Oslo, Norway, are.hoien@vegvesen.no, Phone: +47 918 57 071, ORCID 0000-0001-5478-6377
[b] Norwegian University of Science and Technology, Sem Sælands veg 1, 7491 Trondheim, Norway
[c] Norwegian Geotechnical Institute, P.O. Box. 3930 Ullevål Stadion, 0806 Oslo

Abstract
Adequate rock support in weakness zones that may contain swelling minerals often poses one of the main challenges of excavating tunnels in hard rock conditions. Deformations under such conditions are influenced by several factors, such as the properties of the rock mass, rock stress and the possible swelling potential of the minerals. Thus, dimensioning rock support may be challenging. To increase the knowledge regarding the processes behind deformations in areas of swelling gouge material, an experimental triaxial laboratory test of such material was performed. The main objective was to investigate whether the material may exert pressure under typical in-situ stress conditions or if other processes may be dominant. In addition, the possible elastic and strength properties of such material were indicated. The testing was done on reconstituted cores with material from four different locations in Eastern Norway. The material was dried and then pressed into cores using a compactor. The triaxial testing consisted of four subsequent phases: pre-stressing 1; water addition under constant strain; pre-stressing 2 and failure. The results indicate that factors other than swelling pressure are the main causes of tunnel deformation, as no build-up of swelling pressure was observed during the water addition phase. At first, the E-modulus and strength properties of the samples were very low, which can cause large, immediate deformations in-situ. Furthermore, creep and possibly a reduction of the E-modulus during water addition seemed to cause time-dependent deformations.

Keywords:
Swelling; swelling gouge; weakness zone; triaxial test; deformation

1 Introduction

When tunnelling in hard rock conditions, one of the main challenges is often related to weakness zones containing swelling minerals. Time-dependent deformations, such as swelling and squeezing, are often particularly difficult to cope with. The dimensioning of rock support under such conditions is a challenging task since these deformations are influenced by various factors, such as rock mass quality, rock stresses and swelling pressure. To increase the knowledge of the process behind these deformations regarding swelling, an experimental triaxial laboratory test of reconstituted cores of swelling gouge material has been performed.

A weakness zone gouge may have properties varying within wide ranges and in many cases it has a character similar to moraine. The gouge represents a mix of grain sizes ranging from clay to gravel, and even blocks, and with low to none degree of bonding between the individual grains (Rokoengen 1973). As will be shown later, materials tested in this study are categorized as sandy, gravely and clayey. For materials of this category, the pore pressure and the flow of water may be of great significance with respect to the deformations.

Basically, there are two main types of deformations: immediate and time-dependent (Terzaghi and Peck 1967; Bellwald 1990; Barla 1999), see Fig. 1. The immediate deformations are caused by the in-situ stress, and stress changes that occur due to tunnel excavation, and are dependent on the elastic and plastic mechanical properties of the material. These deformations, which occur in the undrained phase, may result in positive and negative excess pore pressures around the tunnel when the material has a large portion of fine grains. The main types of time-dependent deformations are (mineral) swelling, squeezing, creep, consolidation and mechanical swelling. If certain conditions are present, drained behaviour may occur and as Bellwald (1990) pointed out, the material will either swell or consolidate depending on whether water flows into the material (negative excess pore pressure) or out of it (positive excess pore pressure), resulting in a volume increase or decrease.

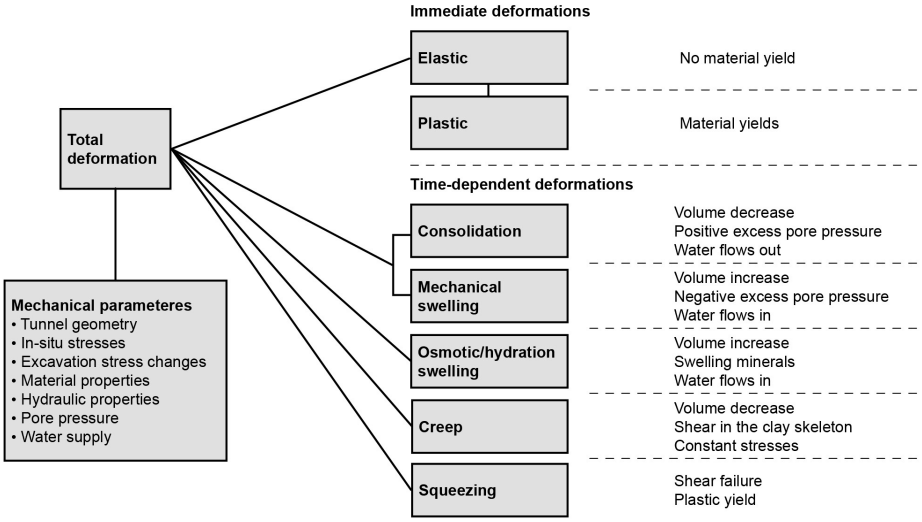

Fig. 1 Types of deformation in weakness zones. Due to the different stress states around a tunnel, different processes may take place at the same time at different locations, and even more than one may occur at the same location

The two main categories of mineral swelling for a gouge material are hydration and osmotic (Barla 1999; Einstein 1996; Bellwald 1990; Selmer-Olsen 1985; Aristorenas 1992). The swelling is in most cases caused by minerals of the smectite group, which most commonly

originate from the weathering of feldspar. The hydration is adsorption of water due to the exchangeable cations between individual clay layers. Osmotic swelling happens between the grains and is driven by the ion concentration difference between grain surfaces and the pore water. The swelling takes place in two stages, with the hydration as the first, followed by the osmotic.

Both swelling and squeezing are common causes of tunnel convergence and Einstein (1996) pointed out that these phenomena are often strongly interrelated and that one may lead to the other. He also provided short definitions for the two, where swelling is defined as the *"Time-dependent volume increase of the ground, leading to inward movement of the tunnel perimeter"* and squeezing is defined as the *"Time-dependent shearing of the ground, leading to inward movement of the tunnel perimeter"*.

Creep is defined as deformations under constant load and occurs after or, under some conditions, at the same time as consolidation. It involves three phases: primary, secondary and tertiary. There are two types of creep associated with these phases: volumetric creep caused by volumetric stress and deviatoric creep caused by deviatoric stress. The primary creep phase is a result of volumetric creep and possibly deviatoric creep if the deviatoric stresses are large enough. Either the rate of strain during primary creep will fade out, and the creep stop, or it decreases until the strain/time is constant. If the rate turns constant, the creep process enters the secondary phase caused by deviatoric creep. Deviatoric creep is a time-dependent shear deformation caused by a serial change in the soil structure caused by rearrangement of the grain contacts. If the creep rate increases rather than fading out, the tertiary phase is entered. The tertiary phase is also caused by deviatoric creep and is important to avoid since it leads to failure.

The in-situ rock stresses are very important for determining which of the above processes that will be dominant. Many researchers (Sheorey 1994; Hoek 2006; Herget 1988; Brown and Hoek 1978; Myrvang 2001) have found that the horizontal stresses near the surface are much larger than they would have been if they were only induced by gravitation. For a case where the ratio between horizontal and vertical stresses, k, is larger than 1, the stresses around the tunnel profile generally will be larger at the crown/invert than the walls. The selected start parameters of the triaxial testing reported in this article are of a range corresponding to a tunnel with approximately k=2 at a depth of approximately 50 m. An important point is that the tests does not try to fit these conditions or a stress path for an advancing tunnel exactly. The main intention has rather been to investigate how the material reacts under the given conditions in order to observe whether swelling can be detected.

Some researchers, including Bellwald (1990), Aristorenas (1992) and Barla (1999), have done triaxial testing on weak rock materials, with focus on testing and tunnel deformation. Yeşil et al. (1993) and Bilir et al. (2008) have described triaxial apparatus and procedures with a focus on finding the swelling characteristics of clay-bearing rock. Wild et al. (2017) have described a multi-stage triaxial procedure for low permeable geomaterials. However, no literature describing research on the behaviour of swelling gouge material from weakness zones under triaxial loads has been found, and a procedure for investigating this issue, with main focus on the swelling process was therefore developed.

The testing was done on reconstituted cores of weakness zone material from four different locations in the eastern part of Norway. The material was dried before reconstituted into cores using a compactor. The triaxial testing consisted of four main phases: 1) pre-stressing 1; 2) water addition under constant strain; 3) pre-stressing 2 and 4) failure.

In addition testing of UCS, swelling pressure in oedometer, and testing of free swelling, grain size distribution and density have been carried out.

The main objective of the triaxial testing described in this paper was to investigate whether swelling gouge material may exert pressure under typical in-situ stress conditions or whether other processes may be dominant. An important objective was also to investigate the material properties, deformability and strength of the swelling gouge material. Very little information is today available in the literature on these parameters, and increased knowledge will provide a better basis to estimate elastic and plastic deformation behaviour.

2 Test material characteristics

Bulk samples of weakness zone materials were collected at four different locations; see Table 1. The samples from Larvik and Drammen represent weakness zone gouge materials from Permian intrusive rocks, monzonite and granite, respectively. The Åsland and Bjørkelangen samples both represent weakness zone materials from Pre-Cambrian gneiss. See Fig. 2.

Table 1 Localities of the different materials

Location number	Test location	Surrounding rock	County
1	Larvik	Monzonite	Vestfold
2	Åsland	Gneiss	Oslo
3	Bjørkelangen	Gneiss	Akershus
4	Drammen	Granite	Buskerud

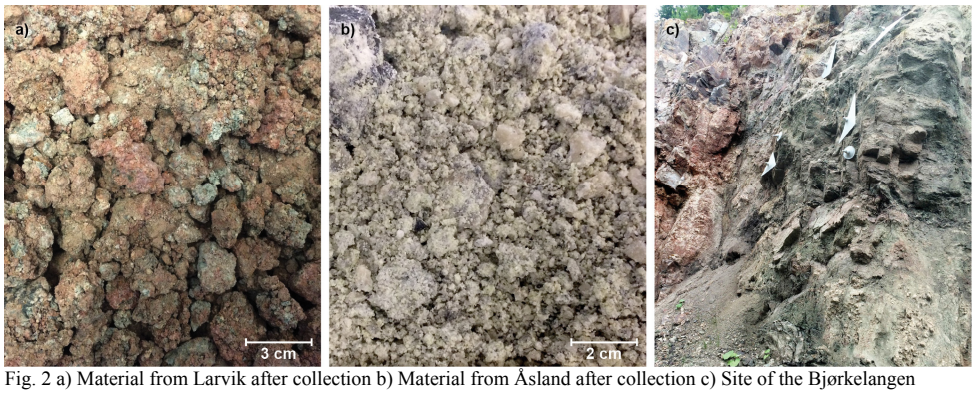

Fig. 2 a) Material from Larvik after collection b) Material from Åsland after collection c) Site of the Bjørkelangen material. The Drammen material is shown in Fig. 4

2.1 Swelling pressure and free swelling

Testing of swelling potential of the gouge material has been done according to Norwegian methodology developed at NTNU, as described in Mao et al. (2011), Nilsen (2016) and others. Briefly explained, for the swelling pressure test 20 g material of the < 20 µm fraction was placed in a 20 cm^2 steel ring and then compacted with a pressure of 2 MPa. The pressure was released and after the expansion caused by the unloading had stopped, the height was set to be constant and water was added. During the swelling process no expansion of the material was permitted and swelling pressure was determined as the final pressure build up.

In the free swell test, the material was prepared in the same manner as for the swelling pressure test described above. Ten ml of loosely packed material was poured into a 50-ml

graded cylinder filled with distilled water and the new volume measured after sedimentation. The free swelling is the volume after sedimentation divided by the dry volume, given as a percentage.

The results of swelling pressure and free swelling tests are shown in Table 2. The swelling pressures obtained from oedometer tests are medium to high (0.1-0.3 MPa and 0.3-0.75 MPa respectively), and the free swelling values high and very high (140-200% and >200% respectively) according to Norwegian classification standards (NBG, 1985). Differences in the categorization between the methods may come from different content of types of montmorillonite, especially Na-montmorillonite (Kocheise 1994).

Although the results in Table 2 are valuable for classification and for evaluating swelling potential, it has to be realized that these test are only index tests, and that the resulting swelling pressures due to sample preparation and discrepancies from in-situ conditions cannot be used directly for dimensioning of support structures.

Table 2 Swelling properties from oedometer and free swelling tests

Number	Location	Swelling pressure [MPa]	Swelling pressure classification	Free swelling [%]	Free swelling classification
1	Larvik	0.43	High	188	High
2	Åsland	0.18	Medium	142	High
3	Bjørkelangen	0.39	High	290	Very high
4	Drammen	0.21	Medium	180	High

2.2 Material grading

For the determination of material grading, wet sieving and sedimentation analysis (< 63 µm) was done according to Statens vegvesen (2016).

Material grains >4 mm were removed in order to facilitate homogeneity in the cores for triaxial testing. As indicated by the material grading curves in Fig. 3, this means that between 70 and 80% of the original material was included in the triaxial testing. As also shown by Fig. 3, materials 1, 2 and 4 have quite similar grain size distributions, while 3 has a larger portion of sand than the others. The material from location 1 is defined as gravely, sandy, clayey material, while locations 2, 3 and 4 are defined as gravely and sandy.

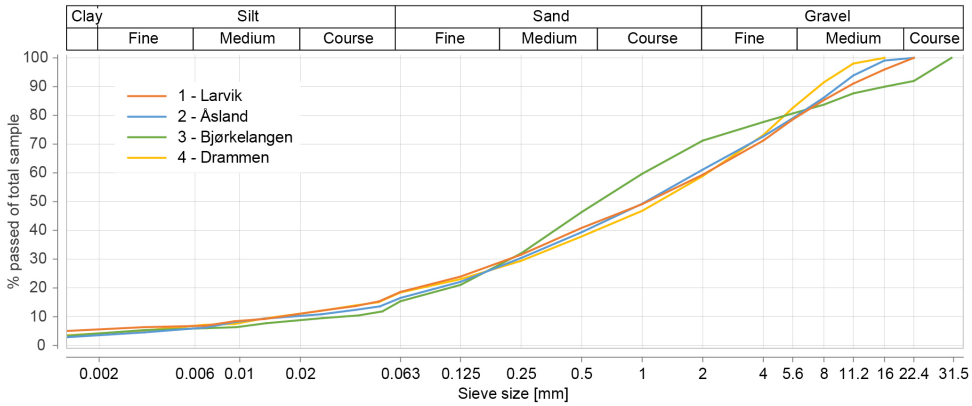

Fig. 3 Grain size distributions of the materials from the four different locations

2.3 Density

Two different methods were used to find the density, depending on the hardness of the sample. For soft materials, a density cylinder with a known volume was pushed into the material and weighed after drying according to Statens vegvesen (2016). See Fig. 4.

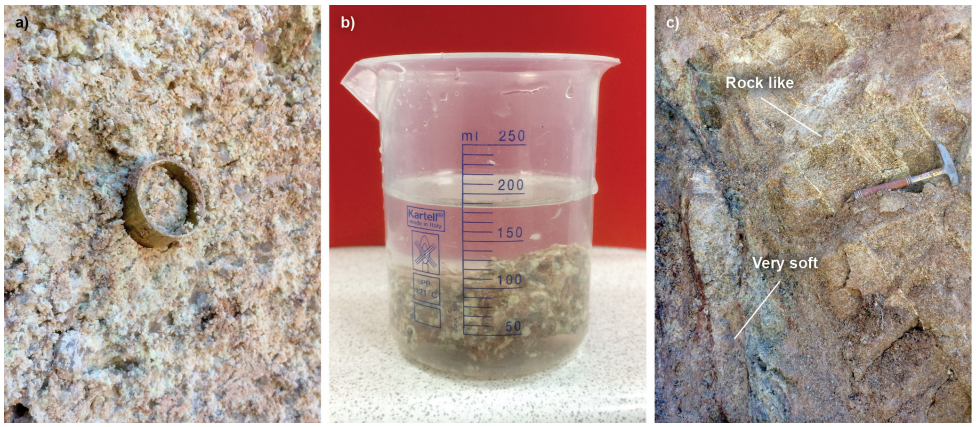

Fig. 4 Sampling density of different types of weakness zone materials. Samples in a) and b) were collected in the very soft and rock-like areas, respectively, both of which are marked in c)

The more solid samples were submerged in water to find the volume. The water volume was determined from photos, for an as accurate as possible recording, taken before and after submergence. The test pieces were weighed after drying and the density was calculated.

Density was measured on material from two of the locations; Drammen and Bjørkelangen. The Drammen material was tested both on soft material with a cylinder and on harder test pieces. For Bjørkelangen, only test pieces were used. In Table 3, the individual test values are presented. The averages of the different test series are 2.23 g/cm^3 for Bjørkelangen (sample piece), 2.14 g/cm^3 for Drammen (sample piece) and 2.00 g/cm^3 for Drammen (soft material).

Table 3 Density of weakness zone material

Bjørkelangen, test piece				**Drammen, test piece**				**Drammen, soft material**			
Sample	**cm^3**	**g**	**g/cm^3**	**Sample**	**cm^3**	**g**	**g/cm^3**	**Sample**	**cm^3**	**g**	**g/cm^3**
3-11	80	170.4	2.13	4-11	35	79.8	2.28	4-21	6.2	12.4	2.02
3-12	74	167.4	2.26	4-12	15	35.6	2.38	4-22	6.1	12.4	2.04
3-13	100	232.3	2.32	4-13	40	85.3	2.13	4-23	6.1	12.3	2.02
3-14	60	134.8	2.25	4-14	40	73.7	1.84	4-24	6.2	12.0	1.96
3-15	88	207.2	2.35	4-15	36	83.6	2.32	4-25	6.2	12.1	1.96
3-16	104	236.2	2.27	4-16	39	67.3	1.73	4-26	6.1	12.2	2.00
3-17	52	116.2	2.23	4-17	21	40.3	1.92				
3-18	100	222.0	2.22	4-18	45	89.9	2.00				
3-19	93	198.8	2.14	4-19	22	52.4	2.38				
3-20	99	209.5	2.12	4-20	38	93.4	2.46				

3 Test methodology and equipment

3.1 Core preparation

To create solid cores of the gouge material, a compactor with an inner diameter of 54 mm was specially designed and produced for this study. The compactor was placed in a workshop hydraulic press with a 10-ton capacity, which provides a possible maximum pressure of 43 MPa. The compactor had pistons at the top and bottom, making it possible to

apply pressure on both sides of the sample. A gauge was used to measure the axial deformation during loading.

Prior to the reconstitution of the gouge material into cores, particles larger than 4 mm were removed by wet sieving as described above. The material batches from each location were divided into suitable specimen sizes using a sample splitter. Before sample preparation, the material was dried at 60ºC for 24 hours and taken out of the oven shortly before sample preparation. The finished cores were stored in a zip-lock plastic bag. While stored the samples may have absorbed humidity from the air through the plastic. It is, however, believed to be very small amounts.

For the preparation of the cores, the following procedure was used:

1. Very cautious hand grinding in a porcelain mortar to separate adhered material from the wet sieving
2. Pouring the sample into the cylinder with the grain size kept as homogenous as possible throughout the process
3. Placing the cylinder in the press, lowering the press piston and removing the cylinder support at the bottom
4. Applying the load stepwise first to 0.5 ton, then to 1 ton and by increments of 1 ton up to 6 or 8 tons and waiting for deformations to stop between each step. Deformations were registered for each step.
5. Removing the bottom piston and extracting the core by applying load on the top. A load very close to the maximum preparation load was usually needed to push the core out of the cylinder.
6. Weighing the final core and measuring the length with a digital sliding calliper

3.2 Test rig

The rig used for uniaxial and triaxial testing was a GCTS RTR-4000 located at the Department of Geosciences and Petroleum, Norwegian University of Science and Technology. The machine is fully computer controlled and has a maximum axial load capacity of 4000 kN and a maximum cell pressure of 140 MPa. The frame stiffness is 10 MN/mm. Axial deformation was measured with two linear variable differential transformer (LVDT) sensors placed at 180 degrees. Radial deformation was measured with one LVDT sensor mounted on a rolling chain placed at the center (lengthwise) on the sample. The LVDT sensors had a range of 5 mm.

3.3 Uniaxial testing

The uniaxial testing was performed to obtain inputs on the mechanical properties of the reconstituted cores as a basis for determining the setup for triaxial testing. The test procedure was based on ISRM's suggested method for determining the uniaxial strength and deformability of rock materials (ISRM 2007).

To determine the E-modulus, the tangent modulus was utilised with ± 15% of 50% of the uniaxial compressive strength defining the regression line. Due to jagged curve, a larger interval than the usual 10% was used.

To protect the equipment from dirt and dust, the test specimens were covered with a sleeve. For the first two UCS-tests a heat shrink sleeve was used, like in the procedure for the triaxial testing. For subsequent UCS-tests, the heat shrink sleeve was switched with cling

foil to see to what degree the results were affected by the confinement from the shrink sleeve and to ensure uniaxial behaviour.

3.4 Triaxial testing

3.4.1 Equipment

The test setup had some modifications regarding the distribution of water to the sample, where the standard setup is to let in water at the bottom end face of the sample and let it out at the top end face. Instead, the water was distributed to the sides of the samples by using specially designed end pieces (see Fig. 5 a) allowing it to flow along the sample in a nonwoven casing (Fig. 5 b). The water inlet was at the bottom of the sample and the water outlet was at the top (Fig. 5 c). The modified setup was designed to ensure a fast and from the outside-and-in soaking of the samples. The drainage valve was open through all stages to ensure as little pore pressure built up as possible. A test with an aluminium core was performed to estimate the additional radial deformation from the nonwoven casing surrounding the sample.

The oil chamber surrounds the whole sample setup making the cell pressure (S_c) act in both radial and axial direction. The deviator stress (σ_d) is the pressure acting from the axial piston. The radial stress (σ_r) is then the same as the cell pressure and the axial stress (σ_a) is then equal to $S_c + \sigma_d$.

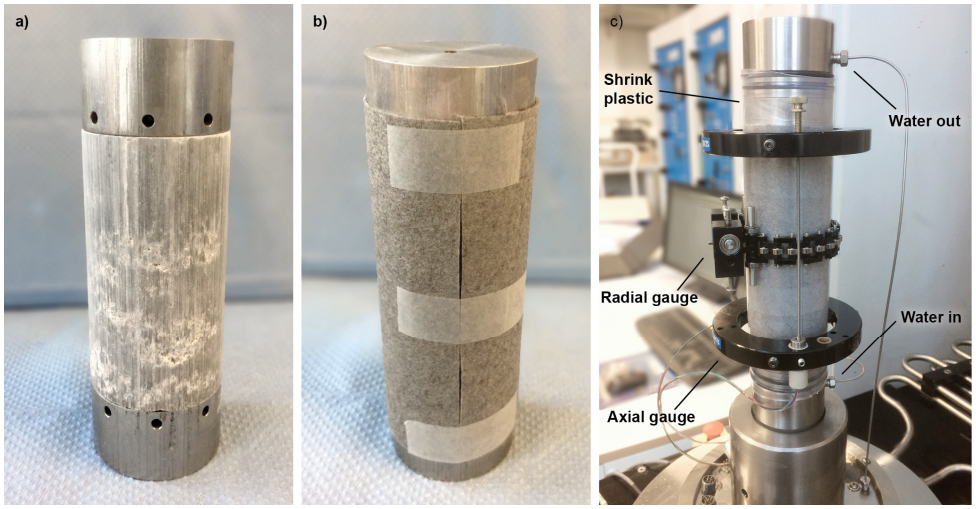

Fig. 5 Sample setup. a) New end pieces to distribute water to the sides of the sample. b) A nonwoven casing covers the sample and the holes in the water distributor. c) Ready for testing with the sample covered with a heat shrink sleeve and the water tubes and deformation gauges mounted

3.4.2 Test procedure

The intention behind the selected test procedure was to investigate whether a build-up of swelling pressure might occur during water addition of a representative gouge material under a stress state that is relevant for typical tunnel projects. The test had four main phases, as described below and illustrated in Fig. 6.

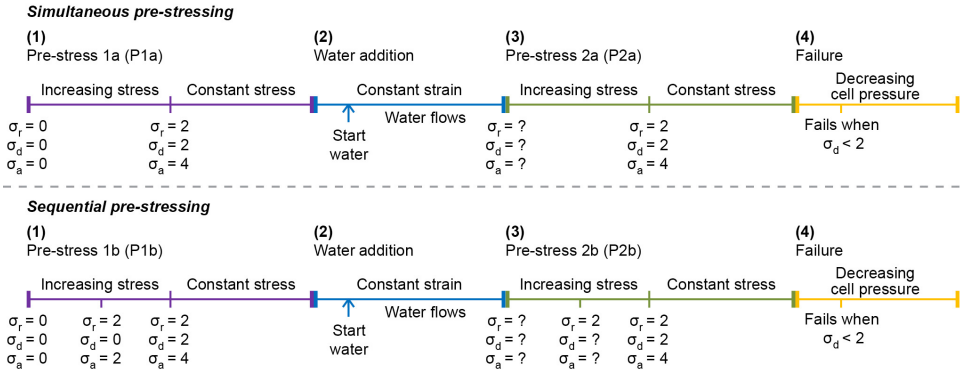

Fig. 6 Timeline for triaxial testing. The lengths of the lines are not representative of the time actually spent on a phase

(1) Pre-stress 1

Two different procedures for increasing the cell pressure and the deviator stress were used; simultaneous, Pre-stress 1a (*P1a*) and sequential, Pre-stress 1b (*P1b*):

- For *P1a*, both the cell pressure and the deviator stress were increased at the same time.
- For *P1b*, the cell pressure was first increased to its pre-set level, immediately followed by an increase of the deviator stress.

Before moving to the next phase, the pre-stress was held for some minutes to ensure stable behaviour.

(2) Water addition

The water addition phase started by switching from constant stress to constant strain. To observe the reaction of the switch, it was waited for some minutes before starting to add water. The goal was not to fully saturate the sample, but to make it sufficiently wet for the minerals to swell. The water was controlled manually to ensure a slow, constant flow along the sample. A minor pressure was needed to push the water through the nonwoven fabric. To ensure that the effect of the water addition on the sample was as small as possible, i.e. to keep the effective stress the same as the total stress, the water pressure was kept below 0.15 MPa. The water addition was maintained until the sample was believed to be wet all the way through.

Since the strain was set to be constant, no expansion or contraction was allowed in either direction. If swelling occurred, the machine would then increase the axial and/or radial stress to keep the strain constant. Correspondingly, if the material tended to shrink, the machine would lower the axial and/or radial stress. The cell pressure was controlled by the radial strain, while the deviator stress was controlled by the axial strain. A close interaction between the two was therefore needed to ensure constant strain behaviour. The nonwoven casing disturbs the constant strain for the actual core as the casing to some degree will expand with lowering of stresses and contract with increasing stresses, resulting in a reduced stress reduction or build-up. However, this effect is believed to small as the allowed radial change of the core is estimated to be on a level below 0.1%.

(3) Pre-stress 2

As for the pre-stress 1 phase, simultaneous, Pre-stress 2a (*P2a*) and sequential, Pre-stress 2b (*P2b*) loading were used. During water addition, a reduction of the cell pressure and the deviator stress occurred, and both were brought back up to 2 MPa.

(4) Failure
The cell-pressure was reduced, making the sample fail, and the test ended when the axial strain reached 30 000 μS.

After testing, the sample was split to conduct a visual examination of whether it was fully soaked.

3.4.3 Parameter calculation

To calculate the E-modulus, the relationship between σ_d and ε_a was used. As for the uniaxial tests, a regression line for a part of the curve was used to find the E-modulus, as described in Section 3.3. For many of the tests there was nonlinear behaviour and, in these instances, the data at the end of the path were emphasized.

The strength parameters were found by using the software RocData (Rocscience Inc. 2015). As indicated in Fig. 6, the sample theoretically fails when the deviator stress is less than 2 MPa. For practical purposes, it seems that the deviator stress slowly started to decrease some time before failure. The point of failure was determined visually in the program combined with an evaluation of the residual error development. For these data, a residual error below 0.010, using the linear regression algorithm and vertical-relative error summation for the Generalized Hoek-Brown criterion, seemed appropriate.

In phase 3 and 4, the unsaturated triaxial tests are performed with open drainage valves. As it is known that the pressure in the water phase is zero, and the air pressure is unknown, the strength and deformability parameters are determined from a total stress analysis. However, due to the used deformation rate, it cannot be guaranteed that no pore pressure have been build up in these phases.

4 Results

4.1 Core preparations

The sample preparation was difficult and time consuming. The most significant problem was that the core got stuck in the cylinder if the maximum load was too large. Therefore, both 6 and 8 tons (representing 26 and 34 MPa, respectively) were used as maximum loads to make the samples. The respective physical properties of the test samples are shown in Table 4. It is believed that the cores have a relatively uniform degree of compaction throughout the sample, but due to friction between the sample and the preparation cylinder, the density is believed to be slightly lower in the middle than on the ends.

4.2 Uniaxial testing

Only sample series 3 and 4 were subjected to uniaxial testing in order to save samples from series 1 and 2 for triaxial testing. Samples 3–2 and 3–3 were tested covered with a heat shrink sleeve, while the rest were loosely wrapped with cling foil. As seen in Fig. 7, samples 3–2 and 3–3 have a considerably greater strength that most likely comes from the radial confinement caused by the heat shrink sleeve. The values for UCS and E-modulus are shown in Table 5.

Table 4 Physical properties of the samples

Sample number	Diameter [mm]	Length [mm]	Weight [g]	Density [g/cm^3]	Max. load [10^3 kg]	Comment/Use[a]
1-5	54	114.79	532.9	2.03	6	Triaxial. Pre-stress b
1-6	54	115.75	542.9	2.05	6	Triaxial. Pre-stress a
2-8	54	112.02	520.6	2.03	8	Triaxial. Pre-stress a
3-2	54	108.01	477.5	1.93	6	Uniaxial (hss). Compacted one side only
3-3	54	106.57	487.9	2.00	8	Uniaxial (hss)
3-4	54	110.74	506.2	2.00	8	Uniaxial (cf)
3-6	54	106.49	490.4	2.01	8	Triaxial. Pre-stress a
3-8	54	107.17	495.9	2.02	8	Triaxial. Pre-stress b
4-1	54	112.27	514.0	2.00	6	Uniaxial (cf)
4-2	54	107.08	490.6	2.00	6	Uniaxial (cf)
4-3	54	112.40	518.3	2.01	8	Uniaxial (cf)
4-4	54	100.94	468.4	2.03	8	Uniaxial (cf)
4-5	54	101.76	482.3	2.07	8	Triaxial. Pre-stress a
4-8	54	102.07	480.2	2.05	8	Triaxial. Pre-stress b
4-9	54	101.92	483.2	2.07	8	Triaxial. P1b and P2a

[a]Uniaxial testing with heat shrink sleeve is marked "hss" and cling foil is marked "cf".

Table 5 Material properties from uniaxial testing

Sample number	Preparation load [10^3 kg]	UCS [MPa]	E-module [MPa]
3-2	6	1.04[a]	62.6[a]
3-3	8	1.20[a]	78.3[a]
3-4	8	0.62	43.7
4-1	6	0.51	48.5
4-2	6	0.64	57.4
4-3	8	0.61	85.5
4-4	8	0.72	77

[a]Samples with heat shrink sleeve

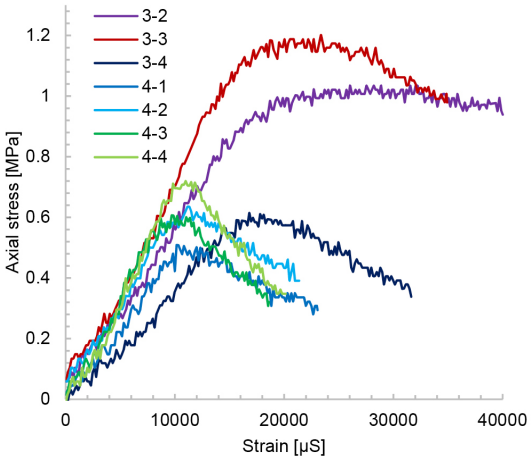

Fig. 7 Uniaxial testing. Samples 3-2 and 3-3 were covered with a heat shrink sleeve while the rest were wrapped in cling foil

4.3 Triaxial testing

Eight triaxial tests were performed: four with *P1a* and *P2a*, one with *P1a* and *P2b* and three with *P1b* and *P2b*. Plots for all tests are not shown in this article since they would require too much space. For additional plots and the raw data, reference can however be made to Online Resource 1.

Testing with aluminium cores showed that the nonwoven casing adds a strain of approx.-imately 2500–3000 µS when the cell pressure is 2 MPa, with a creep of approximately 70

μS for 30 min. When the pressure was lowered the casing showed a (negative) strain of approximately 1300 μS for 2 MPa. There was no change in strain observed due to the wetting of the nonwoven fabric.

Observations from specimens that were not completely saturated indicate that the waterfront moved as shown in Fig. 8. As most of the unsuccessful tests were on samples treated with pre-stress procedure *a*, this may differ for samples treated with pre-stress procedure *b*. Fig. 9 shows a sample after testing that was split with a knife to check whether the water addition was successful.

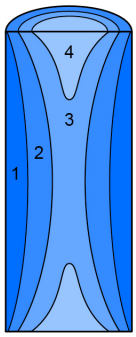

Fig. 8 Probable movement of waterfront of the samples during water addition (with increasing numbers)

Fig. 9 Test sample 2–8 split after testing to check quality of water addition. In the case of dry zones they were easy to detect

4.3.1 Pre-stressing and creep

The test results for the two different pre-stress procedures showed quite different behaviour. The behaviour was however quite similar within each of the different procedures. Two test series representing each procedure are therefore presented: sample 2–8 (pre-stress *a*) and 4–8 (pre-stress *b*). In Fig. 10 and Fig. 11, the test series are presented as stress and strains against time. In Fig. 12 and Fig. 13, the development of τ_{max}, which is the top of the Mohr circle, are plotted for each phase.

After the stresses peaked, one could observe a slow increase in the strains. This is believed to be creep, as described in Section 1, due to the rearrangement of the grains in the skeleton under constant stresses. In Phase 2, the strains are set to be constant. The consequence of the creep in a state of constant strain will be a reduction of the stresses, as the sample will not push back as much as before when the grains rearranges themselves.

For pre-stress procedure *a*, one can observe a small creep in the axial and radial direction. After the switch to constant strain, one can see that the cell pressure decreases while the deviator stress stays at the same level. This indicates that the creep is volumetric.

For pre-stress procedure *b*, one can see that the creep in the axial direction is much larger than in the radial direction. In Fig. 11, one can see at about the 30-min mark that the decrease in cell pressure is evening out and the deviatoric stress is still decreasing. This indicates that the creep has entered its secondary phase with deviatoric creep.

In Table 6, the strains at the end of Phase 1 are listed with the initial and new density of the different samples. One can see that the strains are considerably larger for the samples pre-stressed with the *b* procedure than those pre-stressed with the *a* procedure, which also resulted in a larger density for these samples.

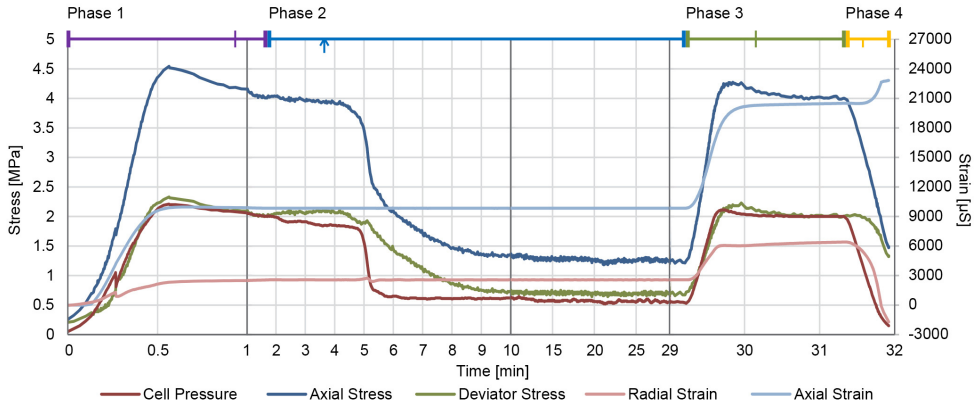

Fig. 10 Stress and strains against time for sample 2–8. Phases, including sub-events, are seen at the top of the chart and correspond to Fig. 6. The flow of water is started at the blue arrow

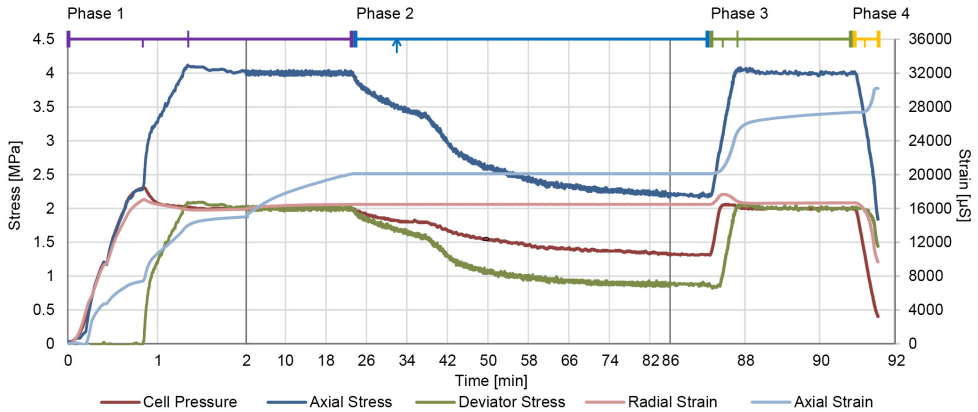

Fig. 11 Stress and strains against time for sample 4–8. Phases, including sub-events, are seen at the top of the chart and correspond to Fig. 6. The flow of water is started at the blue arrow

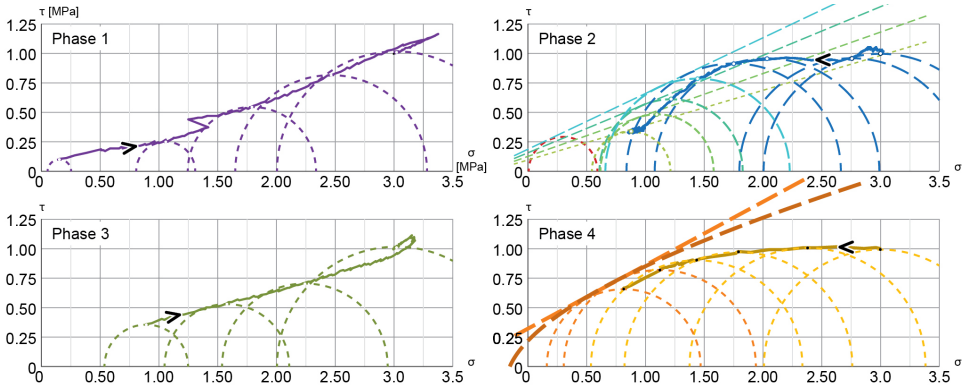

Fig. 12 Stress states illustrated with Mohr circles for sample 2–8 in the different phases. The arrows indicate the direction of progress. The failure envelopes shown for Phase 2 are only suggested/illustrative, while for Phase 4, they are calculated in RocData (Rocscience Inc. 2015). The straight line is Mohr-Coulomb and the curve is Hoek-Brown. The red half circle in Phase 2 represent an average value from UCS tests

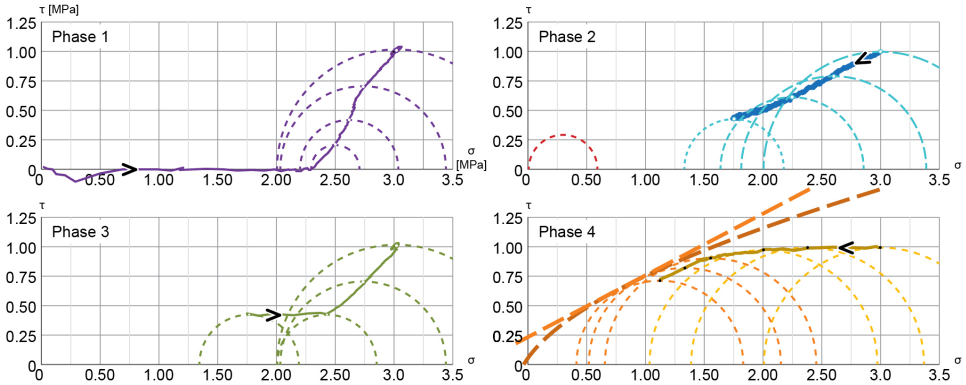

Fig. 13 Stress states illustrated with Mohr circles for sample 4–8 for the different phases. The arrows indicate the direction of progress. The failure envelopes in Phase 4 are calculated in RocData. The straight line is Mohr-Coulomb and the curved is Hoek-Brown. The red half circle in Phase 2 represent an average value from UCS tests

Table 6 Strains and density of the samples at the end of Phase 1

Sample number	Pre-stress procedure	Axial strain, ε_a [µS]	Radial strain[a], ε_r [µS]	Volumetric strain, ε_v [µS]	Initial density [ton/m^3]	New density [ton/m^3]
1-6	a	7688	6943	21420	2.05	2.09
2-8	a	9881	2504	14834	2.03	2.06
3-6	a	11117	7972	26822	2.01	2.07
4-5	a	7719	4325	16283	2.07	2.10
1-5	b	9764	18708	46469	2.03	2.13
3-8	b	21318	18799	57769	2.02	2.14
4-8	b	20109	16476	52133	2.05	2.17
4-9	b	14739	17301	48536	2.07	2.18

[a]Not corrected for strain from the nonwoven casing

4.3.2 Water addition and possible swelling

In Fig. 10 and Fig. 11, the small arrow on the blue line at the top indicates the point of time at which the water started to flow. An increase in the stresses after adding the water was not observed in any of the eight samples, but rather a decrease of both axial and radial stresses. This does not necessarily mean that no swelling occurred, but rather that due to the water saturation, or as a result of the swelling, other processes were dominant.

In Fig. 12 (Phase 2) for sample 2–8, and also in general for the samples that underwent pre-stress procedure *a*, one can see that the path is horizontal and moving to the left before it starts to decline. In the horizontal part, it is believed that the normal stress, σ_n, needed to sustain the radial and axial strain is decreasing. Where the line starts to decline, the shear stress, τ_θ, limit is also met, which indicates that the failure envelope is changing (getting lower), as indicated in the figure. In other words, the friction angle, φ, and cohesion, c, seem to become lower.

In the saturation phase, the samples that underwent pre-stress *b* showed quite different behaviour (Fig. 11 and Fig. 13 (Phase 2)). The creep in the axial direction in the constant stress part of Phase 1 was quite large, while the radial strain was smaller, but still larger than for pre-stress *a*. When switching to constant strain in Phase 2, this creep resulted in a quite significant reduction of the axial stress and a smaller reduction in the radial direction. The water used more time to saturate the sample and the reaction was slower than for the pre-stress *a*. For one sample, 3–8, it was hard to see any reaction at all from the saturation. In sample 4–8, one can see from Fig. 13 that the rate of stress reduction increases when the water starts saturating the sample. Accordingly, no swelling pressure is observed. The reduced stresses of all samples at the end of Phase 2 are listed in Table 7.

Table 7 Stresses at the end of Phase 2

Sample number	Pre-stress procedure	σ_a [MPa]	σ_r [MPa]	σ_d [MPa]
1-6	a	0.8	0.3	0.6
2-8	a	1.2	0.6	0.7
3-6	a	1.6	0.9	0.7
4-5	a	0.9	0.5	0.5
1-5	b	1.7	0.9	0.8
3-8	b	2.8	1.6	1.2
4-8	b	2.2	1.3	0.9
4-9	b	1.5	0.9	0.6

4.3.3 E-modulus

The stress/strain curves used to find the E-modulus are presented in Fig. 14, and the resulting values are listed in Table 8. Compared to the uniaxial tests, one can see that the values from the triaxial test are a bit higher. It does not seem to be a significant difference between the pre-stressing procedures, but it does seem that the values are generally lower on the second pre-stressing.

Table 8 E-modulus from the triaxial test in Phase 1 and Phase 3

Sample number	Pre-stress procedure	E-modulus Phase 1 [Mpa]	E-modulus Phase 3 [Mpa]
1-6	a	250	117
2-8	a	290	133
3-6	a	165	149
4-5	a	301	103
1-5	b	430	203
3-8	b	184	613[a]
4-8	b	295	169
4-9	b/a	357	134

[a]Not a probable value. See discussion

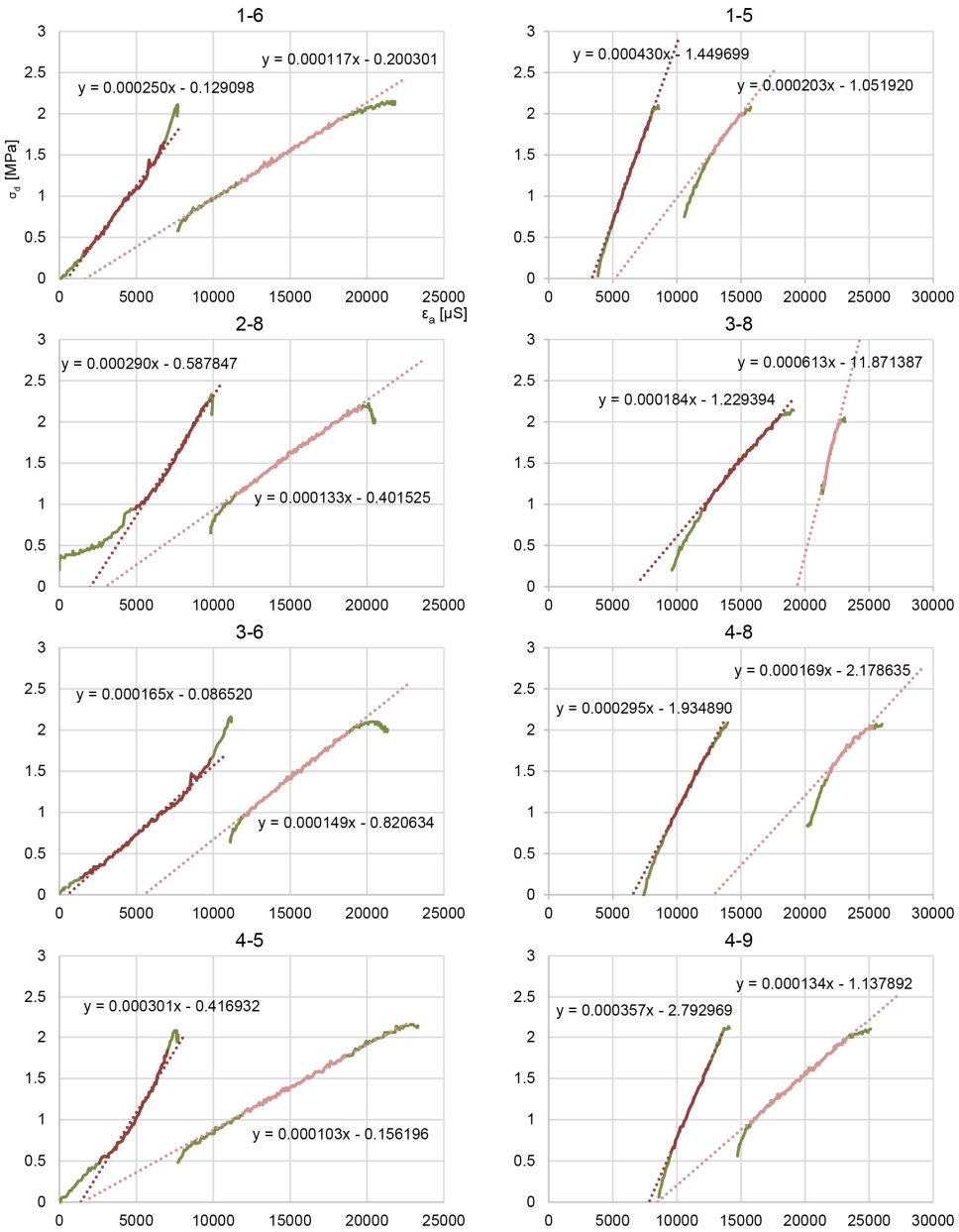

Fig. 14 Curves for the calculation of the E-modulus. The left curve (dark red) is from Phase 1 and the right curve (light red) is from Phase 3

4.3.4 Strength

The strength properties of the samples are listed in Table 9. The stress range for finding these values is quite small, at least for tunnel applications, and the line fitting is therefore quite sensitive to small variations in the raw data. One should therefore be extremely cautious about using such values outside the tested stress range and one should also bear in mind that the samples are reconstituted cores.

The Hoek-Brown m_i value is a material constant and depends upon the frictional characteristics of the component minerals (Hoek and Marinos 2000). The m_i values for 3–6 in particular, but also 3–8 and 4–8, seem too high compared to empirical values where weak and soft rocks have values of approximately 7 and lower (Hoek and Marinos 2000). Looking at the friction angle, samples 3–6 and 3–8 also stand out with high values, but sample 4–8 has one of the lowest values. For more information on this, reference is made to Online Resource 1.

Table 9 Strength parameters calculated by RocData (Rocscience Inc. 2015)

	Pre-stress	Generalized Hoek-Brown		Mohr-Coulomb	
Sample	procedure	σ_{ci} [MPa]	m_i	Cohesion [MPa]	Friction angle
1-6	a	1.1	6.1	0.34	29.7
2-8	a	1.0	5.9	0.32	28.2
3-6	a	0.3	32.4	0.19	36.0
4-5	a	0.9	6.9	0.30	30.6
1-5	b	1.1	5.7	0.34	29.0
3-8	b	0.6	11.9	0.23	34.4
4-8	b	0.4	14.0	0.23	27.5
4-9	b/a	0.8	7.5	0.29	29.0

5 Discussion

The experiment setup was designed mainly to investigate whether a swelling gouge material is likely to exert pressure when exposed to water in a probable and typical stress situation. Since it is very difficult to obtain samples of undisturbed material, reconstituted cores were used.

The main challenge of using reconstituted cores is to recreate the properties of in-situ material. The macrofabric of the sample material was possible to study visually and when splitting the samples after testing (see Fig. 9) the observations indicated that the samples had a quite even distribution of grain sizes. Such even distribution is not the case for most in-situ gouge materials, for which accumulation of e.g. fine grains are often found between the larger fragments (see Fig. 4 a).

The porosity, or occurrence of voids, in the material may be expressed as a function of the density. After the first pre-stressing (Phase 1), the samples had a density of 2.06–2.18 g/cm^3, with the highest values for the samples pre-stressed with procedure *b* (see Table 6). For two of the locations, the density of in-situ material was tested, resulting in average values of 2.23 g/cm^3 (test piece) for the Bjørkelangen location and 2.00 g/cm^3 (soft material) and 2.14 g/cm^3 (test piece) for Drammen (see Table 3). These densities are at similar level as for the sample cores after preparation (see Table 4) and after Phase 2. Based on this similarity, it is assumed that the density, which is correlated to the pore volume, of the samples is quite similar to the in-situ. As stated in the introduction, the bonding between the grains for this type of material, in-situ, is believed to be low to non-existent. Both the in-situ material and the compacted cores are on the verge of disintegrating when handled and are apprehended as being similar.

A main difference from in-situ conditions is that the laboratory tested samples were dry, while in-situ material has an initial water content. This implies two potential main objections: 1) the material properties may be different when the material is wet, and 2) the material has already, to an uncertain degree, swelled when wet. These objections are relevant not only for reconstituted cores, but also for “natural” in-situ samples used in a laboratory.

None of the triaxial tests showed increased pressure during water addition, indicating the build-up of a swelling pressure, even for materials with medium and high swelling pressure obtained by oedometer testing of material < 20 μm.

When performing the tests, one could immediately after the stabilization of the stress, after the pre-stressing in Phase 1, observe a creep behaviour. Creep is originally defined as deformations at a constant load, caused by a serial change in the structure through a rearrangement of the soil contacts (Havel 2004). However, when switching to Phase 2 and constant strain, before the water started to flow, this creep could be observed as a slow decrease of the applied stresses.

For pre-stress procedure *a*, a sudden reaction with a drop in the applied stresses occurred when the sample was saturated. This implies that the material does not need the same stresses to be held in place. As outlined in Fig. 12 (Phase 2), this may be due to a lowering of the friction angle that comes from changes in the contacts between the grains caused by water or swelling. It seems that the material first creeps and then enters a state of shear failure at the same time as the friction angle drops. Since the saturation takes place radially, as outlined in Fig. 8, the sample is not homogenous during saturation as it has a decreasing core of dry material that can "withstand" the axial pressure.

Also, for pre-stress procedure *b* the stresses decrease in Phase 2, but generally at a slower pace and the effect of the water is not that obvious, and for some samples almost invisible. For the pre-stress *b* samples, it almost seems like the water is a "catalyst" of the creep, as in Fig. 13 (Phase 2). As shown in Table 6, the strain after Phase 1 is generally higher for the pre-stress *b* samples, which makes the samples more compact and also probably makes the water move slower in the sample. Because of the different properties of the pre-stress *b* samples, it seems that they do not enter a state of shear failure during water addition as the pre-stress *a* samples did.

The nonwoven casing makes the sample have an unintentional possibility to deform radially during Phase 2. As the casing may expand when the stresses is lowered the core may have a small radial contraction, causing a higher end pressure than if the casing was not there. It is not believed that this effect is very large, at least for most of the samples, as the maximum strain from this effect is probably about 1300 μS for a reduction of 2 MPa, and the strains during pre-stressing shows that the deformability of the samples in such a stress range are far higher. Even with this being a significant effect, it is believed that it does not affect the behaviour in a way that influence the general interpretations of the results, as it only reduces the stress reduction.

The differences between volumetric and deviatoric creep may explain the different results in creep after the pre-stress procedures *a* and *b*. For procedure *a*, where the cell (volumetric) stress was applied at the same time as the deviatoric stress, a quite even creep in the radial and axial direction was observed. For procedure *b*, where the deviatoric stress was applied after the cell (volumetric) stress, an obviously larger axial (deviatoric) creep was observed.

The situation where the strain is constant in Phase 2 is not transferable to the situation in a tunnel, where the rock stresses will continue to push as the material creeps. If the same test was performed with constant stresses in Phase 2, one would obtain better data to determine what processes, creep or shear failure, that would be dominant in the different cases. As shear failure can result in the squeezing of the rock mass, the difference between creep and shear failure may have a significant influence on the tunnel excavation.

For the E-modulus, as shown by Fig. 14 and Table 4, the values are generally lower after the water addition than before, except for the samples from location 3. Looking at the material grading curves (Fig. 3), one can see that the location 3 material has lower clay and silt content and higher sand content than the rest of the locations. This may make it less sensitive to the water addition. The E-modulus values obtained in the triaxial tests were higher than the E-modulus values obtained from the uniaxial tests, which is believed to be due to the increase in compaction from the pre-stressing itself and/or the radial support.

The creep will displace the curves for the second pre-stressing to the right, as sample 4–8 illustrates (see Fig. 14, 4–8 and Fig. 11, axial strain in Phase 1). For sample 3–8, if one subtracts the creep, the strain level would be almost the same after the second pre-stress. This indicates that the decrease of stress in the constant strain phase mainly comes from creep and not a change in the E-modulus. The E-modulus will then be invalid as the stress-strain curve defining it only gets back to the starting point. This also seems to apply to some degree for sample 3–6.

The change in the E-modulus implies an alteration of the material on a grain size level. Since it seemed that the pre-stress *a* samples experienced a shear failure in Phase 2, it is believed that this contributed to the change. The stresses of the pre-stress *b* samples seemed to move below the failure envelope, but still experienced an E-modulus change. The expansion of the swelling clay minerals may have sped up and enhanced the creep deformation by affecting the grain contacts. Because there are voids in the samples, the swelling does not necessarily make the material expand, as grains move because of the swelling; they may rather collapse under the applied stress, making the sample smaller. However, samples without swelling material have not been tested and the effect of swelling versus wet grains and grain contacts is hard to define.

For the test results presented in Table 9 one should in particular be aware of the strength parameters for 3–6, 3–8 and 4–8, where the m_i value is higher than expected for these kinds of samples. In addition, these samples have the lowest σ_{ci} of all the samples, which also indicates that the failure envelope is too steep.

6 Conclusions

Based on the triaxial tests presented in this paper, it seems that there are factors other than the swelling pressure which may be the main reason for tunnel deformation to occur during excavation through a weakness zone containing swelling gouge. The low strength and low E-modulus of the gouge are believed in many cases to be major sources of deformations (elastic and plastic). For the time-dependent deformations, water is a key factor. If the material is fully saturated, water will be exerted and the material will consolidate before possible creep occurs. Creep properties seem to be very important and this phenomenon may cause failure by itself or combined with other processes. The deformation at one location causes a redistribution of the stresses around the tunnel over time that may initiate new deformation processes at places that were previously stable.

A main purpose with the triaxial testing described in this paper was to investigate strength and deformation parameters for swelling gouge materials, for which no previous data were found available in the literature. Valuable additional knowledge has been obtained based on the testing described here, but it should be emphasized that the E-modulus values and strength parameters achieved using the method presented in this paper should be applied with great care for engineering purposes as they are based on a limited stress range and performed on reconstituted samples.

References

Aristorenas GV (1992) Time-dependent behavior of tunnels excavated in shale. Dissertation, Massachusetts Institute of Technology, Cambridge

Barla M (1999) Tunnels in swelling ground: simulation of 3D stress paths by triaxial laboratory testing. Dissertation, Politecnico di Torino, Torino

Bellwald P (1990) A contribution to the design of tunnels in argillaceous rock. Dissertation, Massachusetts Institute of Technology, Cambridge

Bilir ME, Sari D, Muftuoglu Y (2008) A Computer-Controlled Triaxial Test Apparatus for Measuring Swelling Characteristics of Reconstituted Clay-Bearing Rock. Geotech Test J 31 (4):535-541. doi:https://doi.org/10.1007/978-3-319-09060-3_85

Brown ET, Hoek E (1978) Trends in relationships between measured in-situ stresses and depth. Int J Rock Mech Min 15 (4):211-215. doi:https://doi.org/10.1016/0148-9062(78)91227-5

Einstein HH (1996) Tunnelling in difficult ground - Swelling behaviour and identification of swelling rocks. Rock Mech Rock Eng 29 (3):113-124. doi:https://doi.org/10.1007/bf01032649

Havel F (2004) Creep in soft soils. Dissertation, Norwegian University of Science and Technology, Trondheim

Herget G (1988) Stresses in rock. Balkema, Rotterdam

Hoek E (2006) Practical Rock Engineering. www.rocscience.com

Hoek E, Marinos P (2000) Predicting tunnel squeezing problems in weak heterogeneous rock masses. Tunnels & Tunnelling International vol November and December 2000. Polygon Media Ltd, London

ISRM (2007) The Complete ISRM Suggested Methods for Rock Characterization, Testing and Monitoring: 1974-2006. ISRM Turkish National Group, Ankara

Kocheise R-C (1994) Swelling clay in sub-sea tunnels. Dissertation, Norwegian Institute of Technology, Trondheim

Mao D, Nilsen B, Dahl F (2011) Laboratory Testing of Swelling Gouge From Weakness Zone - Principle And Recent Update. Paper presented at the 45th U.S. Rock Mechanics / Geomechanics Symposium, San Francisco, 26-29 June

Myrvang AM (2001) Bergmekanikk. Norwegian University of Science and Technology, Department of Geology and Mineral Resources Engineering, Trondheim

Nilsen B (2016) Reliability of swelling pressure testing for tunnel support evaluation. Paper presented at the ITA-AITES World Tunnel Congress 2016, San Francisco, April 22-28

Rocscience Inc. (2015) RocData. vol 5.003, 5.006 edn. Rocscience Inc., Toronto

Rokoengen K (1973) Swelling properties of clayey zones in rock. Dissertation, Norwegian Institute of Technology, Trondheim

Selmer-Olsen R (1985) Method for determination of dimensional swelling pressure. Paper presented at the Fjellsprengningskonferansen, Oslo, November 21-22

Sheorey PR (1994) A theory for In Situ stresses in isotropic and transverseley isotropic rock. Int J Rock Mech Min 31 (1):23-34. doi:https://doi.org/10.1016/0148-9062(94)92312-4

Statens vegvesen (2016) Laboratory methods. vol R210. Statens vegvesen, Vegdirektoratet, Oslo

Terzaghi K, Peck RB (1967) Soil mechanics in engineering practice. 2nd edn. Wiley, New York

Wild KM, Barla M, Turinetti G, Amann F (2017) A multi-stage triaxial testing procedure for low permeable geomaterials applied to Opalinus Clay. Journal of Rock Mechanics and Geotechnical Engineering 9 (3):519-530. doi:https://doi.org/10.1016/j.jrmge.2017.04.003

Yeşil MM, Paşamehmetoğlu AG, Bozdağ T (1993) A triaxial swelling test apparatus. Int J Rock Mech Min 30 (4):443-450. doi:https://doi.org/10.1016/0148-9062(93)91725-X

Paper IV

Oedometer testing of swelling gouge materials at different water contents

Høien, Are Håvard[a]
Nilsen, Bjørn[a]
Olsson, Roger[ab]

[a]Norwegian University of Science and Technology, Sem Sælands veg 1, 7491 Trondheim, Norway
[b]Norwegian Public Roads Administration, Postboks 8142 Dep, 0033 Oslo, Norway
[c]Norwegian Geotechnical Institute, PO Box 3930 Ullevaal Stadion, 0806 Oslo, Norway

E-mail:
Høien, A.H. are.hoien@vegvesen.no, corresponding author (all stages)
Nilsen, B., bjorn.nilsen@ntnu.no
Olsson, R., Roger.Olsson@ngi.no

Abstract
The swelling of gouge material is an important factor to consider when excavating tunnels through weakness zones. The swelling that occurs in a weakness zone is mainly caused by the expansion of clay minerals belonging to the smectite group. The objective of this paper is to examine the behaviour of the swelling fraction of gouge material with different initial water contents. Oedometer testing of the fraction < 20 µm was used to identify potential swelling pressure and the behaviour of swelling gouges. A test setup with different degrees of initial water content was applied for two different materials originating from a road tunnel at highway E18 in Vestfold and highway E39 in Bergen, Norway, respectively. Seven tests were performed on the first material and eight were performed on the second. For each material, two tests were conducted on dry material and the rest of the material with various water contents. In these experiments, a correlation was found between the sample height and the swelling pressure. It was also found that the water content had a significant influence on pre-compacting, with higher water content giving lower samples heights. Based on this, it may be possible to identify a water content when all the intracrystalline swelling/hydration has completed. This is assumed to be important in assessing the test results for the *in-situ* material as one may consider to what degree swelling has already occurred based on the *in-situ* water content.

Keywords
Swelling; swelling gouge; weakness zone; oedometer; intracrystalline swelling; osmotic swelling

1 Introduction and background

When excavating tunnels in hard rock conditions, the crossing of weakness zones, which often contain swelling minerals, poses a significant challenge, and knowledge about the swelling potential is important for decisions regarding excavation and rock support. The swelling that occurs in weakness zone gouge material is an expansion caused mainly by clay minerals in the smectite-group (Brekke and Selmer-Olsen 1965; Selmer-Olsen 1985).

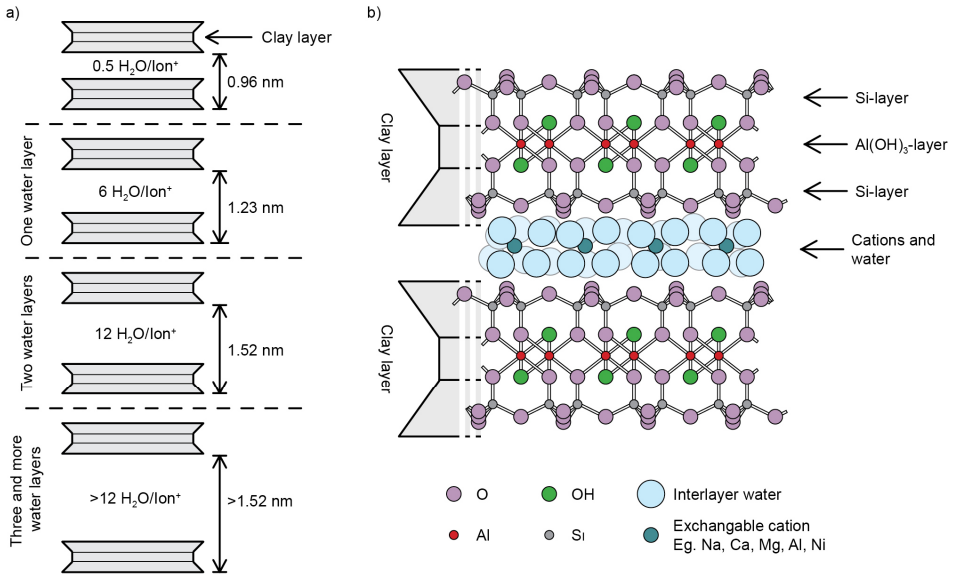

Fig. 1 a) Intracrystalline swelling/hydration of sodium montmorillonite with distances as a function of water adsorption. b) The basic structure of montmorillonite. Each clay layer consists of two Si-layers (tetrahedral) and one $Al(OH_3)$-layer (octahedral). Based on Kraehenbuehl et al. (1987), Selmer-Olsen (1980), Nilsen (2016) and Weil and Brady (2017)

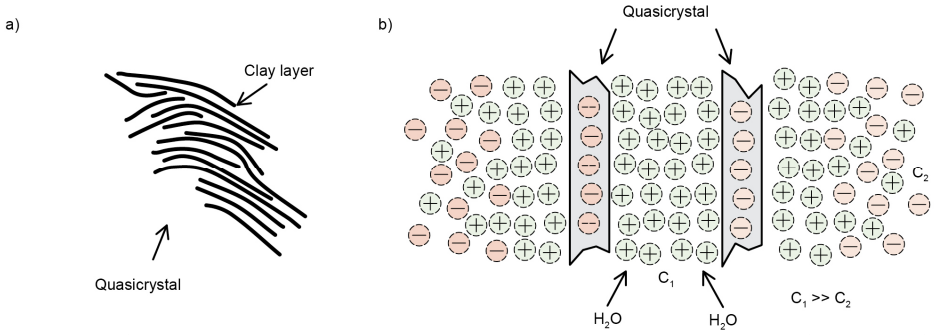

Fig. 2 a) Example of a quasicrystal consisting of fifteen clay layers. b) Osmotic swelling. Quasicrystals are negatively charged at the surfaces and between them there is a high ion concentration, C1. This concentration is much higher than in the pore water, C2, and an equilibrium is reached through the penetration of the water between the quasicrystals. Based on Madsen and Müller-Vonmoos (1989) and Laird (2006)

According to Madsen and Müller-Vonmoos (1989), there are two swelling processes for this kind of material, intracrystalline/hydration (see Fig. 1) and osmotic (see Fig. 2), which occur in sequence. A clay quasicrystal (see Fig. 2 a) consists of two to thousands of individual clay layers (Laird 2006), and this first swelling process is caused by the hydration of the exchangeable cations between these layers. The intracrystalline swelling/hydration can expand the quasicrystal by up to about 100% and in a specific type of montmorillonite, swelling pressures ranging from several hundred MPa for one layer of water between the clay layers to about 27 MPa for three and four layers of water have been identified. The

second process relates to the ion concentration differences near the quasicrystal surface and in the pore water. The osmotic swelling in the second phase can create pressure reaching up to about 2 MPa.

Because swelling gouge material is too loose to form undisturbed test specimens, the ISRM's suggested methods (ISRM 2007) are not feasible. At the Norwegian University of Science and Technology (NTNU), a swelling test for remoulded specimens, giving a relative, potential swellability, was introduced several decades ago, and is still common in the Norwegian tunnelling industry. One of the first publications describing and developing the method was written by Brekke (1965). Further research conducted by Selmer-Olsen (1985) linked the measured values to rock support applications. The latest paper on the subject was published by Mao et al. (2011), who described the method in detail and provided an overview of their test results.

In short, the method is performed by extracting the material under 20 µm through sieving or sedimentation. After drying, the material is ground in a porcelain mill, creating a fine powder. Twenty grams of the material is placed in a 20-cm^2 oedometer ring. The sample is then pre-compacted at 2 MPa for 24 h and after that it is unloaded and set to rest until no height change is recorded (approximately 2 h). Further, distilled water is filled in the test cell, causing the material to swell. During swelling, no expansion is allowed, and a swelling pressure builds up. A more detailed description of this process is given in the methodology section.

According to Mao et al. (2011), 40% of gouge samples tested at the NTNU laboratory had 0 to 10% content of the fraction < 20 µm, 30% of the samples had 10 to 20% and 15% had 20 to 30 %. As illustrated in Fig. 3, the tested fraction have inactive as well as swelling grains of different types, which also had different swelling capabilities (Kocheise 1994).

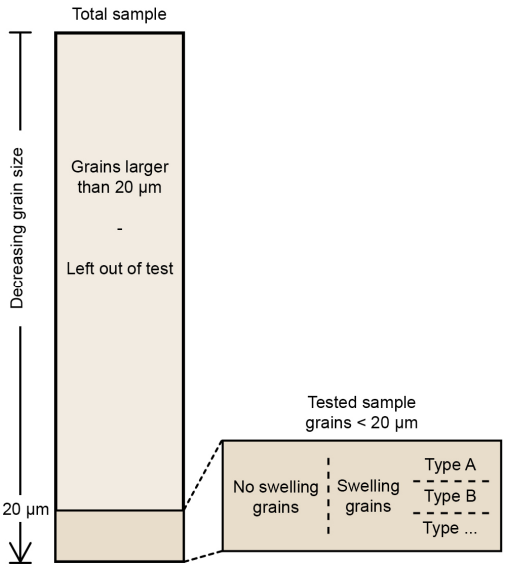

Fig. 3 Content of tested sample fraction in relation to the total collected sample

The in-situ material has a natural water content, while the standard laboratory procedure uses a dry material. In the current study, the behaviour of the fraction of swelling gouge material under 20 µm with various water contents has been considered. However, the results

of the water content tests in the lab must not be matched with the natural water contents as their behaviour in the pre-compacting stage, combined with other factors, means they do not represent comparable features.

The objective of this paper is to examine the behaviour of the swelling fraction of gouge material at different degrees of initial water content based on oedometer testing. A test setup with different degrees of initial water content for two different materials, called sample series 1 and sample series 2, has been used in this study. In addition to the normal test practice, a consolidation stage has been performed after the swelling to explore the behaviour of swollen material when it is exposed to counter pressure.

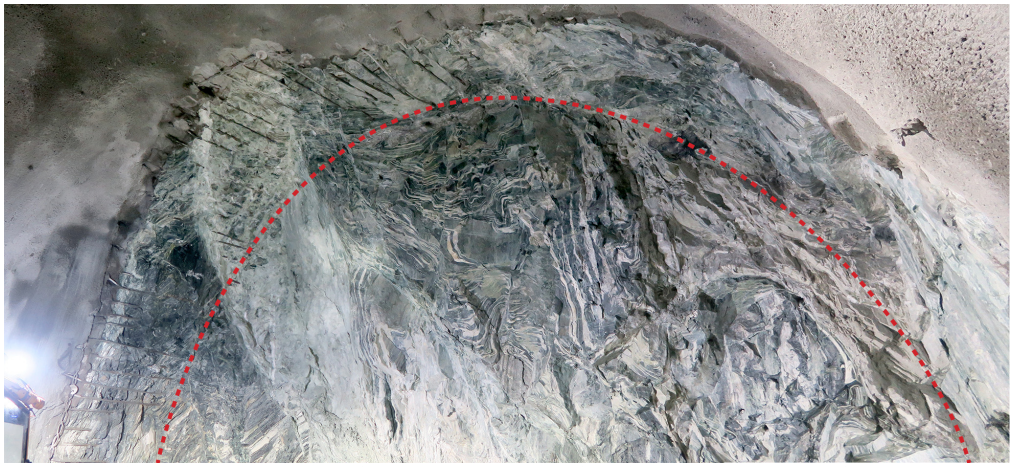

Fig. 4 The weakness zone where the material for sample series 2 was collected, E39 Svagatjørn – Rådal, located in Bergen, Norway. The red dashed line is the approximate location of the transition between the walls/roof and tunnel face. Exposed spiling bolts can be seen in the left wall and in the roof

2 Sample materials

The material for sample series 1 originated from a road tunnel at highway E18 in Vestfold, Norway. The material is a mix of leftover material from the ordinary test of several zones and was used as a preliminary series to test the method.

Sample series 2 was collected from highway E39 in Bergen, Norway at a single spot, with approximately 16% of the grains being < 20 µm. In Fig. 4, the weakness zone of the collected material is shown.

2.1 Plasticity and particle density

The material (< 20 µm) was tested for its liquid limit (W_L) based on the cone penetrometer and plastic limit (W_P), according mainly to the procedure described by Statens vegvesen (2016) and Statens vegvesen (2013). The usual method of testing the plasticity limit is to use the rolling test. This was not applicable for both materials, however, and the cone penetrometer was used on material 2. The plasticity index (I_P) is given by $W_L - W_P$.

The particle density was determined by using a pycnometer according to Statens vegvesen (2016). The pycnometer method is based on determining the volume of a dry mass by monitoring the displacement of water. The particle density was calculated based on the dry mass determined by weighing, and the net volume was determined using the pycnometer.

Table 1 shows the measured values of particle density and plasticity. As can be seen, the plastic limit and liquid limit for sample series 1 are lower than for sample series 2.

Table 1 Particle density and plasticity of the tested materials

Sample series material	Particle density [g/cm^3]	Plastic limit (W_P) [weight %]	Liquid limit (W_L) [weight %]	Plasticity index (I_P) [weight %]
1	2.76	26	79	53
2	2.83	38	149	111

2.2 Intact material density

The density was tested by using a brass density cylinder with approximate dimensions of Ø19 x 22 mm, according to Statens vegvesen (2016). The cylinder was pressed by hand into pieces of test material that were still intact. The material had been stored in plastic bags for some time, and a change from the original water content was to be expected.

Table 2 shows the densities and water contents of intact material from sample series 2, E39 Svegatjørn – Rådal. The dried samples are shown in Fig. 5. Intact material for this test of sample series 1 was not available. The different water contents in the samples may be explained by their different locations in the sample bag before they were collected.

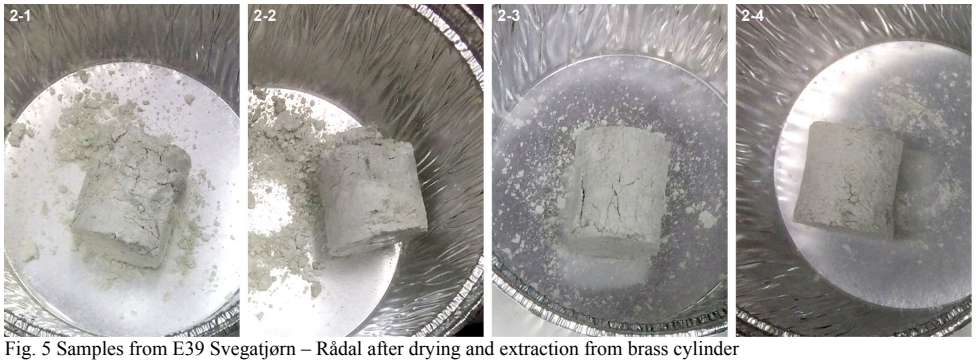

Fig. 5 Samples from E39 Svegatjørn – Rådal after drying and extraction from brass cylinder

Table 2 Density of samples from E39 Svegatjørn – Rådal

Sample	Cylinder volume [cm^3]	Wet weight [g]	Wet density [g/cm^3]	Dry weight [g]	Dry density [g/cm^3]	Water content [weight %]
2-1	6.28	11.73	1.87	9.7	1.55	21
2-2	6.26	12.08	1.93	10.18	1.63	19
2-3	6.30	12.09	1.92	11.23	1.78	8
2-4	6.29	11.07	1.76	8.04	1.28	38

3 Swelling test methodology

The setup of the oedometer test will be described below, along with the equipment and sample preparation.

3.1 Sample preparation

To separate the material < 20 µm for series 1, settling as described in Mao et al. (2011) was used and for series 2, wet sieving as described in Statens vegvesen (2016) was applied. The material was then dried at 60°C. After drying, the material was milled down to a fine powder. For each sample series, two dry samples and samples with increasing water content were tested. For the two dry samples, one was dried for a week (called x-dry-1) and one was dried overnight (called x-dry-2).

No data was found in the literature to suggest suitable water contents for the wet samples. To acquire a value that could be used as a basis for the water contents, one of the dry tests for each series was performed with no post-swelling consolidation stage. After testing, the weights of the water in the samples were measured (m_w). For the wet samples, a water amount of 10, 20, 40, 60 and 80% of m_w was added. For series 2, 90% of m_w was also tested. The samples were called x-wet-1 for 10%, x-wet-2 for 20%, x-wet-3 for 40% and so on. The water was added by using a spray bottle, while the material was spread out on a plastic sheet placed on a scale with an error margin of ± 0,01 g (see Fig. 6). The plastic sheet was then folded and closed with a rubber band. A small amount of air was left in the bag to make it possible to mix the material inside the bag. To make sure the water was homogeneously distributed, the samples were stored for a minimum of a week before testing. The sample bags were stored in a desiccator with water at the bottom to prevent them from drying. For sample series 1, the samples were successively prepared during the test period of the series, while for sample series 2, all samples were prepared at the same time, except 2-wet-6, which were prepared closer to the time of use.

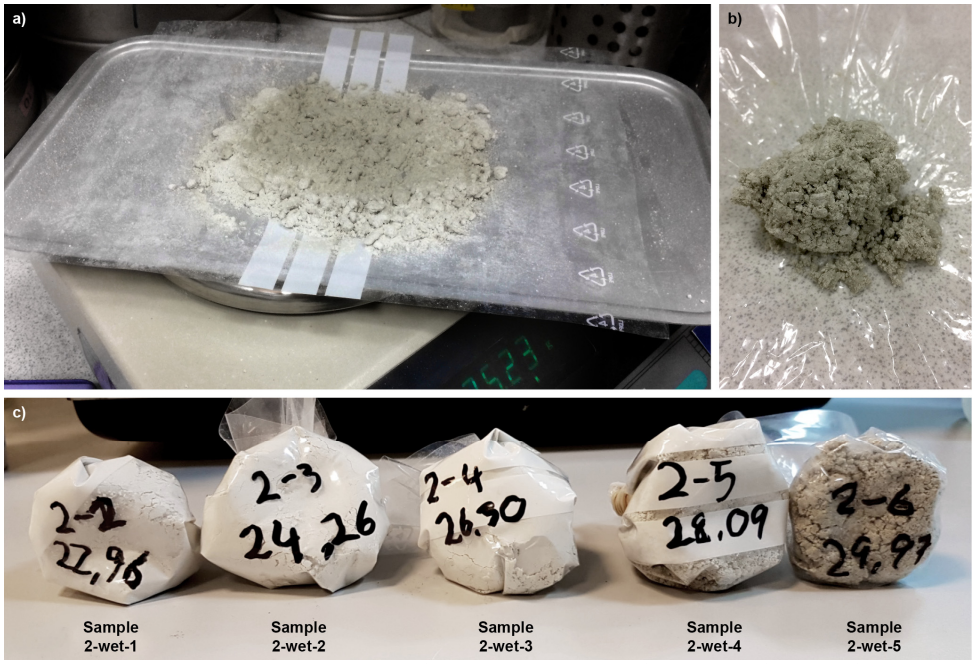

Fig. 6 Sample preparation. a) Adding water on sample 2-wet-5 with a spray bottle. The material was mixed with a spatula while the water was added. b) Sample 2-wet-5 before applying the rubber band. A spatula was used to collect all material and water in the middle of the plastic sheet. c) Sample series 2. The total weight was marked on the bag for easy control of any water leaving or entering the material. Bag marked 2-2 is later called 2-wet-1, 2-3 is called 2-wet-2 and so on

3.2 Cell setup

A standard consolidation cell from GDS Instruments was used, except for the sample ring, which was higher than normal. The main parts of the oedometer cell are as follows (see Fig. 7):

- Tray
- Bottom porous disc
- Sample ring, with a diameter of 50 mm and a height of 30 mm
- Loading plate, including the upper porous disc
- Fastening plate

To minimize the risk of water disappearing during the pre-compacting stage, modifications were made to the standard setup. The sample was placed between two paper filters, which were stored in a desiccator with water in the lower tray to keep them moist. The sample material was weighed to find the actual water content before it was placed in the cell. A piece of overhead transparency film was placed between the bottom porous disc and the bottom paper filter to try to prevent evaporation downwards (Fig. 7 a). The loading plate was covered in plastic to try to prevent the porous disc on the loading plate from attracting water from the sample (Fig. 7 c). When the loading plate was placed in the ring, there was a thin gap between inside of the ring and the plate. When the pre-compacting was started, and the first large deformation stopped (after a few minutes), a strip of cling foil was carefully put into the gap to seal it.

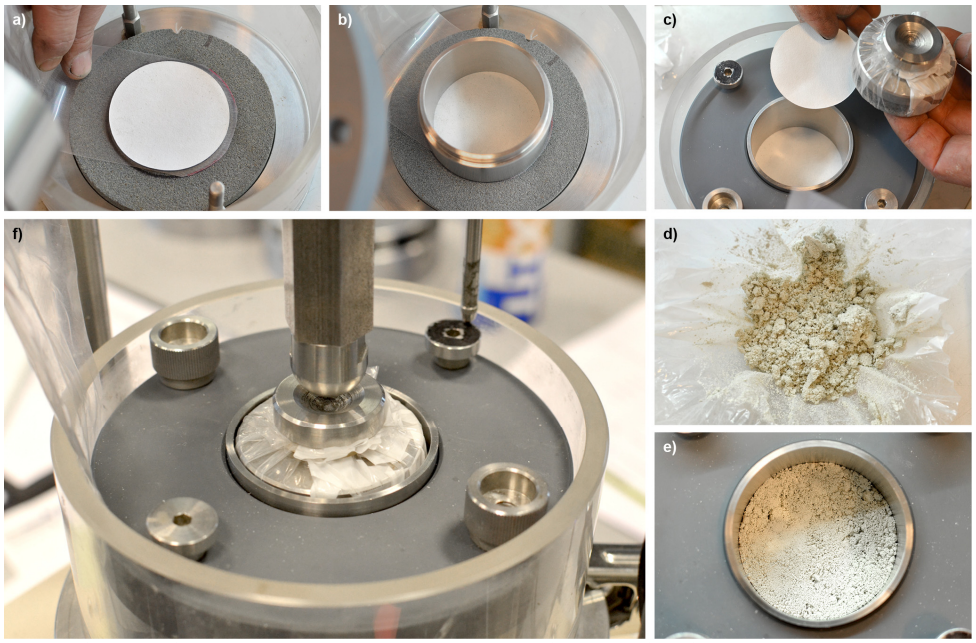

Fig. 7 Oedometer cell setup for wet samples. a) The bottom porous disc is placed inside the tray. Between the porous disc and the paper filter, a piece of overhead transparency is placed. b) A sample ring is placed on the paper filter, covering its edges. c) The fastening plate that fixates the ring and filters, top paper filter and loading plate is shown. d) Material ready to be placed in the ring. e) Sample material cautiously packed in the ring. f) Cell placed in the oedometer and ready to be loaded. The pin to the upper right is the tip of the extensometer

3.3 Testing

The oedometer testing had two main stages, pre-compacting and swelling. For sample series 2, a consolidation stage was performed after swelling as a third stage. The oedometer used in the tests is shown in Fig. 8.

The bottom plate was moved up and down to create and release pressure in the sample. The load cell was placed on the transverse beam at the top. The extensometer was placed on the rod from the loading cell, eliminating any apparatus deformation. The bottom plate also had its displacement monitored and the difference between this and the extensometer monitoring is the apparatus deformation.

Before the pre-compacting started, the initial height of the sample was measured. For sample series 1, the initial heights of the samples were measured using a sliding calliper. This method had a systematic error of approximately 0.7 mm depending on the sample height,

yielding initial heights that were too low which is corrected for in the presented data. During the testing of sample series 1, it was found that the initial height and the pre-compacting height data would be more interesting than initially believed. Therefore, a more accurate method of measuring the initial height was chosen for sample series 2, based on using the apparatus extensometer.

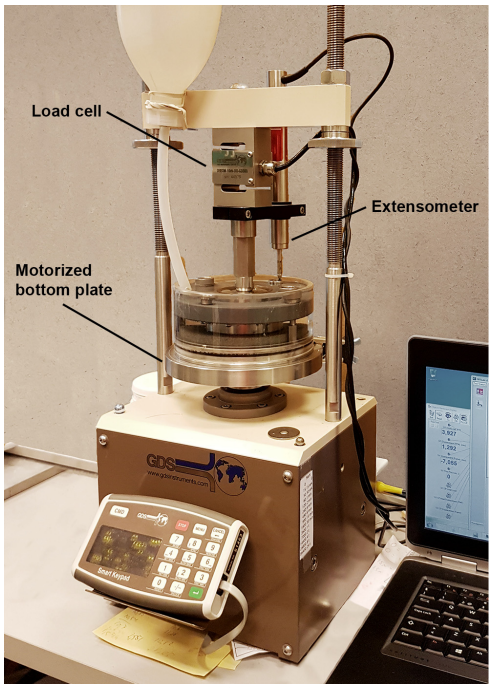

Fig. 8 GDS Oedometer used in the tests

3.3.1 Stage 1 – Pre-compaction

The term "consolidation" is often used to describe this stage. This term is originally used when water is drained out of the material. The drainage of water is not necessarily the case, particularly not for most of the samples discussed in this paper. The term "pre-compact" has therefore been used in this paper.

In the standard procedure, the pre-compacting is performed at 2 MPa for 24 h or until the sample has reached a constant height. For the samples in this test, the height change did not stop after 24 h, and the stop criterion was defined as a height change of less than 0.008 mm in the last 4 h. The longest pre-compacting period was 19 days. For samples with high water content, the height decreased quite quickly before it again increased. The first drop in height development was ignored in such cases.

For sample series 2, the cell was weighed before it was placed in the oedometer. This was done in order to survey the water content in the sample during pre-compacting. The scale had 0.01-gram readability and an error of ± 0.02 g.

After pre-compacting, the sample was unloaded. The standard procedure is to wait until no height change is registered (approximately 2 h). Also for the unloading a stop criteria was needed and the one described above, < 0.008 mm/4 h, was also used here. To register the height change, a small counter pressure was needed and 8 kPa was used in this case.

3.3.2 Stage 2 – Swelling

First, the oedometer cell was removed from the oedometer and for series 2 it was weighed. Then the plastic film between the bottom porous disc and the bottom paper filter and the cling foil strip was removed. The cell was then placed back in the oedometer and a pressure of 8 kPa was applied. For the tests on dry material, it was not necessary to remove the cell since no plastic film was used. The swelling was then started by adding distilled water on top of the oedometer cell. The height change due to the removal of the plastic film is corrected for in the presented data.

Since there was some apparatus deformation during swelling, and the control software unfortunately did not have options to compensate for this, the height change during swelling was not completely zero, as described for the original method. However, the extensometer records the actual height of the sample and the height change due to this deformation was therefore known and reported in the results section.

3.3.3 Stage 3 – Post-swelling consolidation

For sample series 2, a consolidation phase was carried out after the swelling to see how the already swollen material was reacting to a counter pressure. The consolidation pressure was 2 MPa or at least 0.5 MPa more than the swelling pressure; that is, a swelling pressure of 1.7 MPa would yield a consolidation pressure of 2.2 MPa. The increase in pressure was done in the first hour. The stage was planned to last until the samples showed stable behaviour. However, for most of the samples, the stage held much longer, for up to about three days.

Table 3 Water content data for the respective samples. Samples 1-dry-2 and 2-dry-1 were weighed after swelling and used as a basis for calculating the water to be added.

Sample name	Added water [% of m_w]	Prepared weight [g]	Initial weight[a] [g]	Initial water content [Weight %]	Weight at finished pre-compact [g]
1-dry-1	0	20	20	0	-
1-dry-2	m_{w1}=9.54 g	20	20	0	-
1-wet-1	10	20.95	20.83	4	na
1-wet-2	20	21.91	21.73	9	na
1-wet-3	40	23.82	23.87	19	na
1-wet-4	60	25.72	25.74	29	na
1-wet-5	80	27.63	27.98	40	na
2-dry-1	m_{w2}=9.61 g	20	20	0	-
2-dry-2	0	20	20	0	-
2-wet-1	10	20.96	21.8	9	19.57[b]
2-wet-2	20	21.92	22.32	12	19.89[b]
2-wet-3	40	23.84	23.77	19	22.4
2-wet-4	60	25.77	25.35	27	22.36
2-wet-5	80	27.69	27.29	36	22.55
2-wet-6	90	28.65	28.17	41	21.86

[a]Weight at start of pre-stressing. Changed from prepared weight due to storage. [b]Values less than 20 g may have been caused by a loss of material during preparation.

4 Results

Each test was quite time consuming and the test period was eight months. The total time used for testing added together was as much as 188 days.

4.1 Sample water content

Data concerning the water content of the samples are shown in Table 3. The samples were stored in a humid environment, and as shown, the water content of sample series 2, which had the longest storage time, the content of the driest samples showed a small increase and the content of the wettest samples showed a small decrease. During the testing of sample

series 1 an interest in the actual water content after pre-compacting arose, and this was monitored for series 2. As can be seen in Table 3 below, the samples lost a considerable amount of water during this phase.

4.2 Pre-compaction

As shown in Fig. 9, the pre-compacting stage took from < 1 to 29 days. Some samples (such as 2-wet-2) were pre-compacted more than required by the < 0.008mm/4 h stop criteria, which was due to personnel situations (vacations, etc.).

Looking at series 1, one can observe that the sample height after approximately one day was lower with increasing water content until sample 1-wet-5, which was higher than 1-wet-4. Also, a flat section was observed before the height again started to decrease, which is commented on further below. For sample series 2, similar behaviour was observed. The height of sample 2-dry-1 was lower than expected. This may have been caused by the powder being very light and pushed into the small gap between the ring and the loading plate during the on-loading.

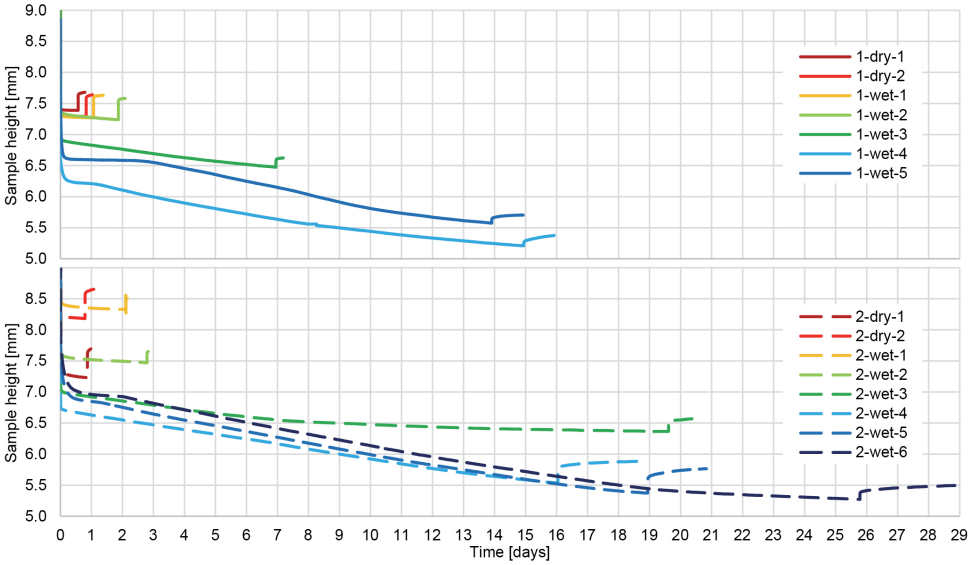

Fig. 9 Sample height versus days of pre-compacting for series 1 (top) and series 2 samples (bottom). The rise of the graph at the end is the unloading phase

For series 2, after approximately one day, the samples 2-wet-5 and 2-wet-6 were higher than sample 2-wet-4 and had a longer semi-flat section with increasing water content. The same behaviour can be seen in sample series 1. The weights for the samples at the end of pre-compacting presented in Table 3 show that even with very different initial water contents, they end up with quite similar final water contents. This despite drying was tried to be prevented. Water being pressed out was not directly observed, but small amounts might still have been pressed out without being observed.

4.3 Swelling

The maximum swelling pressures for the different samples are shown in Table 4, along with sample heights and densities. The swelling pressures given are the maximum pressures monitored during testing.

In Fig. 10, the dry-1, dry-2, wet-1 and wet-2 samples for both series are plotted against time. The dry samples reach an upper value before dropping and sample series 2 also has a second upper value. Further, in looking at Fig. 11, one can see that over the next two days the pressure decreases for the dry samples. The drop in the beginning and the continuous drop in pressure over time may be caused by grains sliding on other grains as a creep response, acting under its own pressure.

Fig. 11 also shows that the more water the sample initially contained, the higher the swelling pressure became. Also, the time it took to reach the maximum swelling pressure generally increased with increasing initial water content. In Table 4, one can see that for both series the swelling pressure increased with decreasing height. This is illustrated by Fig. 12, where the maximum swelling pressure is plotted against the sample height. It is quite clear that there is a correlation between the two parameters for each sample series. The dry samples seem to be able to create pressure that is a bit higher, according to their sample height, than the initial wet samples. However, in looking at the long-term swelling pressure for the dry samples in Fig. 11, they seem to converge to about the same level.

Table 4 Maximum swelling pressures, sample heights and densities.

Sample name	Initial height [mm]	Height before swelling [mm]	Height at max. swell. [b] [mm]	Max. swell. pressure [b] [MPa]	Time at max. swelling [dd hh:mm]	Density initial[a] [g/cm^3]	Density at max. swell[a] [g/cm^3]
1-dry-1	10.31	7.68	7.79	0.47	00 00:12	0.99	1.31
1-dry-2	10.46	7.64	7.75	0.47	00 00:15	0.97	1.31
1-wet-1	11.38	7.74	7.82	0.37	00 00:45	0.90	1.30
1-wet-2	11.42	7.57	7.68	0.42	00 01:09	0.89	1.33
1-wet-3	12.39	6.52	6.80	1.08	00 13:06	0.82	1.50
1-wet-4	7.76	5.52	5.90	1.65	01 00:09	1.31	1.73
1-wet-5	8.85	5.84	6.25	1.79	00 13:49	1.15	1.63
2-dry-1	13.45	7.75	7.91	0.49	00 05:13	0.76	1.29
2-dry-2	13.82	8.67	8.85	0.45	00 00:57	0.74	1.15
2-wet-1	15.76	8.65	8.76	0.39	00 01:07	0.65	1.16
2-wet-2	16.53	7.80	7.90	0.44	00 13:14	0.62	1.29
2-wet-3	18.21	6.70	6.99	1.39	00 23:30	0.56	1.46
2-wet-4	17.42	6.02	6.47	2.15	02 04:41	0.58	1.57
2-wet-5	15.80	5.88	6.44	2.26	02 06:42	0.64	1.58
2-wet-6	14.39	5.63	6.29	2.93	03 16:29	0.71	1.62

[a]Water not included and assumed 20-g sample weight. [b]Apparatus deformation during swelling was approximately 0.25 mm/MPa.

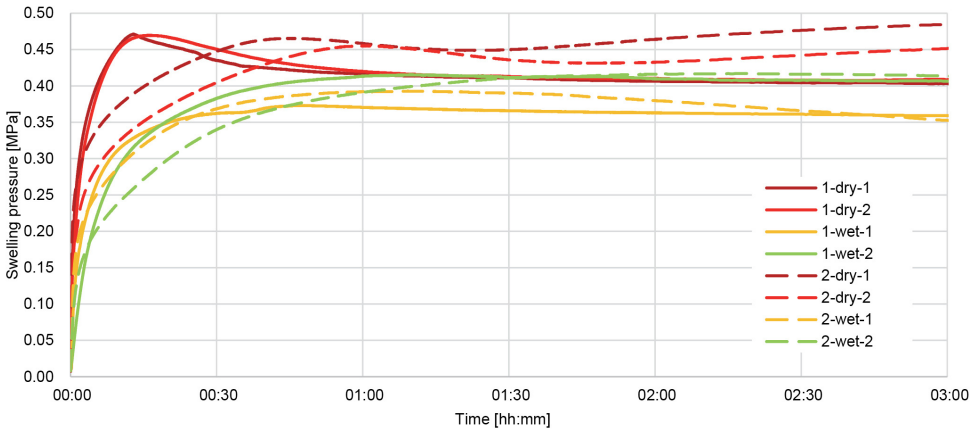

Fig. 10 Swelling pressure versus time for the four driest samples of both series

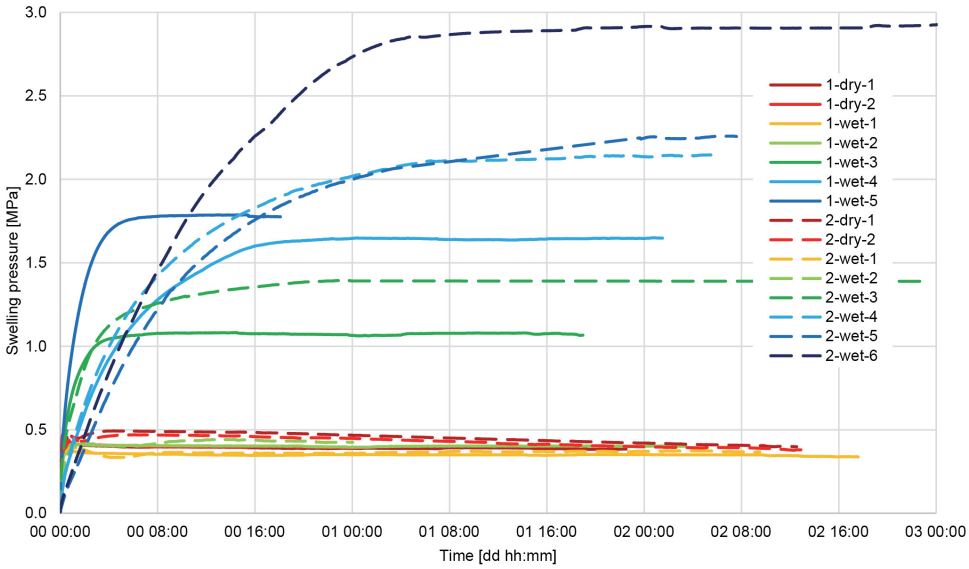

Fig. 11 Swelling pressure versus time for all samples

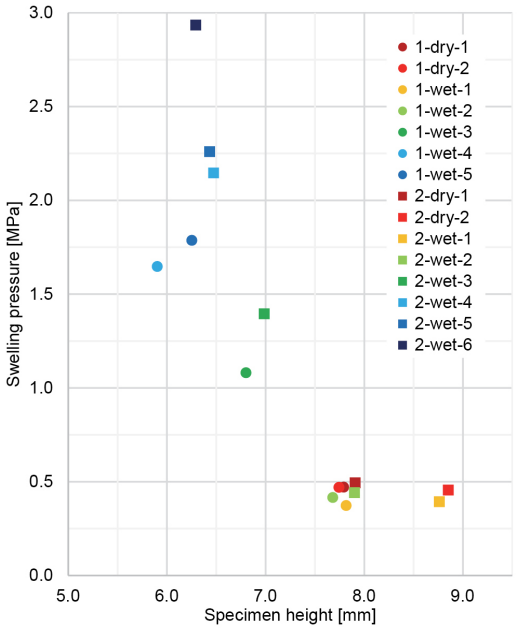

Fig. 12 Maximum swelling pressure versus height for all samples

4.4 Post-swelling consolidation

In Fig. 13, the reaction of a counter pressure to an already swollen sample is shown. The consolidation was held for three days for most of the samples, but as shown, deformation generally stopped after about six hours. One can see that the four highest samples all end up at around, and just below, 7 mm. This deformation progress is very similar to that of the wettest samples in the pre-compacting stage, which are included in Fig. 13 for reference.

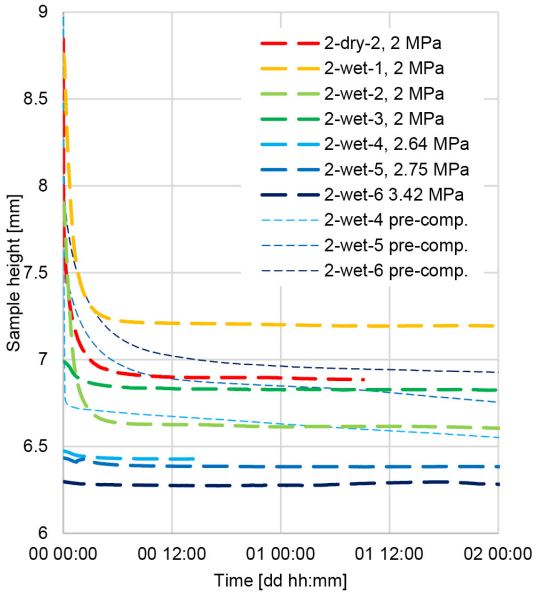

Fig. 13 Post-swelling consolidation, with consolidation pressure for each sample shown to the upper right. Three curves from pre-compacting are added as reference points

5 Discussion and conclusions

This experiment was designed to study the behaviour of samples of swelling gouge material with different water contents. One main finding is that there seems to be a correlation between the sample height and the swelling pressure. Further, the water content has been found to have a significant influence on pre-compacting, yielding lower samples, and it has also been found that it may be possible to identify the water content when all the intracrystalline swelling/hydration is completed. This last issue should be emphasized as intracrystalline swelling may create the largest swelling pressures.

As shown by Fig. 10 and Fig. 11, the swelling pressure generally increased with increasing initial water content. However, during pre-compacting, the samples dried and created sample heights that were lower with increasing initial water content. It is believed that the lower sample heights created the increased pressures, as shown in Fig. 12. For sample series 1, this correlation seems to be mostly linear and for sample series 2, it seems to be curved. Since all samples have the same material weight, the height is representative of the volume and based on that, the density.

Sample 1-wet-4 had a slower swelling development (see Fig. 11) compared to the rest of the curves and also a lower swelling pressure than expected considering the sample height. Looking at the apparatus deformation data (not presented), sample 1-wet-4 had a divergent development compared to the other samples, the reason for which is unknown. As previously mentioned, the standard test allows no expansion during swelling, while in this test setup, apparatus deformations had to be allowed due to the lack of this option in the system control software. Since the apparatus deformation was similar for all samples, except for the aforementioned sample 1-wet-4, the only effect is believed to be slightly lower swelling pressures due to the allowed sample expansion.

Table 4 shows that the initial height was generally much higher for sample series 2 than for sample series 1. This indicates that the samples have different amounts of swelling material and also different types of swelling material, as some swelling minerals expand more than others when pressure is not applied (Kocheise 1994). The sample heights and swelling pressures in Fig. 12 are quite similar, but it seems that sample series 1 has a slightly lower pressure build-up with respect to the sample height.

Fig. 9 shows that with increasing water content, the samples get lower after pre-compacting for both sample series prior to samples 1-wet-4 and 2-wet-4. This behaviour is assumed to be caused by lower friction between the grains due to the water. The heights at about day one for the samples wetter than 1-wet-4 and 2-wet-4 increased, which is believed to be a result of the material swelling.

In considering the two initially wettest samples for both series, one can observe a flat or semi-flat section of the pre-compacting curve immediately after the first large deformation has completed. In this period, it is assumed that the water between the grains that originally caused osmotic swelling is evaporating and that the grain matrix is able to withstand the pressure. When the curves start to drop again, it is assumed that the intracrystalline swelling is reversed due to further evaporation of the water. Since the reversal of the intracrystalline swelling will decrease the volume of the grains, it is reasonable to believe that the volume of the sample will also decrease. The amount of water evaporation during the pre-compacting stage can be viewed in Table 3 for initial and final weights.

Regarding post-swelling consolidation for sample series 2 (Fig. 13), all samples that were higher than 7 mm dropped to about 7 mm when exposed to a pressure of 2 MPa, which also occurred for the wettest samples during pre-compacting. During this stage, the samples were still covered with water. A stable behaviour for three days indicates that the long-term reduction in sample height in pre-compacting was because of drying, and not creep or other material property dependent deformations.

In the post-swelling phase, the three wettest samples showed very little reaction when subjected to an additional counter pressure of 0.5 MPa. Based on this finding, one can assume that no swelling was reversed by the pressure. Since both the original pressure from the swelling and the post-swelling consolidation pressure are above the 2 MPa osmotic swelling potential, one can further assume that the main swelling mechanism for these samples was intracrystalline swelling.

The water content at the finishing point of intracrystalline swelling is believed to be important since the potential swelling pressures of more than tens of MPa would be hard to counteract with a support construction, while the osmotic pressure of 2 MPa would be much easier to counteract. However, the fraction lower than 20 μm is only a small part of the in-situ material, which also has other material properties affecting its behaviour. For further study of the amount of water needed to complete the intracrystalline swelling, the material of sample series 2 can be used as a case. Assuming all voids are filled with water, a height of 7 mm for the sample provides a water content of 6.7 g for 20 g of material, which is a 34 weight %. In the in-situ material, the fraction lower than 20 μm is 16% of the total sample volume. If the percentage of water in the sample is distributed in the in-situ material, this yields a water content of approximately 5%. The water content of the actual material was between 8 and 38% (see Table 3). Since the swelling happens in sequence with the intracrystalline swelling occurring first, it is quite likely that this material has already undergone intracrystalline swelling and is well into osmotic swelling. According to Haigh

et al. (2013), the plastic limit relates to the point at which the water phase ceases to act as a continuum. This means that at a water content equal to the plastic limit, the swelling is likely to be well into the osmotic phase as there is water in the pores of the material.

Transferring the findings of the tests discussed in this paper to large-scale in-situ conditions, such as the actual weakness zones in tunnels, is quite challenging. Some factors are, however, believed to be of particular interest, such as the portion of swelling grains, their swelling potential and the natural water content. Together these factors may be a measure of how much swelling has already taken place in-situ, as indicated in the previous paragraph. In addition, the density of the material in-situ is of interest as the swelling pressure increases with the increasing compaction of the material.

In addition to the above-mentioned factors, the in-situ material also has other mechanical properties that would influence the *in-situ* behaviour, combined with the rock stresses and the installed support. If samples of undisturbed in-situ material were possible to obtain, one would be able to produce interesting and useful data describing the probable minimum and maximum values for a material regarding, for example, swelling pressures and compressibility. One is not likely to know the precise rock mass stress conditions and the influence of the rock support, but by assessing the suggested values in *in-situ* conditions, one might be able to anticipate a range of behaviour in a zone to suggest applicable rock support.

As is the case for results from the standard test, the test results from this study must not be considered as a measure of the in-situ swelling pressure. However, this study shows that some supplementary tests and/or an extension of the current method may provide a better basis for assessing the results for in-situ conditions:

- The plasticity limit and the natural water content of the total sample may be used to assess the degree to which the in-situ material has already swollen and if the intracrystalline swelling/hydration process is complete.
- The post-swelling stage may have water content where osmotic swelling is well underway. This may be used also to assess to what degree the in-situ material has already swollen.

Acknowledgments
The authors would like to thank Mr. Tom-Andrè Kynbråten and Mr. Jan-Inge Senneset at the Sentral Laboratoriet at the Norwegian Public Roads Administration for their excellent work and technical input.

Conflict of interest
The author wishes to confirm that there are no known conflicts of interest associated with this publication and there has been no significant financial support for this work that could have influenced its outcome.

References

Brekke TL (1965) On the measurement of the relative potential swellability of hydrothermal montmorillonite clay from joints and faults in pre-Cambrian and Paleozoic rocks in Norway. Int J Rock Mech Min 2 (2):155-165. doi:https://doi.org/10.1016/0148-9062(65)90011-2

Brekke TL, Selmer-Olsen R (1965) Stability problems in underground constructions caused by montmorillonite-carrying joints and faults. Eng Geol 1 (1):3-19. doi:https://doi.org/10.1016/0013-7952(65)90004-9

Haigh SK, Vardanega PJ, Bolton MD (2013) The plastic limit of clays. Geotechnique 63 (6):435-440. doi:https://doi.org/10.1680/geot.11.P.123

ISRM (2007) The Complete ISRM Suggested Methods for Rock Characterization, Testing and Monitoring: 1974-2006. ISRM Turkish National Group, Ankara

Kocheise R-C (1994) Svelleleire i undersjøiske tunneler. Universitetet i Trondheim, Norges tekniske høgskole, Institutt for geologi og bergteknikk, Trondheim

Kraehenbuehl F, Stoeckli HF, Brunner F, Kahr G, Müller-Vonmoos M (1987) Study of the water-bentonite system by vapour adsorption, immersion calorimetry and X-ray techniques; I, Micropore volumes and internal surface areas, following Dubinin's theory. Clay Miner 22 (1):1-9. doi:https://doi.org/10.1180/claymin.1987.022.1.01

Laird DA (2006) Influence of layer charge on swelling of smectites. Appl Clay Sci 34 (1):74-87. doi:https://doi.org/10.1016/j.clay.2006.01.009

Madsen FT, Müller-Vonmoos M (1989) The swelling behaviour of clays. Appl Clay Sci 4 (2):143-156. doi:https://doi.org/10.1016/0169-1317(89)90005-7

Mao D, Nilsen B, Dahl F (2011) Laboratory Testing of Swelling Gouge From Weakness Zone - Principle And Recent Update. Paper presented at the 45th U.S. Rock Mechanics / Geomechanics Symposium, San Francisco, 26-29 June

Nilsen B (2016) Reliability of swelling pressure testing for tunnel support evaluation. Paper presented at the ITA-AITES World Tunnel Congress 2016, San Francisco, April 22-28

Selmer-Olsen R (1980) Ingeniørgeologi: Generell geologi, vol 1. 3rd edn. Tapir, Trondheim

Selmer-Olsen R (1985) Method for determination of dimensional swelling pressure. Paper presented at the Fjellsprengningskonferansen, Oslo, November 21-22

Statens vegvesen (2013) Measurement of plastic limit of cohesive soils. Statens vegvesens rapporter. Statens vegvesen, Oslo

Statens vegvesen (2016) Laboratorieundersøkelser. vol R210. Statens vegvesen, Vegdirektoratet, Oslo

Weil RR, Brady NC (2017) The Nature and Properties of Soils. 15th edn. Pearson, Boston